Università degli Studi di Cagliari

INTERNATIONAL Ph.D IN INNOVATION SCIENCES AND TECHNOLOGIES

Cycle XXIX

TITLE

Spark Plasma Sintering and Characterization of Bioceramics

Scientific Disciplinary Sector:

Materials Engineering

Presented by:	Ing. Luca Desogus
Ph.D Coordinator	Prof. Roberto Orrù
Tutor	Prof. Roberto Orrù

Final Exam, Academic Year 2015 – 2016

Thesis presented in the examination session - March 2017

Index

Preface

The present work, mainly conducted at the Mechanical, Chemical and Materials Engineering Department, University of Cagliari (Italy), is part of a research activity addressed to the fabrication and characterization of innovative ceramic systems. The focus of this thesis is on a particular subclass of these materials, that have attracted their interest in the last decades for their compatibility with living tissue: hydroxyapatite and bioactive glass-based ceramics.

Musculoskeletal problems including bone and joint pathologies that lead to tissue degeneration and inflammation, are among the main causes of chronic pain, physical disability and work absenteeism in both developed and developing countries. These problems involve millions of people worldwide, especially those aged over 50 years. In addition, it is expected that the percentage of target population affected by these diseases will double by the next 5 years[1]**.** These diseases typically require surgery, including bone substitution, partial or total joint replacement. Furthermore, the treatment of most bone traumatism and malfunctions also need the use of different devices made of suitable biocompatible materials. All the features above have driven the great efforts made by research groups for the development of new implant biomaterials for prosthesis and implants in the last 50 years. For instance, Figure 1 (a-b) shows two implants dating back forty years ago.

To perform successfully in vivo, an implant material must possess particular and well controlled properties suited to each individual application. In major load-bearing situations, such as joint replacement, emphasis may be placed on the strength of the material and its ability to withstand repeated cycles of loading and unloading. The focus in repairing small bone defects, on the other hand, may lie on the chemical composition of the material and whether it is able to bond with surrounding bone tissue or trigger new growth.

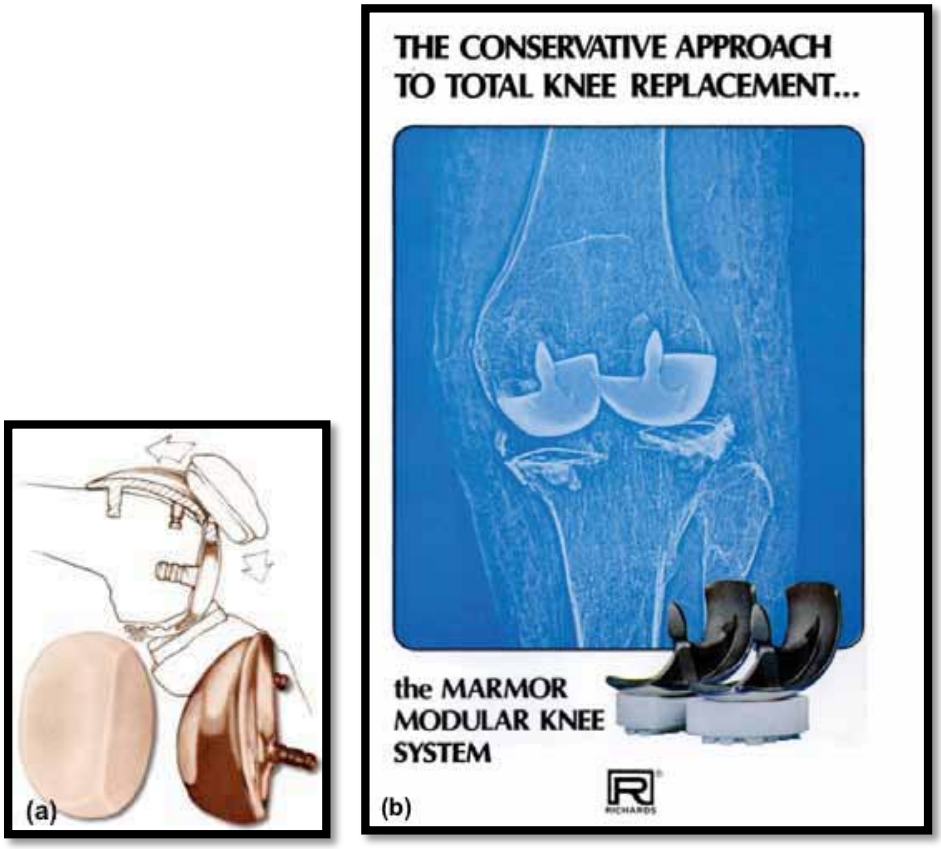

Figure 1. Bechtol patellofemoral component (1974) (a) and Marmor Modular Knee Ad from JBJS (1970)(b)[2]

In general, it is also not easy to give a unique comprehensive definition of biomaterial. In fact since the end of the 20th century there have been several modifications in this regards, caused by shifts in both the conceptual ideas and the expectations of biological performance, which mutually changed in time. We can use the definition introduced in September 2009: "A biomaterial is a substance that has been engineered to take a form which, alone or as part of a complex system, is used to direct, by control of interactions with components of living systems, the course of any therapeutic or diagnostic procedure, in human or veterinary medicine" [3].

The biomaterials discipline is founded on the knowledge of the synergistic interaction of material science and technology, biology, chemistry and medicine. The input of comprehension from all these areas are required for the development of implants able to operate adequately in a living body and interrupt normal body functions as little as possible [4]. Since clinical implantology is the main

purposes of biomaterials, biomedical sciences become the key part of the research. These include cell and molecular biology, histology, anatomy and physiology. The final aim is to obtain the correct biological interaction of the artificial grafts with living tissues of a host. To achieve such goal, several stages have to be performed. These include: material synthesis, design and manufacturing of prostheses, followed by various types of tests. Furthermore, before any kind of clinical application, potential biomaterials must also pass all regulatory requirements [5].

Indeed, when a synthetic material is placed within the human body, tissue reacts towards the implant in a variety of ways depending on the material type. The mechanism of tissue interaction depends on the tissue response to the implant surface. Living organisms can consider artificial implants as [6]:

- biotoxic (or bioincompatible), when materials release to the body substances in toxic concentrations and/or trigger the formation of antigens that may cause immune reactions ranging from simple allergies to inflammation with possible severe health consequences. They may cause atrophy, pathological change or rejection of living tissue near the material as a result of chemical, galvanic or other processes;
- bioinert, which indicates material that, once placed in the human body has minimal interaction with surrounding tissues, (the term “bioinert” should be used with care, since it is clear that any material introduced into the physiological environment will induce a certain response);
- biotolerant (or biocompatible), when materials do not release any toxic constituents but also do not show positive interaction with living tissues;
- bioactive, consisting of materials which dissolve slightly and promote the formation of a surface layer of biological apatite: afterwards such materials are able to interface directly with the tissue at the atomic level, resulting in the formation of a direct chemical bonds to bones;
- bioresorbable**,** made of materials that dissolve over time (regardless of the mechanism leading to the material removal) and allow a newly formed tissue to grow into any surface irregularities but may not necessarily interface directly with the tissue. Consequently, the

functions of bioresorbable materials are to participate in dynamic processes of formation and re-absorption occurring in bone tissues; thus, they are used as scaffolds or filling spacers allowing to the tissues their infiltration and substitution [7].

Regardless the classification made above, we can also divide biomaterials into 4 major groups: bio-metals, bio-polymers, bio-ceramics and bio-composites. All of them play very important roles in biomedicine, for both replacement and regeneration of various human tissues.

However, as mentioned previously, this work is entirely focused on bioceramics, specifically hydroxyapatite and bioactive glass-based. The fabrication of the latter ones in massive form will always take advantage of the innovative Spark Plasma Sintering (SPS) technology. In particular, after the Introduction section, this thesis is divided in five additional chapters, as follows:

- Chapter II: sintering and characterization of dense biomaterials, starting from conventional 45S5 and innovative bioglass powders;
- Chapter III: preparation and characterization of composite material, based on the combination of innovative glass and hydroxyapatite.
- Chapter IV: in-vitro test to investigate the behavior of a human cells' line on three different calcium phosphate materials obtained by SPS dorm hydroxyapatite powders.
- Chapter V: concluding remarks.

Luca Desogus gratefully acknowledges Sardinia Regional Government for the financial support of her PhD scholarship (P.O.R. Sardegna F.S.E. Operational Programme of the Autonomous Region of Sardinia, European Social Fund 2007-2013 - Axis IV Human Resources, Objective l.3, Line of Activity l.3.1.)

Chapter 1

Introduction

1.1 Bioceramics and bioactive glasses

Ceramics and glasses represent some of the more durable materials being developed for applications in several industrial field, such as refractory, aerospace, electronics, biomedicine, etc. The majority of ceramics produced in the world have a crystalline structure while glasses are noncrystalline solids. The use of these materials for the repair and reconstruction of diseased or damaged parts of the body has led to a great innovation in biomedicine in the last 60 years. In this contest, the are formally termed as bioceramics [8]. From the mechanical point of view, they have high hardness, generally a low friction and a good wear resistance. In addition, interest in bioceramics is related to their behavior when implanted in a living organism. In this regard, as mentioned in therefore, bioceramics are classified as bioactive, bioinert and bioresorbable materials (see the preface). Their applications in medicine are rather wide, i.e. components for implants to repair hard tissues of the skeletal system (bones, teeth), as well as diagnostic instruments, thermometers, tissue culture flasks, eye glasses, and others. In Figure 2 (a-b) is shown an example of bioceramic used for repairing an orbital floor.

As mentioned above, in general, bioceramics comprise various polycrystalline materials, amorphous materials (glasses) and blends thereof (glass-ceramics). Nevertheless, the chemical elements used to manufacture bioceramics is just a small set of the Periodic Table. Specifically, bioceramics can be prepared from alumina, zirconia, magnesia, carbon, silica and calcium-containing compounds, as well as from a limited number of other chemicals. All these compounds can be manufactured as bulk

bodies in dense and porous forms, or as crystals, powders, particles, granules, scaffolds and/or coatings[6]. Figure 3 shows schematically four different ceramics in contact with living tissue.

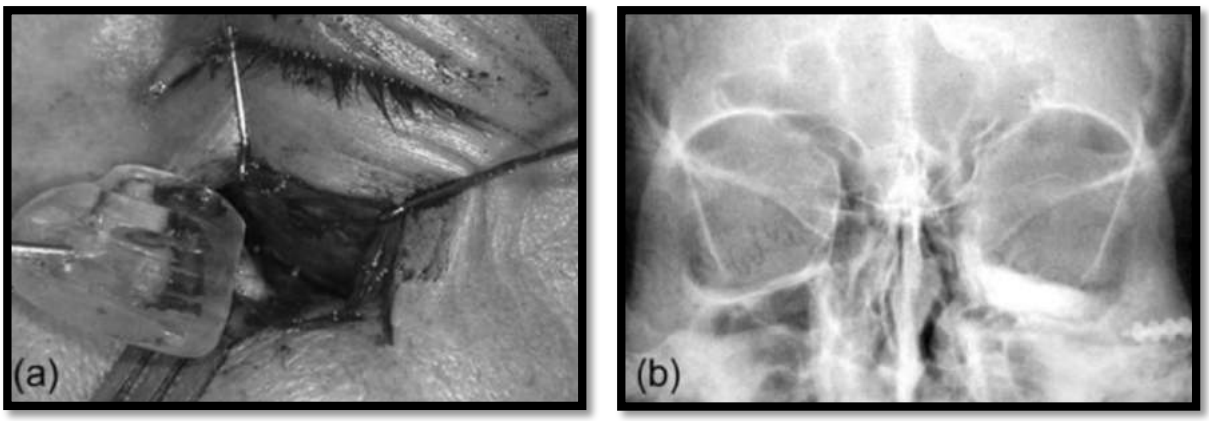

Figure 2. Orbital floor reconstruction (a) Inserting glass implant beneath the eye, (b) Post-operative X-Ray[9].

In the present thesis, the attention is focused on the preparation and characterization on two groups of bioceramics, i.e. calcium phosphates (in particular Hydroxyapatite based ceramics), and bioactive glasses system, which will be discussed in detail in the following sections.

1.1.1 Hydroxyapatite-based Bioceramics

Ap atite (Greek, 'to deceive') was the name given by Werner in 1788 to describe a group of mineral crystals appearing in different colors that were often mistaken for the more precious gems such as aquamarine, amethyst and topaz[10]. Based on the X-ray diffraction patterns of sintered bone similar to those of mineral apatites, as well as on chemical analyses, which evidence the main presence of calcium and phosphate ions, it was concluded that the inorganic phase of bones and teeth is basically a calcium phosphate called Hydroxyapatite, commonly referred to as HA (or HAp) [11].

In his pure form, HA has the specific chemical composition of $Ca_{10}(PO_4)_6(OH)_2$, with Ca/P stoichiometric ratio of 1.67, and displays the crystallographic structure shown in Figure 4.

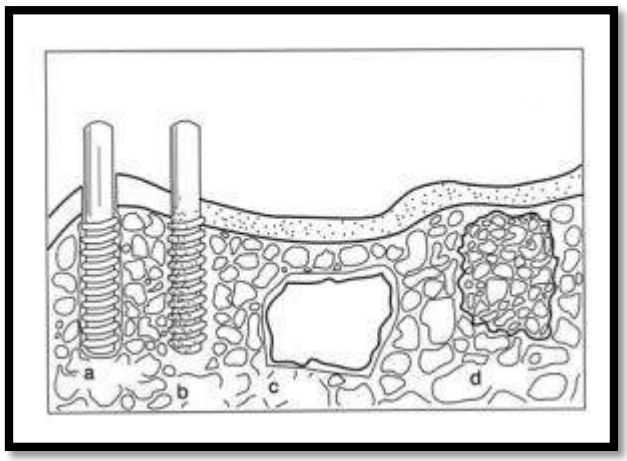

Figure 3. Example of Bioceramics: (a) bioinert alumina dental implant, (b) bioactive hydroxyapatite $[Ca_{10}(PO_4)_6(OH)_2]$ coating on a metallic dental implant, (c) surface active bioglass and (d) bioresorbable tricalcium phosphate $[Ca_3(PO_4)_2]$ implant[12].

Actually, biological apatites also contain important minor substituents (e.g. CO_3^{2-}, Na^+, Mg^{2+}), so that are more accurately described as carbonated apatite or carbonate apatite, CHA or HCA. The structure of human bones can be quite well reproduces by synthetic HA (cf. Figure 5).

A lack of HA leads to the development of pathologies like osteoporosis; on the other hand, apatite is also found in some pathologic calcifications (dental calculus, heart calcifications, urinary stones, soft-tissue calcifications, etc) [8].

Since hydroxyapatite represents the main inorganic component of hard human tissues, it is not surprising that it is regarded as one of the most investigated ceramics for biomedical application in either bulk form or as coating. In this regards, it is known that the heat treatment required for the consolidation of HA powders may lead to the partial or total decomposition of the original phase to

generate less suitable ones (β-TCP and others)[14]. Starting powders characteristics and the adopted sintering method play a relevant role in this contest.

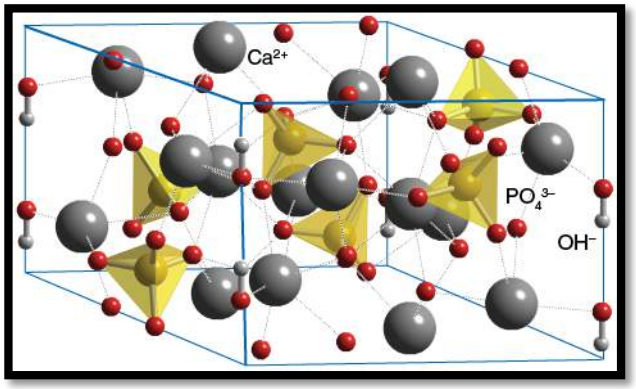

Figure 4. Mineral structure of HA[13].

Synthetic HA is used in a number of different ways throughout the body, covering all areas of the skeleton. These include healing of bone defects, fracture treatment, total joint replacement, bone augmentation, orthopedics, craniomaxillofacial reconstruction, spinal surgery, otolaryngology, ophthalmology and percutaneous devices, as well as dental fillings and periodontal treatments[6].

It should be noted that hydroxyapatite of synthetic or biologic origin (animal bones) have also diverse non-medical applications including: protein chromatography, water defluoridation, components of dental products and as abrasives for orthopedic and dental implants[7].

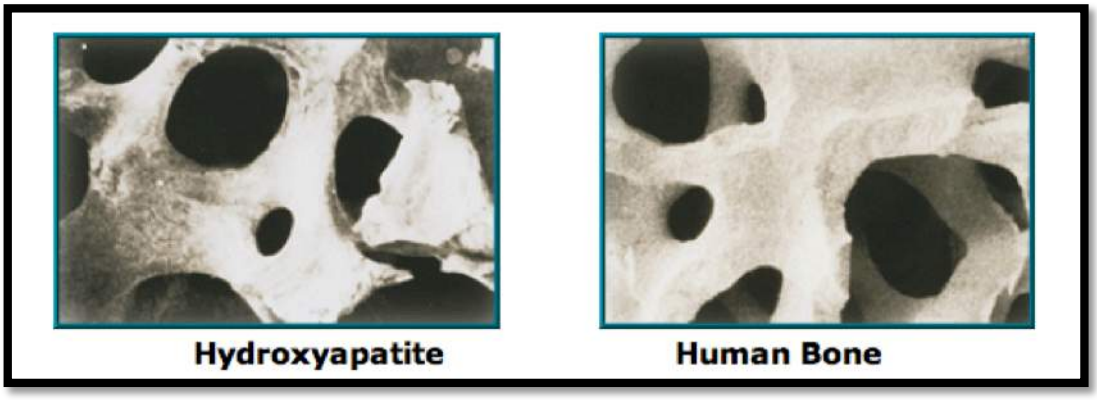

Figure 5. Structural similarity between HA and human bone[15].

The most important aspect related to the use of hydroxyapatite-based bioceramics comprises their inclusion in the metabolic process of the organism, adaptation of either surface of the entire material to the biomedium, integration of a bioactive implant with bone tissues at the molecular level or the complete replacement of a resorbable bioceramics by healthy bone tissue[6].

The mechanism proposed to interpret how hydroxyapatite surfaces are recognized when implanted in organisms is shown in Figure 6[16] . The entire phenomenon can be divided into 8 steps:

1-2) Solubilization of the hydroxyapatite surface start to occur;

3) achievement of the equilibrium condition between physiological solutions and the modified surface of hydroxyapatite;

4) adsorption of proteins and organic material;

5-6) cell adhesion and proliferation;

7) beginning of new bone production;

8) new bone formed and natural bone metabolism.

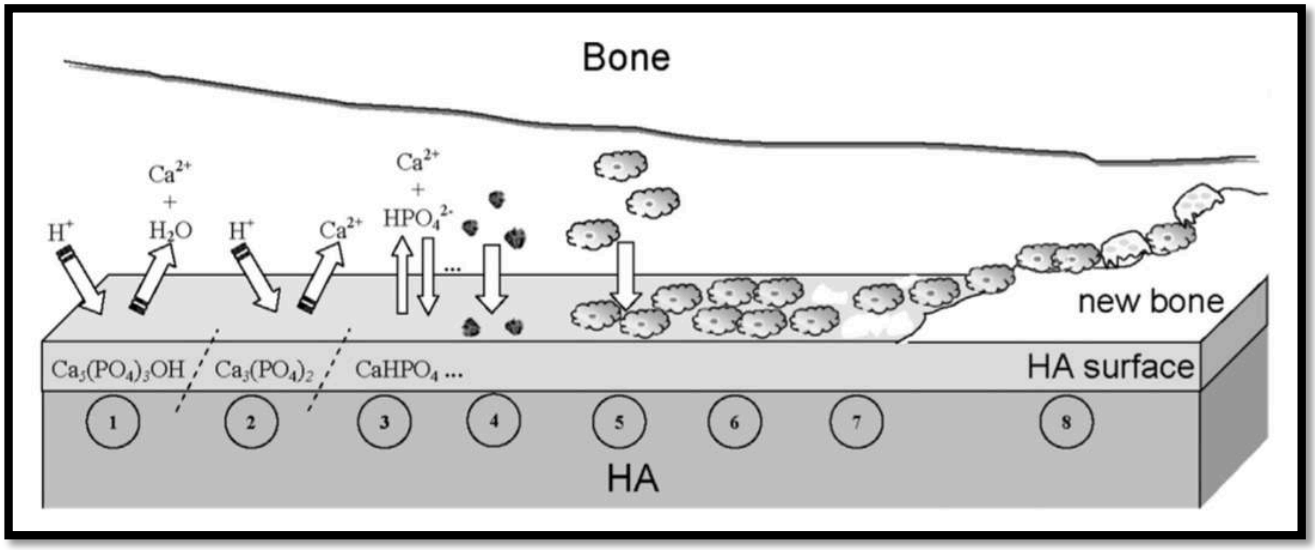

Figure 6. Schematic representation of the phenomena that occur on the surface of hydroxyapatite after implantation[16].

HA and the other calcium phosphates fall into the categories of bioresorbable or bioactive bioceramics. Indeed, in the first case, they dissolve slightly while also promoting the formation of a surface layer of biological apatite before interfacing directly with the tissue. Alternatively, they can act as a bioresorbable one if the bioceramics dissolve over time, so that they can be used as scaffolds or filling spacers, allowing to the tissues their infiltration and substitution. It is important to emphasize that a difference between the bioactive and bioresorbable bioceramics might be associated with structural factors only. In fact, an implant made from dense and crystalline HA behaves as a bioactive material, and is retained in an organism for at least 5-7 years[6]. In contrast, a highly porous ceramics of the same composition can be resorbed approximately within a year[6]. Furthermore, as shown in Figure 7, two different bioceramics (calcium deficient hydroxyapatite HHA, and stoichiometric hydroxyapatite SHA) with the same porosity degree (70%), can exhibit different behaviors, i.e. bioresorbable and bioactive, respectively[17].

Therefore, the final biological behavior of HA materials can be strongly affected by its stoichiometry as well as porosity degree.

1.1.2 Bioactive Glass-based Bioceramics

Bioactive glass discovery happened in the late 60s, early 70s by Prof. Larry Hench after a challenge set out by a colonel of U.S. Army on the way back from Vietnam[18]. At that time Hench was studying the interactions between materials and high frequency radiation. Thus, on the way to a conference in 1967 he had the chance to speak with the colonel, about his discoveries concerning to gamma rays on semiconductors. During their conversation, the colonel, made the following question that changed Hench's life:

"If you can make a material that will survive exposure to high energy radiation, can you make a material that will survive exposure to human body?"

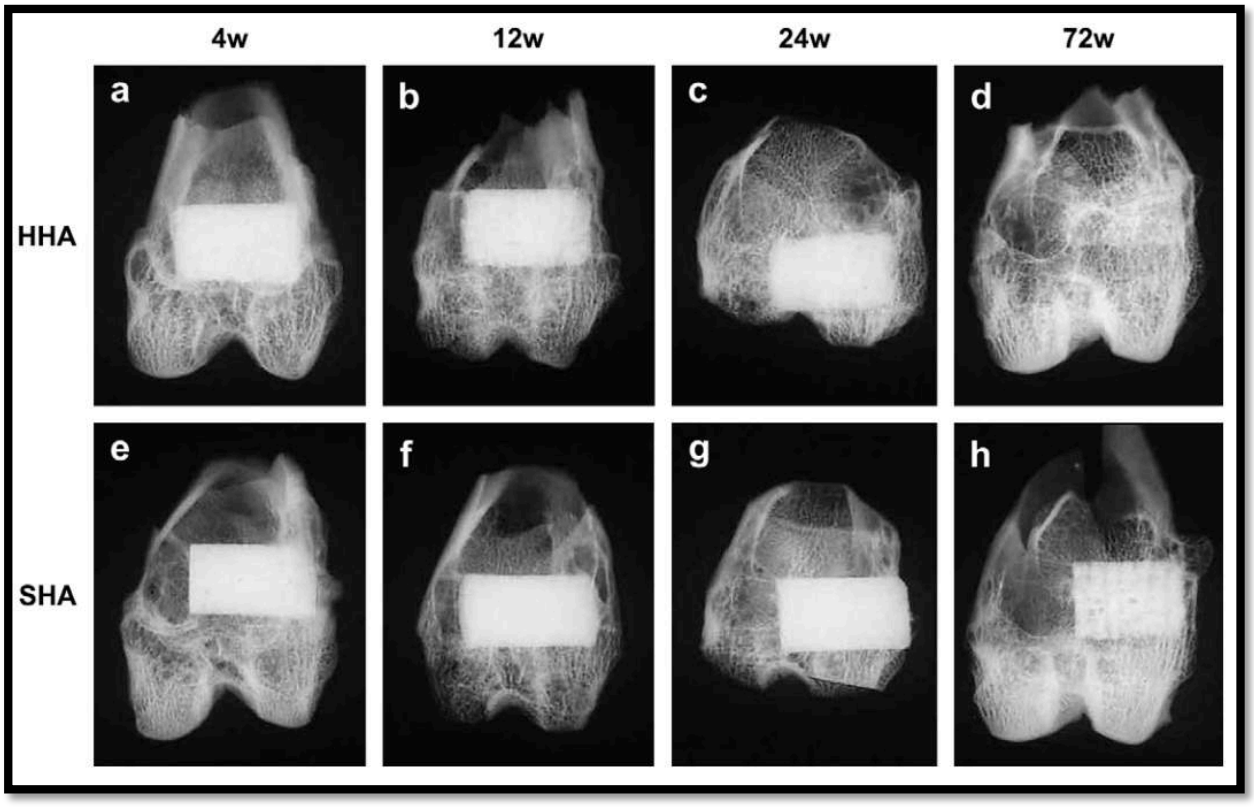

Figure 7. Soft X-ray photographs of the operated portion of the rabbit femur. Four weeks (a), 12 weeks (b), 24 weeks (c) and 72 weeks (d) after implantation of HHA, 4 weeks (e), 12 weeks (f), 24 weeks (g) and 72 weeks (h) after implantation of SHA[17].

The motivation for such question was related to the colonel experience in Vietnam, where soldiers' limbs containing implants generally made of metals and plastic, had to be cut because the outset of rejection problems. Then the request was the development of one or materials family able to bond with living tissues, rather than forming scar tissues, and composed by the constituents similar to human bones.

Hench was fascinated by this challenge, so that accepted his request. To this aim, he formed a research group that, after two years and several experiments, came up with the first bioglass formulation, called Bioglass® and often indicated as 45S5, consisting of: 45% SiO_2 – 24,5% Na_2O – 24,5% CaO – 6% P_2O_5.

Specifically, Hench and his staff designed and produced small 45S5 samples, that were implanted in test subjects for trials. After six weeks, they found that implants formed strong bonds at bones interfaces. An example of Bioglass 45S5 implanted into a rabbit femur after 8 weeks from surgical procedure is reported in Figure 8. Other in-vitro experiments proved that when bioglasses characterized by such specific formulation were contacted with simulating biological fluids solution, a layer of hydroxyapatite was formed on samples surface, as for the case of in-vivo tests. Consequently, bioactive glasses started to be used in the biomedical field.

Nonetheless, research studies involving the utilization of 45S5 Bioglass continued. In this regard, in 1981 June Wilson and coworkers[19] discovered that was possible to induce bonds between 45S5 and not only hard, but also soft tissues (gums, cartilage...), this outcome opened the way for the utilization of Bioglass® in the substitution of tiny ear bones and in periodontics applications.

Further research by Wilson and Nolleti[19], pointed out that the bone formation between soft tissue and bioglasses was possible only for compositions with sufficient reaction time. Glasses with this property fall within the S region indicated in Figure 9. Specifically, the diagram reported in the latter figure applies to glass with 6%wt of P_2O_5 and percentages of SiO_2, CaO and Na_2O from 0 to 100%.

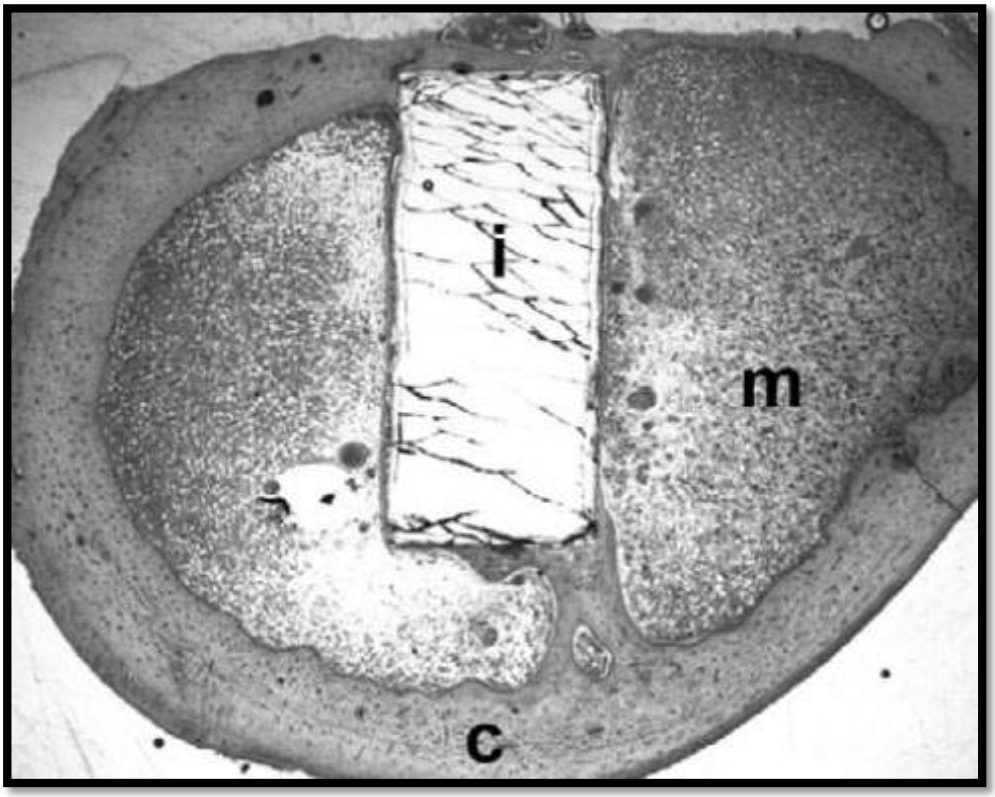

Figure 8. Bioglass 45S5 implant into rabbit femur 8 weeks after surgical procedure (C, cortical bone, I implant, M medullary bone) [20].

Only for compositions included in region A is possible to obtain bonds with bone. This is also possible with soft tissues if glass composition falls in the sub-region S. It should be noted that Bioglass® is included inside the latter region. It is important to stress that if SiO_2 content is higher than 60% (region B), the corresponding glass doesn't form bonds even with bone and behaves as a bioinert material.

Additional bioactive glasses have been proposed as an alternative to the Bioglass®. Some of them are reported in Table 1. For example, the 13-93 and 6P53B also contain MgO and K_2O, not present in the 45S5. The 58S type belongs to the SiO_2-CaO-P_2O_5 system with no Na_2O. In addition, the 70S30C consists on SiO_2-CaO only. The 13-93B3 and 13-93B1 systems are borate glasses. Finally, glasses like $P_{50}C_{35}N_{15}$ have a lattice formed by P_2O_5 and modified with CaO and Na_2O. Further compositions have been also proposed more recently[21].

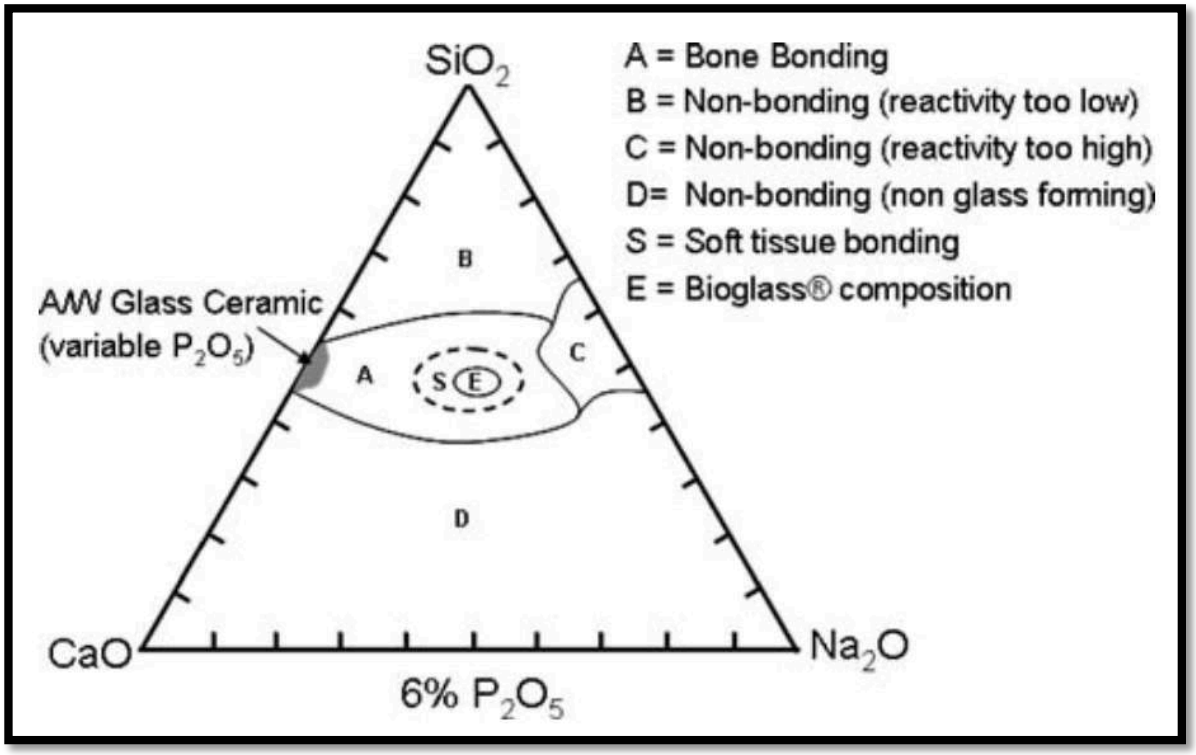

Figure 9. Compositional diagram for bone-bonding[18].

After Bioglass discovery, studies aimed to clarify the bond formation mechanism in suitable water solutions, which simulate human body fluids, were intensified. Based on the results obtained in these studies, the following steps are involved for the formation of bioglass-tissue bond: (cf. Figure 10)

1) Na^+ and Ca^{2+} ion exchange from glass and H^+ from the solution. This fact leads to an increase of the pH.
2) Dissolution of the glass network followed by the formation of Si-OH (silanol) bonds.
3) Polymerization reactions with consequent superficial formation of a SiO_2-rich and alkali-poor layer on glass surface.
4) Ca^{2+}, and PO_4^{3-} and Ca_3^{2-} migration from the solution and their chemiadsorption on the surface. A CaO-P_2O_5 rich amorphous layer is then formed.

5) Crystallization from the $CaO-P_2O_5$ rich layer, with consequent hydroxycarbonate apatite (HCA) formation.

6) Growth factors adsorption and desorption in HCA. These factors are able to stimulate cellular differentiation (this phenomenon continues during the entire process).

7) Release of superficial site set by macrophages. These sites will be occupied by cells.

8) Stem cell adhesion over the bioactive surface.

9) Stem cell proliferation and differentiation into osteoblasts.

10) Bone matrix production and mineralization made by osteoblasts, with mature osteocytes obtainment as final products.

11) Inorganic matrix crystallization consisting of calcium phosphates.

12) Bone growth.

Composition (wt. %)	45S5	13-93	6P53B	58S	70S30C	13-93B1	13-93B3	$P_{50}C_{35}N_{15}$
Na_2O	24.5	6.0	10.3	0	0	5.8	5.5	9.3
K_2O	0	12.0	2.8	0	0	11.7	11.1	0
MgO	0	5.0	10.2	0	0	4.9	4.6	0
CaO	24.5	20.0	18.0	32.6	28.6	19.5	18.5	19.7
SiO_2	45.0	53.0	52.7	58.2	71.4	34.4	0	0
P_2O_5	6.0	4.0	6.0	9.2	0	3.8	3.7	71.0
B_2O_3	0	0	0	0	0	19.9	56.6	0

Table 1. Compositions of various bioactive glasses[22].

Bonding with bone can take place due to similarities between bone inorganic component and HCA layer formed over the implant. On the other hand, bonding with soft tissues can occur thanks to chemiadsorption of collagen fibrils over the porous silica layer. It is important to stress that the

accumulation of dissolution product is strictly connected with pH and composition of the solution. In this regard, it should be noted that during the early stages, the solution becomes poorer of H^+, so that pH increases, and relatively richer of other cations. Subsequently, when cations release rate from bioglass decreases, pH tends to return to normal values.

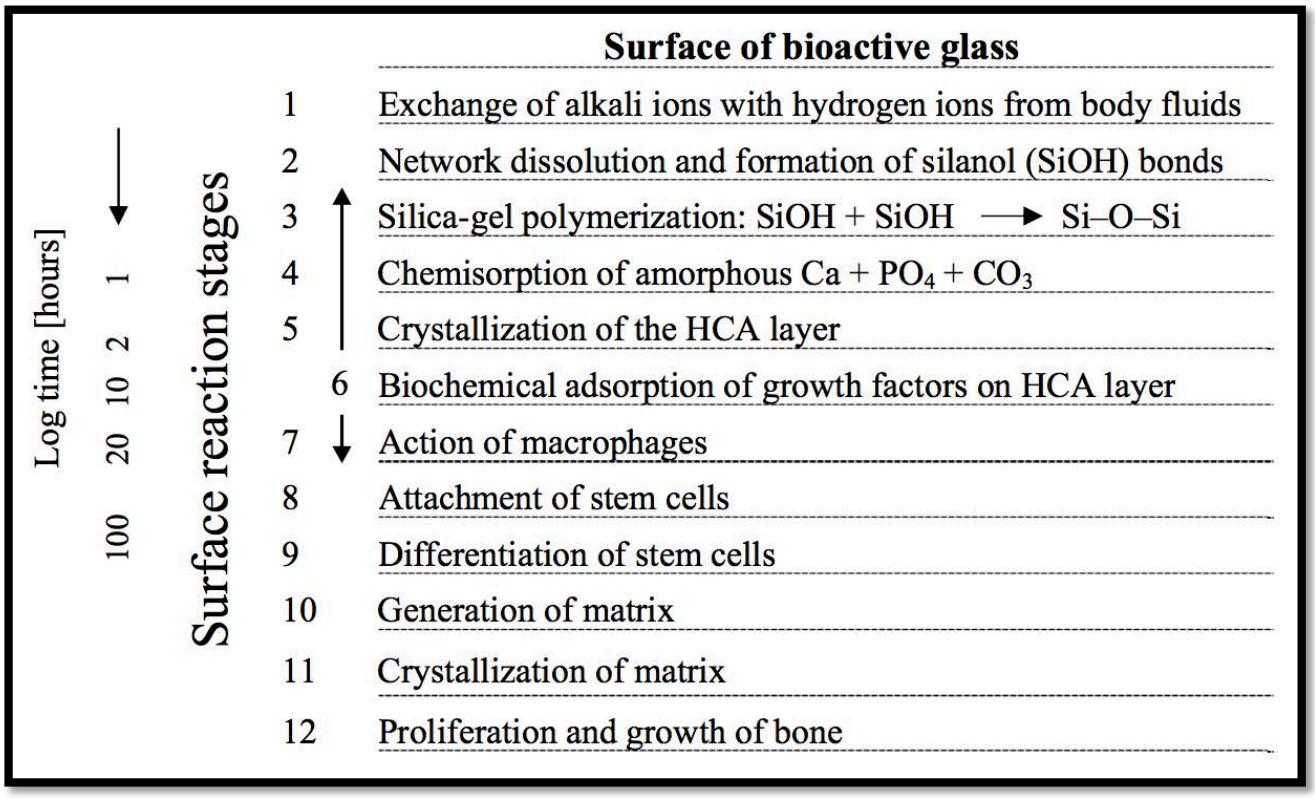

Figure 10. Stages involved during the formation of bonds between tissues and bioactive glasses[23].

To be able to achieve some particular application, bioactive glasses have to be produced in appropriate shapes. In this context, particular interest was devoted to scaffolds, tridimensional objects able to reproduce the extra-cellular matrix, so that the right support as a substrate for the newly formed tis The first bioglass based implant was used in U.S. to treat conductive hearing loss[18]. This disease causes ear-weakness as a result of damages or degenerations. The device, aimed at middle ear reconstruction, was called “Bioglass Ossicular Reconstruction Prosthesis” (or MEP®). sue can be provided. These examples of bioglass scaffolds are reported in Figure 11[9].

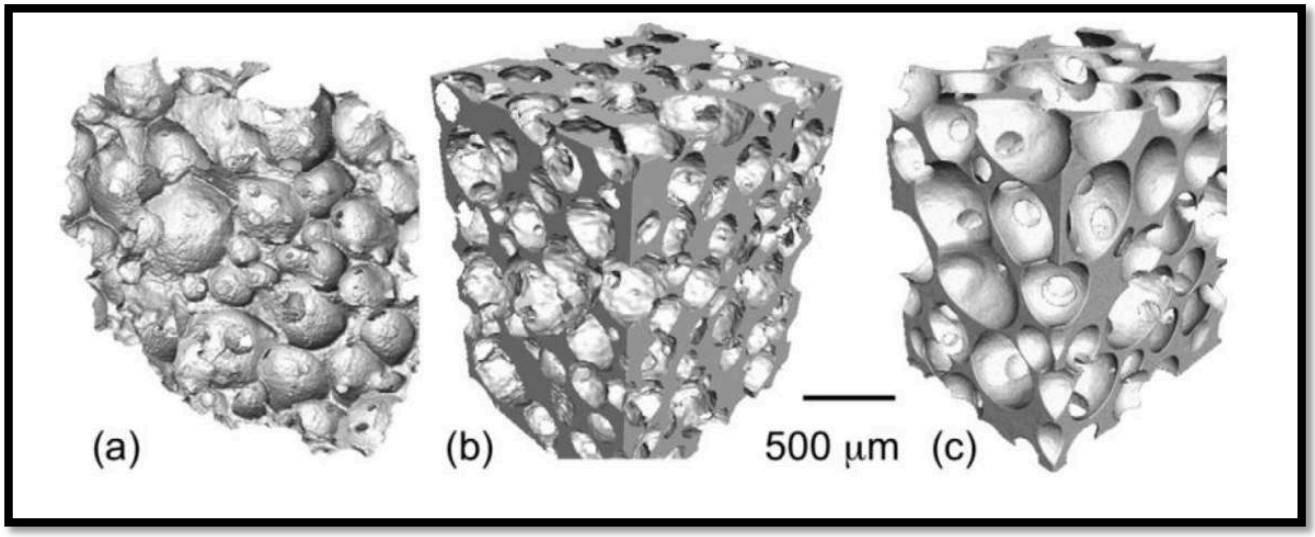

Figure 11. Three examples of bioactive glass-based scaffolds[9].

It was made of a solid bioglass structure that conduced sound from tympanic membrane to cochlea. The advantage of the MEP® over the other devices in use at the time was the ability to bond with soft tissue (tympanic membrane) as well as bone tissue. A modification of MEP® design was made to improve handling in the surgery and it is used clinically with the trademark name of the DOUEK MED®[18]. The first and the second versions of the MEP® are reported in Figure 12.

The second bioglass device available on the market was the Endosseous Ridge Maintainence Implant [ERMI®][18]. This device was designed to provide a more stable ridge for denture construction following tooth extraction. These implants were simple cones of 45S5® to be placed into fresh tooth extraction sites. Numerous clinical studies demonstrate that ERMI® was not only extremely stable, but a lower failure percentage was also found with respect to same devices realized with other materials[18].

None of the products mentioned previously are widespread clinically used, this is because surgeons need to cut the implants to shape them suitably and obtain the required final size. This feature prevented commercial success on this kind of product. Indeed, monolithic bioglass is more suited to implants that are custom made for the patient's need[9].

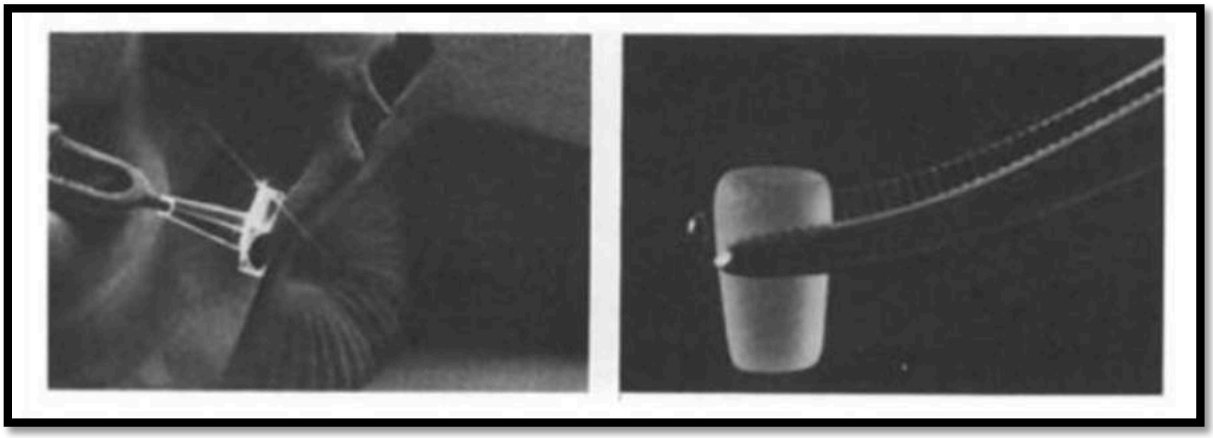

Figure 12. Classic MEP® implant is shown on the left, whereas the second version (DOUEK MED®) is reported to the right[24].

One of the major commercial utilization of bioglasses is as an active repair agent in toothpaste, under the name NovaMin® (GlaxoSmithKline, UK) [9]. This is composed by a 45S5® based particulate with 18μm particle size, used for treating tooth hypersensitivity, which affect 35% of people. Clinical studies show that Bioglass particles adhere to the dentine and then form a HCA layer, so that pain for long period can be alleviated. Figure 13 shows the action of glass particles once in contact with dentine surface, which is totally covered by a HCA layer just after 24h.

Despite the numerous potential applications, so far the use of bioactive glasses in implants which have to bear certain loads is extremely limited because of their unfit mechanical properties, first of all the high fragility. The comparison between those ones of Bioglass 45S5®, hydroxyapatite and human bone is reported in Table 2.

To overcome such drawbacks, new bioglass formulations and production technologies are in development, in order to obtain monolithic bodies with improved mechanical properties. On the other hand, the obtainment of the latter goal should not be accompanied by a worsening of bioglass bioactivity.

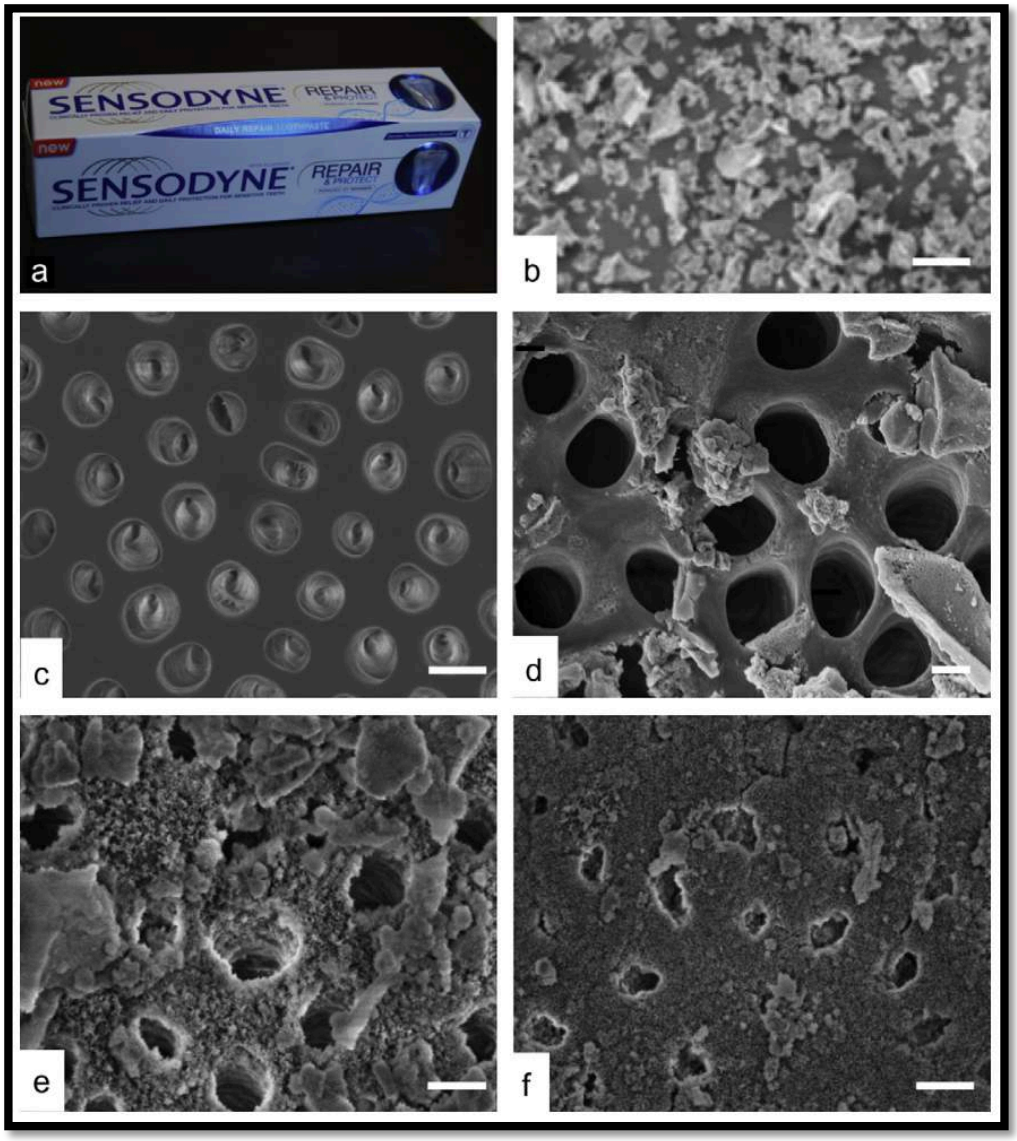

Figure 13. (a) Photograph of Sensodyne® Repair and Protect toothpaste, which contains NovaMin®; (b) SEM image of NovaMin® particles. (c-f) SEM micrograph of human dentine: (c) untreated, (d) immediately after application of Novamin® in artificial saliva (AS); (e) 24 h after application of NovaMin® in AS; (f) 5 days after application[9].

Indeed, the temperature and pressure levels required for the preparation of dense bodies, can also produce modification in the bioglass amorphous nature and composition. To better clarify this aspect, structural and compositional transformations which occur, depending on the temperature, in the 45S5 bioglass are reported in Figure 14.

		Strenght [MPa]		Young's Modulus [GPa]	Fracture Toughness, KIC [MPa m1/2]
		Compressive	Bending		
Bioglass® 45S5		-	42	35	-
HA		500-1000	115-200	80-110	1.0
Human bone	Cancellous	2-12	-	0.05-0.5	-
	Cortical	100-230	50-150	7-30	2-12

Table 2. Mechanical properties of Bioglass 45S5®, hydroxyapatite (HA) and cortical and cancellous bone[25].

Several studies have been reported that crystallization phenomena, which starts at about 610°C (cf. Figure 14**)**, produce a deterioration in bioglass bioactivity performance. In particular, a strong correlation between the crystalline phase percentage in the 45S5-based material and the HCA formation rate was found by Filho et al. [26], as shown in Figure 15.

Briefly, it was observed that the formation of the HCA layer was progressively delayed as the crystallization degree was increased from 0 to 60vol.%. No significant changes are observed when the volume fraction of crystallites was further increased. In contrast, based on the results obtained in a more recent study[27], the preferential dissolution taking place at the glass-crystallites interface promotes the formation of the HCA layer. Thus, a certain crystallization degree might provide beneficial effects in terms of bioactivity. Nevertheless, crystallization phenomena have to be properly controlled to avoid negative consequences in this regards.

Since mechanical properties are generally superior in crystalline or glass-ceramic products with respect to fully amorphous ones, a good compromise should be found.

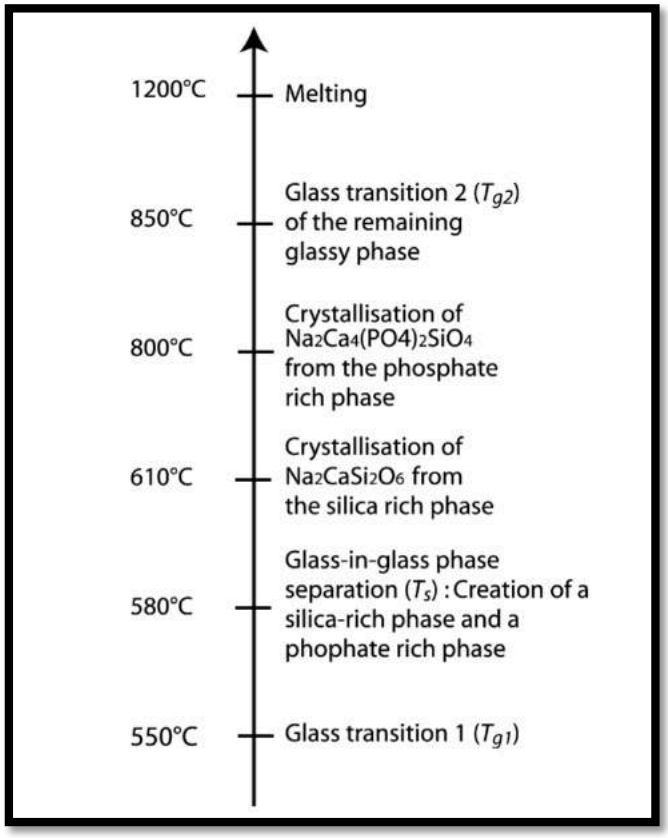

Figure 14. Summary of Bioglass structural transformation[28].

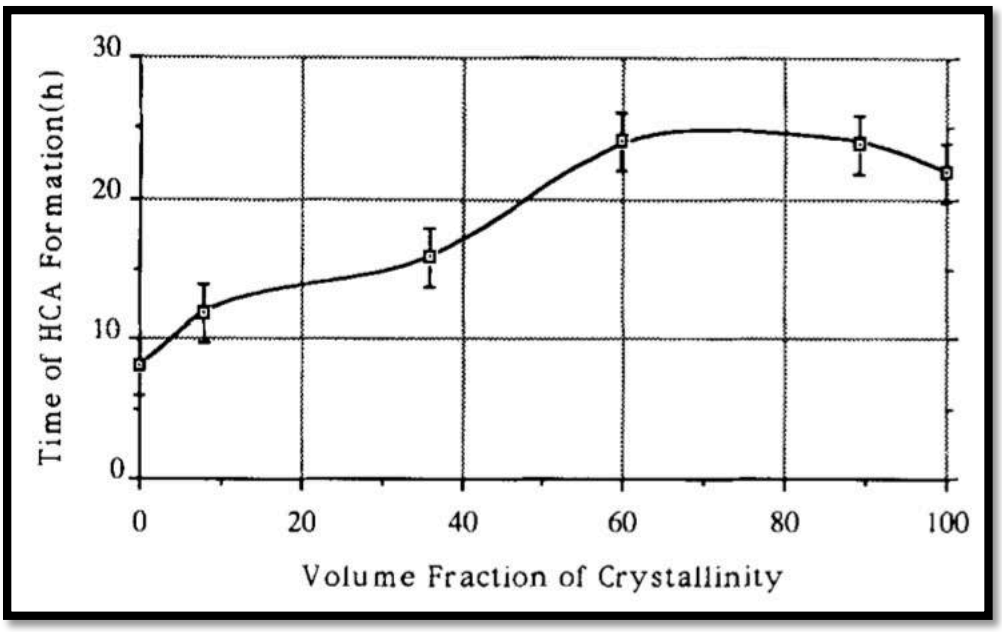

Figure 15. Onset time of HCA formation (stage 5 in Figure 10) with percent crystallization of the bioactive glass-ceramic[26].

Three possible complimentary strategies along this direction that will be considered in this work, are:

1) Take advantage of an innovative and efficient sintering technique, able to densify bioceramics in relatively shorter times and lower temperatures, thus avoiding or limiting crystallization phenomena;
2) Use of recently developed CaO-rich bioactive glasses, which exhibit a lower tendency to crystallize;
3) Formulation of novel composite materials obtained by combining bioglasses and HA.

As mentioned previously, the sintering step is crucial to proper control the structural and compositional changes of the powders under consolidation. In the next session, sintering phenomena and techniques will be considered in details.

1.2 Sintering

Sintering is defined as a thermal treatment for bonding particles together into a coherent, predominantly solid structure via mass transport phenomena that occur largely at the atomic level[29]. The sintering process has been known for thousands of years. For example, first sintered products were bricks heated to add strength. Today, sintering is the primary processing stage for the production not only of most common ceramics, like white wares, refractories, abrasives and others, but also for the fabrication of a wide variety of advanced materials in innovative sectors like aerospace, microelectronic and biomedicine.

Theories about the mechanism occurring during sintering have provided the subject matter of several conferences and learned scientific papers. Related to ceramics, we can say that it is the hardening process of green bodies when exposed to sufficiently high temperature, but lower than the melting point of a material. Indeed, when solids are heated to high temperatures, constituent ions or atoms are driven to move to compensate for the surface energy differences among their convex and concave

surfaces. Bottlenecks are formed and grow among powders at the initial stage (cf. Figure 16). As a result, strong chemical bonds are formed among powders, and loosely compacted green bodies are hardened to ceramic materials.

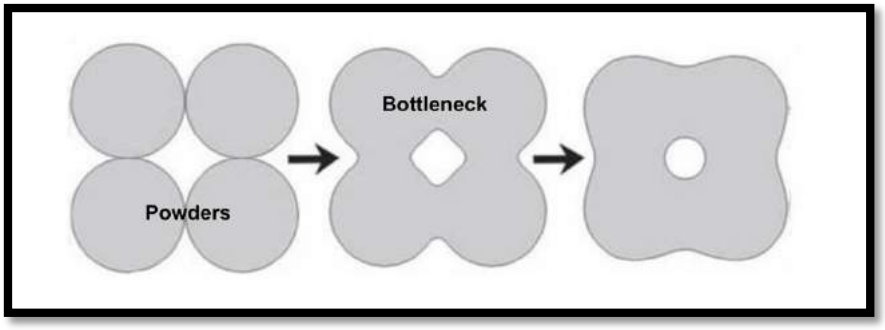

Figure 16. Bottleneck formation between particles under the sintering[30].

Thus, for the thermodynamic point of view, the driving force for the sintering process is the reduction of surface free energy of powdered compacts, by replacing solid-vapor interfaces (or surface energy Γ_{SV}) with solid-solid (Γ_{SS}) interfaces, where $\Gamma_{SS} < \Gamma_{SV}$. Sintering is an irreversible process in which a free energy decrease is obtained through a surface area reduction.

The change of system energy dE due to sintering is therefore composed of two contributions: one relative to the increase due to the creation of new grain boundary areas, $dA_{SS} > 0$, and the second one due to the annihilation of vapor-solid interfaces, $dA_{SV} < 0$. The thermodynamic condition to be fulfilled for the sintering to proceed is

$$dE = \Gamma_{SS} dA_{SS} + \Gamma_{SV} dA_{SV} < 0$$

The sintering process will stop when $dE = 0$

$$\Gamma_{SS} dA_{SS} + \Gamma_{SV} dA_{SV} = 0$$

The following three categories of sintering can be identified, depending on the composition being fired and the extent to which second phases are formed during the heat treatment:

- Solid-state sintering: the shaped green body is heated to a temperature that is typically 1/2 – 9/10 of the melting point. No liquid is present and atomic diffusion in the solid state produces joining of the particles and reduction of the porosity.
- Liquid-phase sintering: a small amount of liquid, typically less than a few volume percent of the original solid mixture, is formed at the sintering temperature. The liquid volume is not sufficient to fill the pore space so that additional processes are required to achieve full densification. Liquid-phase sintering is an important method for the industrial fabrication of several ceramics.
- Viscous sintering: most silica-containing ceramics, including traditional porcelains as well as advanced silicon nitride, sinter in the presence of viscous glass-type liquids, with predominant mass transport through viscous flow.

1.2.1 Main stages

Sintering phenomena can be divided into three stages:

Initial stage of sintering

As schematically represented in Figure 17, the first sintering step results in the densification of the powder compact up to about 10vol%. Specifically, if the relative green density of the original particle compact was 60%, after the initial stage this value could achieve at most about 70% of the theoretical density (TD). It should be noted that such modest densification in the initial stage is reached very quickly (seconds or minutes) after exposing powder to high temperature. This is because of the large surface area and the high driving force for sintering under such conditions.

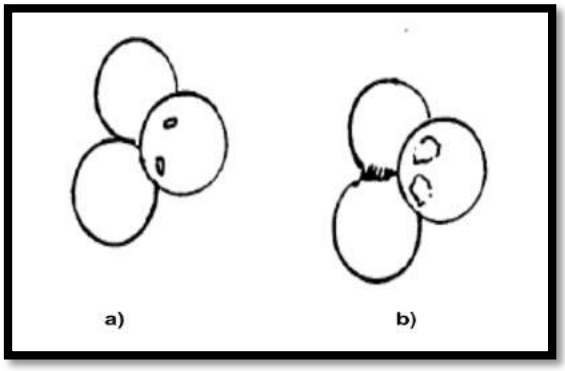

Figure 17. Local point of contact formation or ‘’fusion’’, without shrinkage of compact. This is accompanied by smoothing of the free surface of particles (a). Neck formation at the contact point (b)[31].

Intermediate stage of sintering

The sample shrinkage, i.e. the contraction of the compact normally referred a decrease in linear dimensions, obtained in the intermediate stage can result in the additional densification of at most 25%, equivalent to a compact density of about 95% of the TD value. During this stage the main feature taking place are: neck growth, pores forming arrays of interconnected cylindrical channels, particle centers approaching one another, with the resulting compact shrinkage (cf. Figure 18). However, shrinkage does not necessarily have to take place in a marked way during the intermediate stage of sintering. For example, shrinkage would occur at low level if matter is transported from the particle surface, and proceeds through either gas, solid or along interface as surface diffusion.

Final stage

The final sintering stage begins at about 93-95% of theoretical density, when porosity is already isolated. Ideally, at the end of this step all residual porosity is eliminated. However, the latter goal can be achieved in the final stage of sintering only when all pores are connected to fast, short diffusion paths along grain boundaries, (or, equivalently, if the grain boundaries remain attached to the pores).

In Figure 19 the final stage of sintering is schematically shown, where isolation of pores (a) and grain growth (b) are evidenced.

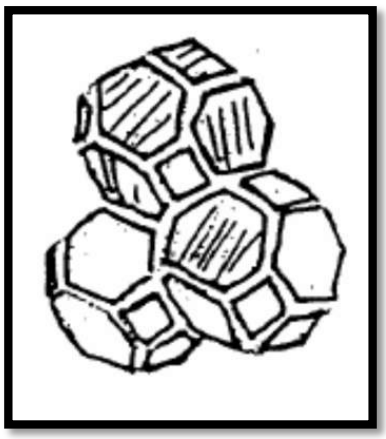

Figure 18. Intermediate stage of sintering[31].

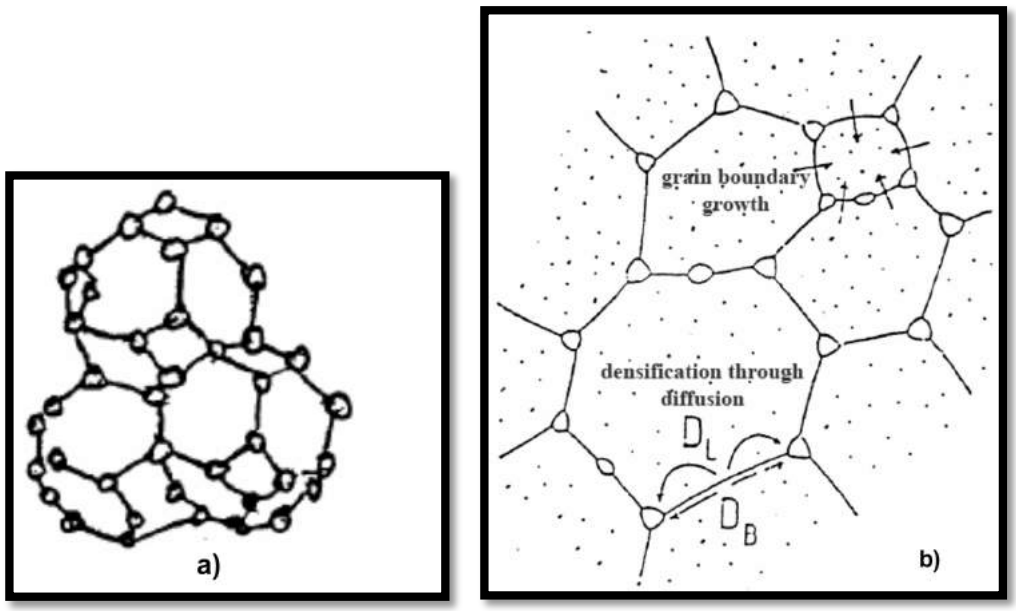

Figure 19. Final stage of sintering[31].

The graph plotted in Figure 20 summarizes how the relative density of the compact increases in each stage as a function of sintering time. As said before, initial stage is very quick with small increase of density, while intermediate and final stages take longer time to reach high consolidation levels, near to the theoretical value.

1.2.2 Techniques

The microstructure of bioceramics affects significantly their mechanical and biological properties which play an important role in biomedical applications. Such characteristics is strongly dependent on the used sintering techniques. The most frequently adopted conventional and innovative sintering methods will be described in the following sections.

1.2.2.1 Pressureless Sintering

Most sintering processes are performed by heating powders without the application of an external pressure, i.e. the so called pressureless sintering (PLS). This method is based on the preliminary pressing of powders in a mold to form a compact. Afterwards, the pressed powders are heat treated in a oven for their densification.

There are different heating schedules adopted in PLS:

- constant rate of heating (CRH): consisting of heating the green compact at a constant rate up to the sintering temperature;
- rate controlled sintering (RCS): non-linear and non-isothermal heating schedule. Specimens sintered under RCS conditions are generally characterized by finer grain sizes and pore-free structures;

- two step sintering (TSS): the sample is first heated to T_1, then cooled to T_2 and held at the latter temperature until densification is completed.

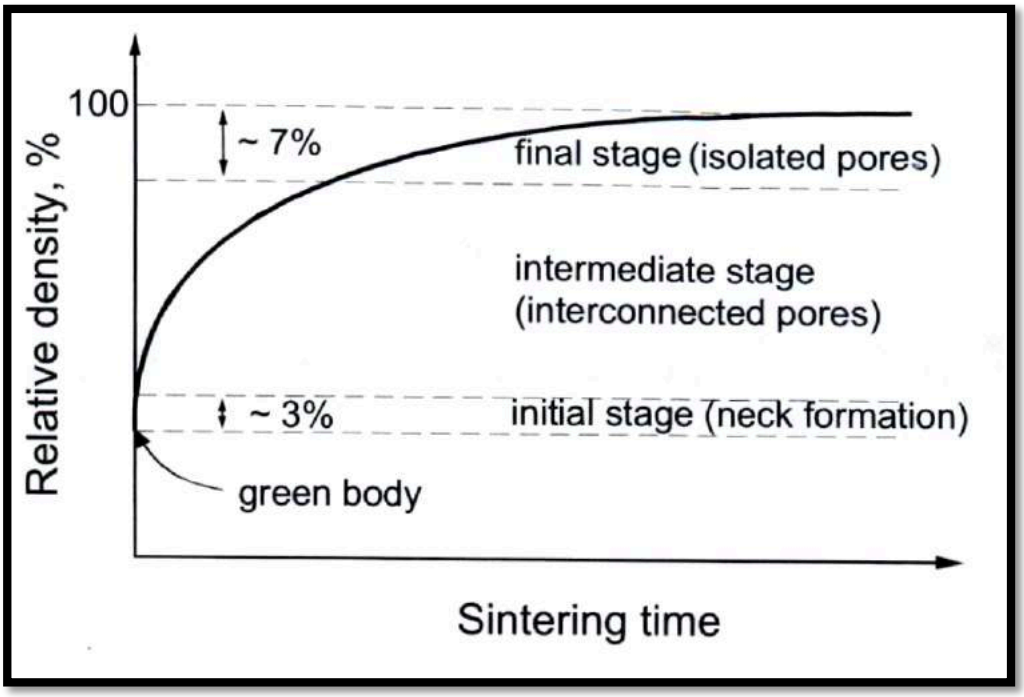

Figure 20. Influence of the sintering time on the relative density of powder compacts[32].

In general, high densification levels can be achieved with PLS only when the powders undergoing sintering are processed at high temperatures and long time intervals. Very often, the resulting samples are characterized by residual porosity.

1.2.2.2 Pressure-Assisted Sintering

The sintering process described previously can be promoted when powder heating is also assisted by the simultaneous application of a pressure. Indeed, pressure increases the driving force for densification, so that the temperature needed for sintering can be reduces to a level as low as half of

the melting point of the ceramic. Furthermore, shape forming and densification can often be accomplished in a single step. The two more often adopted pressure-assisted sintering methods are the so-called hot pressing (HP) and hot isostatic pressing (HIP), which will be briefly described in the following section.

Hot Pressing (HP)

Conventional HP makes use of external heating elements as an energy source (cf. Figure 21). At the same time, a mechanical load is applied along the axial direction. The material composing or lining the rams and die walls is extremely important, since it must not react with the ceramic being hot-pressed. Unfortunately, it is hard to process complex shapes by hot pressing. Moreover, the most relevant concern associated to this method is related to the rather slow heating rates which makes the processing times significantly long, on the order of hours. This feature corresponds, in turn, to a relatively high energy consumption, particularly for the case of ceramics when severe temperature conditions have to be achieved[32].

Hot Isostatic Pressing (HIP)

As shown in Figure 22, during HIP process the green compact is placed inside a closed chamber containing a high-pressure fluid (usually an inert gas) at elevated temperature. The compact must first be presintered to the closed porosity stage (no open, interconnected pores), or encapsulated with a viscous coating such as glass. During HIP under the action of the high-pressure fluid, residual gases enclosed within the sample bubble out and are eliminated. Preformed complex shapes such as turbine blades, rotors, and stators can be densified by HIP.

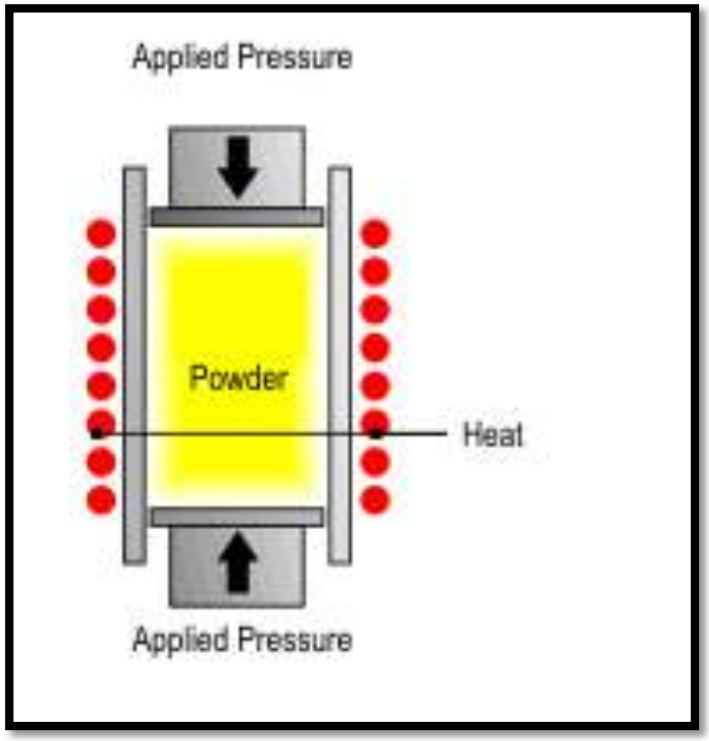

Figure 21. Classical Hot Pressing method[34].

1.2.2.3 Spark Plasma Sintering

In the precious sections, it as evidenced that one of the most relevant concerns associated to the utilization of conventional sintering methods is the use of external energy sources which make powders heating relatively slow. Consequently, the sintering conditions, temperature and processing time, required to reach adequate densification levels in ceramic bodies are generally very high. This fact also leads to an increase of the energy consumption and, consequently, production costs. Furthermore, the microstructure of the resulting products are typically quite coarse since grain growth is promoted by wither an increase in the sintering temperature or the processing time. To overcome such drawbacks, some innovative, more efficient, sintering methods are proposed in the last decades.

These include the Selective Laser Sintering (SLS), the Capacitor Discharge Sintering (CDS) and the Spark Plasma Sintering (SPS). The latter technique, which is adopted in the present thesis for the fabrication of various bioceramics, will be described in detail in the present Chapter.

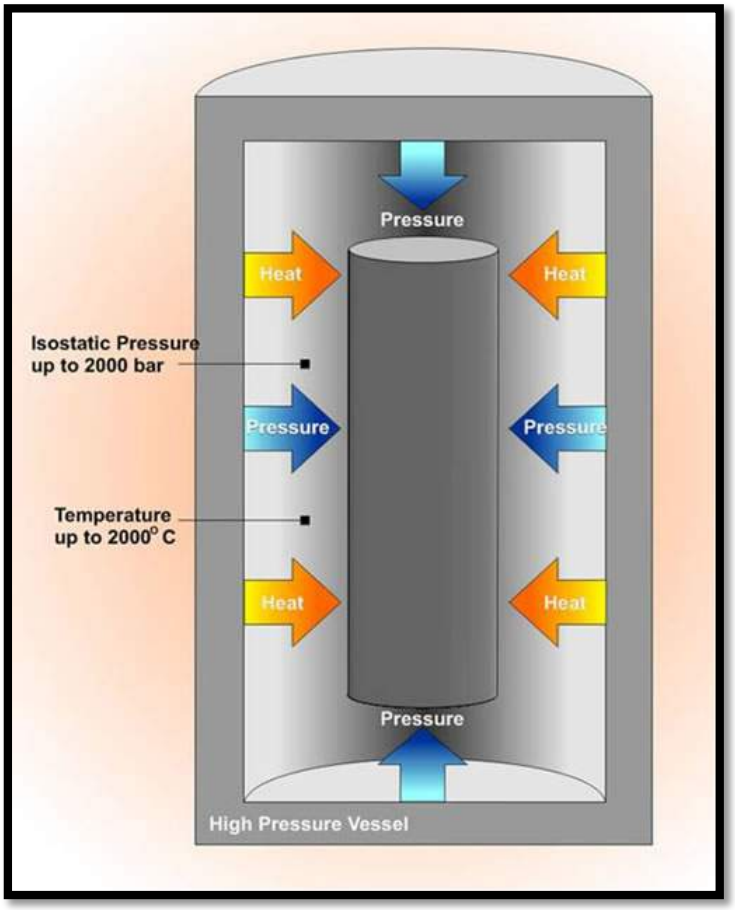

Figure 22. Schematic representation of the Hot Isostatic Pressing process[35].

SPS, also referred in the literature to as field assisted sintering (FAST) or pulsed electric current sintering (PECS), is a novel pressure assisted pulsed electric current sintering process utilizing ON-OFF DC pulse energizing[36].

Principle of SPS can be deduces from Figure 23. Powders are compacted into a graphite mold which is placed inside a vacuum chamber. The powders container is inserted in an electric circuit using suitable graphite plungers and spacers. During a SPS experiment, a pulsed current flows through powders (if conductive) and the die with subsequent heat generation via Joule effect. The Simultaneous application of this low-voltage high current power along with a mechanical axial load generally leads to high densification levels at lower temperatures and, above all, shorter times with respect to conventional PLS and HP methods. A wide variety of advanced monolithic and composite

materials have been produces so far using the SPS technology[36]. More recently, the latter technique has been exploited also for the fabrication of Functional Graded Material (FGM) [37].

The most important SPS parameters, i.e. temperature, current, voltage between the machine electrodes, mechanical load and vertical sample displacement, can be monitored and recorded in real time. In particular, the displacement output provides an indication of the evolution of the powders densification during SPS. However, the thermal expansion of sample, electrodes, graphite blocks, spacers and plungers is also responsible for the measured value[36].

As previously mentioned, high relative densities can be reached by SPS in very short time. This feature, along with the generally lower temperature required, is responsible for the relatively finer product microstructure. In particular, nano-sized powders can be sintered without considerable grain growth, which is not possible when considering conventional sintering process. Hence, high dense nano-structured ceramics or nano-composites with fewer defects can be successfully prepared by SPS. This holds true for all types of materials, even those difficult to densify. Moreover, to advantage of high heating rate and shorter holding time, SPS can significantly restrict the unwanted reactions in highly reactive systems, which may occur in conventional sintering, so that the formation of undesirable product phases can be avoided. It should be noted that the only phenomenon which is experimentally proved to be driven by the current flowing through the plunger/die/sample ensemble is Joule effect. Other phenomena, i.e. plasma formation, high localized temperature at the contact area between particles, enhanced diffusion of materials at forming particle necks, may also take place simultaneously. Nonetheless, they are not yet unequivocally demonstrated, probably because they are masked by the dominant Joule effect[36].

In the present thesis the SPS technology has been exploited for the fabrication of various monolithic and composite bioceramics to be subsequently characterized form the microstructural, mechanical and/or biological points of view.

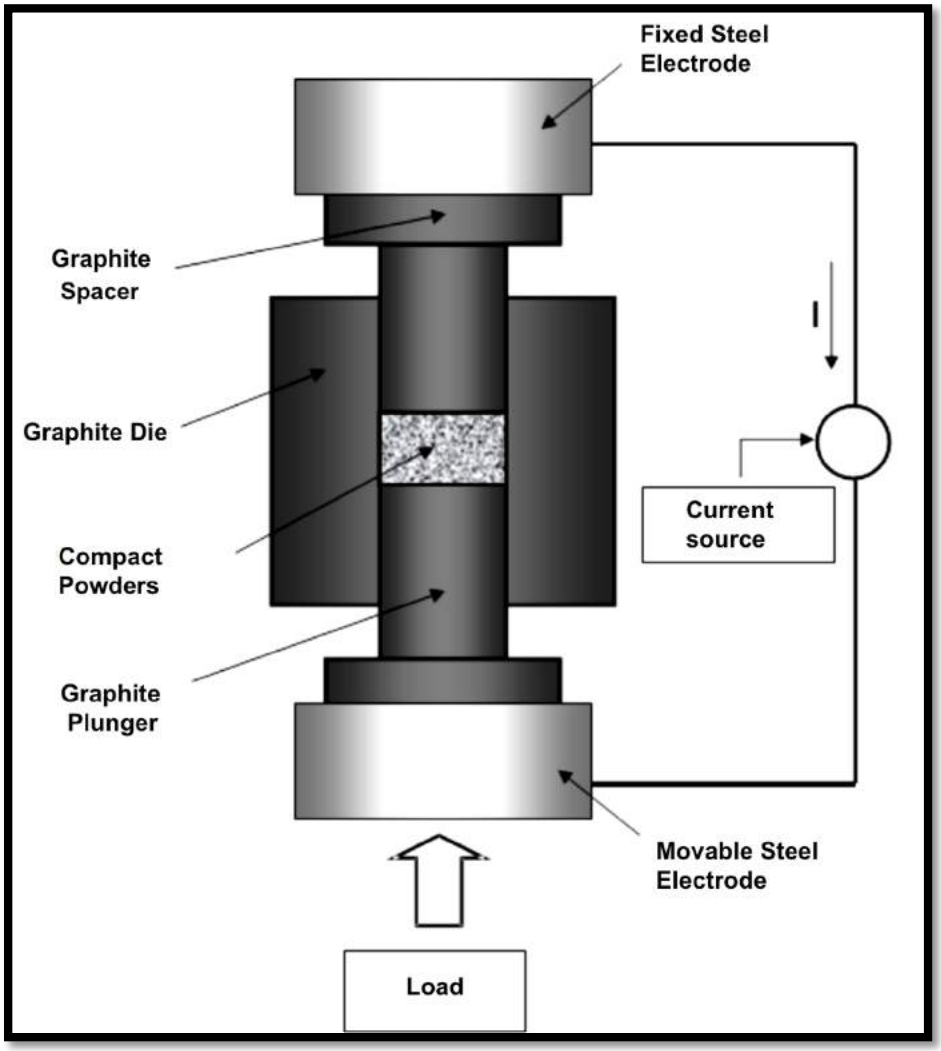

Figure 23. Principle of SPS technique.

In particular, the optimization of the SPS conditions for the obtainment of nearly full dense products when starting from conventional 45S5 and a recently developed CaO-rich bioglass powders is described in Chapter 2. Thus, the fabrication of three different dense glass-ceramic composite systems obtained via SPS by combining HA with the previously mentioned innovative bioglass is considered in Chapter 3. Finally, the preparation of three diverse calcium phosphate products in dense form is carried out by SPS for their subsequent characterization in-vitro using human cells.

Chapter 2

Conventional 45S5 and Novel CaO-rich Bioactive Glasses

2.1 Introduction

As mentioned in Chapter 1, thanks to the favorable response displayed during their interaction with biological tissues, bioglass materials have become one of the most important and investigated classes of ceramics for biomedical application[18,27]. In particular, as a consequence of the several chemico-physical phenomena involved at the glass-physiological fluids interface, a bone-like hydroxycarbonate apatite (HCA) layer is formed on the biomaterial surface, so that a strong bond between the latter one and the surrounding tissues can be established[26].

It is well known that mechanical and biological properties of bioactive glasses are significantly affected by the relative amounts of the different oxide constituents as well as the sintering conditions adopted to consolidate the initial amorphous powders. One of the most important aspects to consider in this regard is represented by the tendency of the material to crystallize during heat treatments, as the extensive crystallization of the bioglass negatively influences its bioactivity properties. In particular, as reported and discussed in the previous chapter (cf. Figure 15), the onset time for the formation of the HCA layer during glass exposure to a simulated body fluid (SBF) solution is delayed by crystallization[26,38]. On the other hand, the partial crystallization of glass-ceramics is often beneficial in terms of mechanical properties with respect to the completely amorphous product.

Therefore, the crystallization degree has to be properly controlled to guarantee adequate biological and mechanical characteristics in the bulk material.

The classical 45S5 Bioglass® originally developed by Hench, exhibits a rapid tendency to crystallize at temperature values in the range 550-650°C (cf. Figure 14). Thus, when corresponding powders are exposed to the thermal levels required by pressureless sintering to obtain bulk materials, fully crystallized ceramics or glass-ceramic composites are produced[39,40]. In contrast, highly porous samples characterized by poor mechanical properties are obtained when operating below the crystallization temperature.

Based on the consideration above, several efforts have been recently made to identify more efficient powder densification techniques and/or different bioactive glass formulations which display reduced tendency to crystallize with respect to 45S5 Bioglass®.

As far as the first issue is concerned, the SPS technique, has already demonstrated to provide an efficient consolidation method for ceramic powders[36]. In particular, due to the relatively milder temperature/time conditions generally required during SPS, with respect to the low heating rates established in conventional sintering methods, crystallization phenomena in bioglass powders undergoing consolidation might be suppressed or mitigated. This fact is confirmed by the various studies conducted so far relative to 45S5 Bioglass® powders processed by SPS either singularly[41-43] or in combination with other phases[43-45].

As pointed out above, the crystallization of bioglass depends on the relative amounts of oxide constituents. For instance, the onset of crystallization is known to take place at significantly higher temperature levels as the amount of CaO in the bioglass is increased at the expenses of Na_2O[46].

Along these lines, new compositions with relatively higher CaO/Na_2O ratio with respect to 45S5 Bioglass® were recently developed[47,48]. Furthermore, the introduction of suitable amounts of K_2O in these CaO rich bioglass materials was also examined[21,48]. It was found that the amorphous nature

in the latter systems is preserved when the starting powders are processed at 800°C for 3h by pressureless sintering.

The aim of this part of the thesis is to compare the densification and crystallization behavior during spark plasma sintering of commercial 45S5 Bioglass® and lab made CaO-rich, K_2O containing, bioactive powders. Specifically, the starting materials are both characterized by laser scattering, X-ray diffraction, SEM, and TGA/DTA analyses. Afterwards, a systematic study is conducted to find the optimal dwell temperature, holding time and applied pressure to obtain fully dense products by SPS. Furthermore, the sintering conditions corresponding to the incipient crystallization of both bioglass systems are identified. The obtained amorphous and crystallized dense products are finally compared from the mechanical point of view.

It should be noted that the choice to focus our attention on the fabrication of dense samples, instead of porous bodies that are more frequently utilized for biomedical applications, is because the effect of crystallization on mechanical properties is significantly facilitated and the obtained results can be interpreted and compared more easily. This fact holds also true when the biological response of such materials will be investigated.

Thus, the final aim of this investigation is to provide useful preliminary insights in view of developing porous architectures from standard or novel bioglass and bioglass-ceramics able to exhibit the best combination of mechanical and biological properties.

2.2 Experimental

The designation and the chemical composition of the two types of bioglass powders considered in this Chapter are reported in Table 3.

Bioglass type	Na_2O	K_2O	CaO	P_2O_5	SiO_2
BG_45S5[Hench, 1991]	24.4	-	26.9	2.6	46.1
BG_Ca/Mix[Bellucci et al., 2012]	2.3	2.3	45.6	2.6	47.2

Table 3. Composition (oxide mol%) of bioglass powders used in the present investigation

Bioglass® 45S5 Glass Spheres (Cod. GL0160P) were provided by Mo-Sci Corp. (USA) whereas the preparation of CaO-rich bioactive powders was made at the Dipartimento di Ingegneria "Enzo Ferrari", Università degli studi di Modena e Reggio Emilia (Italy) [21] .From the compositional point of view, the main difference between the two bioglass powders relates to the CaO/Na_2O molar ratio, which is equal to about 1 (1.1) and about 20 (19.8) for the classical and innovative bioglass, respectively. In addition, the latter one also contains about 2.3 mol.% of K_2O. For the sake of brevity, the two bioglass systems will be heretoafter referred to as BG_45S5 and BG_Ca/Mix, respectively.

A detailed particle size analysis of the two powders was performed taking advantage of the laser light scattering analyser (CILAS 1180, France) shown in Figure 24. The raw and thermally treated powders were characterized by XRD analysis using a Philips PW 1830 X-rays diffractometer reported in Figure 25 equipped with a Ni filtered Cu Kα radiation (λ=1.5405 Å). Powders morphology was examined by high resolution scanning electron microscopy (HRSEM, mod. S4000, Hitachi, Japan) using the equipment reported in Figure 26. The thermal stability of the bioglass powders was studied by simultaneous thermogravimetric analysis-differential thermal analysis (TGA/DTA). The initial powders have been heated at different rates, in the range 5-50 °C/min, from room temperature to 1000°C using a **NETZSCH STA 409PC** Simultaneous DTA-TGA Instrument (cf. Figure 27) under 100 mL/min air flow.

Figure 24. Particle size analyzer (mod. Cilas 1180).

Figure 25. X-Ray Diffractometer (mod. Philips PW 1830).

Figure 26. High resolution Scanning electron microscopy equipment (mod. Hitachi S4000).

Figure 27. Simultaneous TGA/DTA Analyzer (mod. NETZSCH STA 409PC).

Bioglass powders were sintered in the form of cylindrical disks (about 15 mm diameter, 3 mm thickness) using the Spark Plasma Sintering machine (SPS 515S model, Sumitomo Coal Mining Co Ltd) shown in Figure 28 under vacuum conditions (20 Pa).This apparatus is based on the combination of a uniaxial press (50 kN) with a DC pulsed current generator (10 V, 1500 A, 300 Hz), to provide simultaneously a pulsed electric current through the graphite die containing the nonconductive bioglass powders, along with a mechanical pressure through the punches. A sequence of 12 ON pulses followed by 2 OFF pulses is adopted, being the characteristic time of single pulse equal to about 3.3 ms.

Figure 28. Spark Plasma Sintering apparatus (mod. 515S) used in this work.

The die and the plungers shown in Figure 29 (a) and (b), respectively, were both made of AT101 graphite (Atal s.r.l., Italy). The powders to be sintered (1.35-1.40 g) were poured inside a cylindrical die with outside diameter of 35 mm, inside diameter of 15 mm, and 30 mm high. To protect the die/plungers and make sample release easier after sintering, the compact was lined with a 0.13 thick

graphite foil (cf. Figure 29 (c)) (Alfa Aesar Karlsruhe, Germany). In addition, the die was covered with a layer of graphite felt (3 mm thick, Atal s.r.l., Italy) for thermal insulation purpose (cf. Figure 29 (d)).

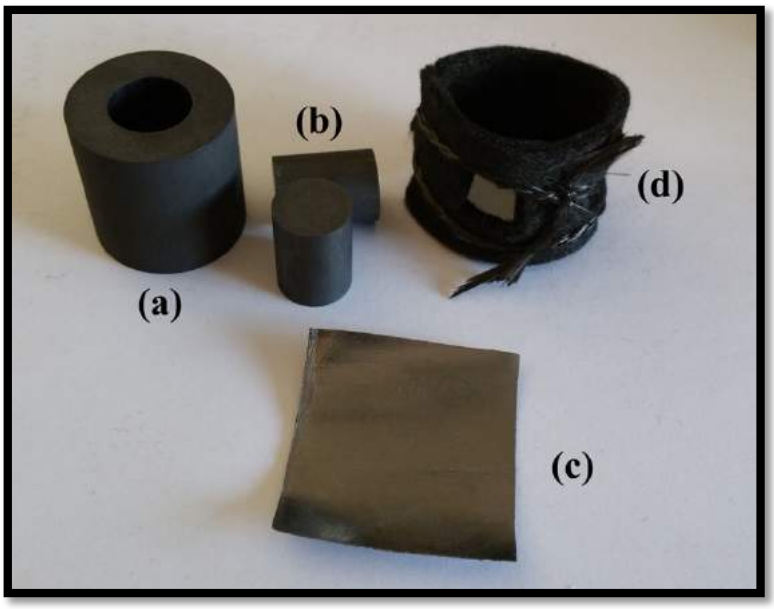

Figure 29. Graphite die (a), plungers (b), foil (c) and felt (d). Used for SPS experiments.

The most important SPS parameters, i.e. temperature, current, voltage between the machine electrodes, applied load, vertical sample displacement and displacement-rate, were recorded in real time. The thermal expansion of electrodes, graphite blocks, spacers and plungers have to be subtracted from the displacement output to determine the evolution of the powders densification during SPS[49]. The sample shrinkage (S), is correspondingly obtained. In any case, the final consolidation level is determined by measuring the density of the samples obtained at the end of the sintering process.

SPS experiments were conducted under temperature controlled mode using a K-type thermocouple (Omega Engineering Inc., USA) inserted inside a small hole drilled near the centre of the external surface of the graphite die. The effect of the dwell temperature (T_D), holding time (t_D) and mechanical

pressure (P) on the product density was investigated. A two-step heating rate was adopted. Firstly, the temperature of the sample was increased from the room value at 50°C/min. Afterwards, when the temperature of the sample achieved 100°C below the T_D value, the heating rate was lowered to 10°C/min. After exposure for the prescribed holding time at the T_D level, the sample was cooled to 300°C at 50°C/min under a mechanical load of about 16 MPa. Afterwards, the current was turned off, the sintered specimen allowed to cool to room temperature and then removed from the die. For the sake of reproducibility, each experiment was repeated at least twice.

The microstructure of the sintered specimens was analyzed by SEM. In particular, the SPS products were first mirror polished and then chemically etched for 30 s using a 1 vol.% HF solution.

The selected samples were also investigated from the mechanical point of view at the Dipartimento di Ingegneria "Enzo Ferrari", Università degli studi di Modena e Reggio Emilia (Italy). Specifically, in order to determine the local elastic modulus as well as the micro-hardness of the SPS products, a depth-sensing micro-indentation technique was applied, working with an Open-Platform instrument (CSM Instruments, Peseux, Switzerland), equipped with a Vickers indenter tip. For each indentation, the applied load and the corresponding penetration depth were recorded and the elastic modulus was deduced from the unloading part of the load–depth curve by means of the Oliver-Pharr method[50]. For each glass sample, at least ten indentations were performed using standard parameters, i.e. maximum applied load of 1 N; loading/unloading rate equal to 1.5 N/min, and loading time at maximum applied load of 15 s.

2.3 Results and discussion

2.3.1 Powders Characterization

Laser light scattering and SEM analyses evidenced that, beside their composition, the initial powders also differ in terms of particle size. In particular, the results related to the powders' granulometry

reported in Table 4 indicate that BG_45S5 displays relatively finer particles, with an average size below 5 μm, whereas the CaO-rich product is characterized by powders about 20 μm sized (average value).

This measurement is in agreement with SEM observations (cf. Figure 30).

System ID	d_{10}	d_{50}	d_{90}	Average size
BG_45S5	0.70±0.04	2.28±0.18	12.34±1.02	4.51±0.33
BG_Ca/Mix	1.50±0.04	15.03±1.26	45.58±2.89	19.88±1.41

Table 4. Particle size characteristics (μm) of starting powders as determined by laser light scattering analysis.

Indeed, Figure 30(a) shows that BG_45S5 is mostly made of 1-2 μm sized particles, although a small amount of sub-micrometer grains is also found. In contrast, the BG_Ca/Mix material is significantly coarser (cf. Figure 30(b)), consisting of particles generally larger than 5 μm, albeit a minor fraction of finer powders is also present.

The XRD patterns of the two bioglass powders are reported in Figure 31. This analysis confirms the amorphous nature of both materials.

The thermal stability and crystallization features of the initial powders were first evaluated by performing TGA/DTA tests in air flow up to 1000°C. The corresponding curves obtained for the case of the BG_45S5 product at 5, 30 and 50°C/min heating rates are plotted in Figure 32(a) as a function of the temperature.

As far as the DTA curves are concerned, it is observed that the characteristic endothermic peak corresponding to the glass transition at about 550°C is better evidenced when the test is conducted at

relatively higher heating rates. This finding is in agreement with other studies reported in the literature[40]. The related compositional changes are correspondingly monitored by XRD and the obtained results are shown in Figure 32(b) for the case of the test conducted at 30°C/min.

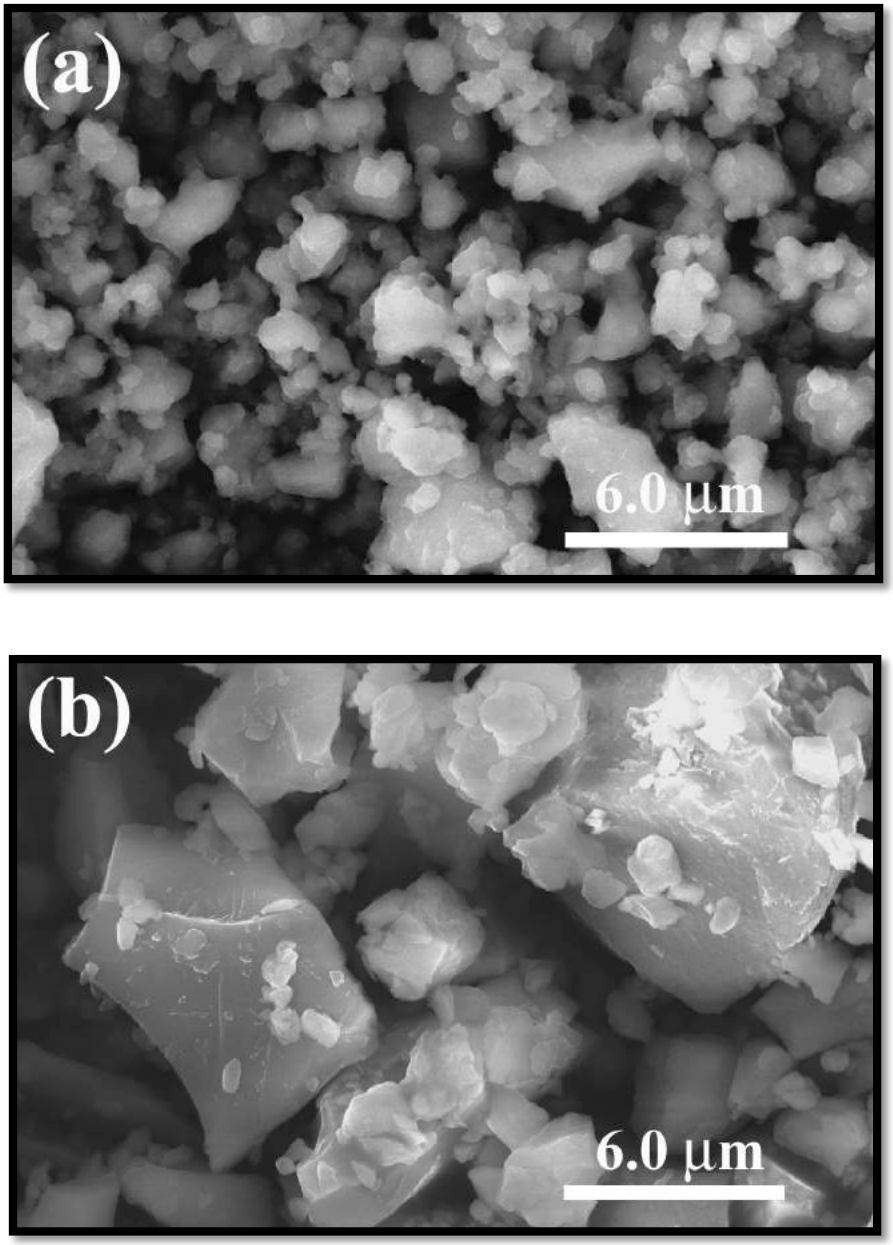

Figure 30. SEM images of the initial bioglass powders investigated in the present work: (a) BG_45S5 and (b) BG_Ca/Mix.

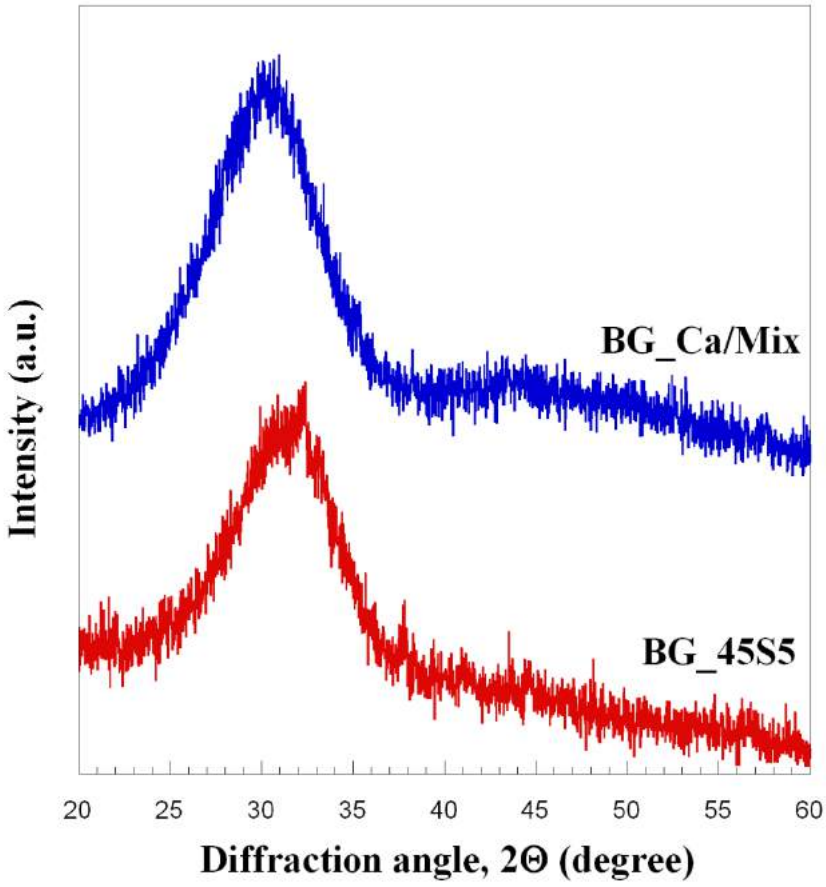

Figure 31. XRD patterns on the initial powders investigated in this part of the thesis.

Analogous results are obtained when operating at different heating rates. The XRD analysis of powders corresponding to the thermal analysis interrupted at 550°C (endothermic peak) did not evidence the formation of crystalline phases. On the other hand, when the temperature level was increased slightly above (about 620 °C), and a broad exothermic peak starts to appear in the DTA curve, a crystalline phase, namely $Na_6Ca_3Si_6O_{18}$ (or $Na_2CaSi_2O_6$), was detected by XRD. The formation of $Na_2CaSi_2O_6$ as a result of the crystallization of 45S5 bioglass is consistent with similar studies addressed in the literature[27,28,42].

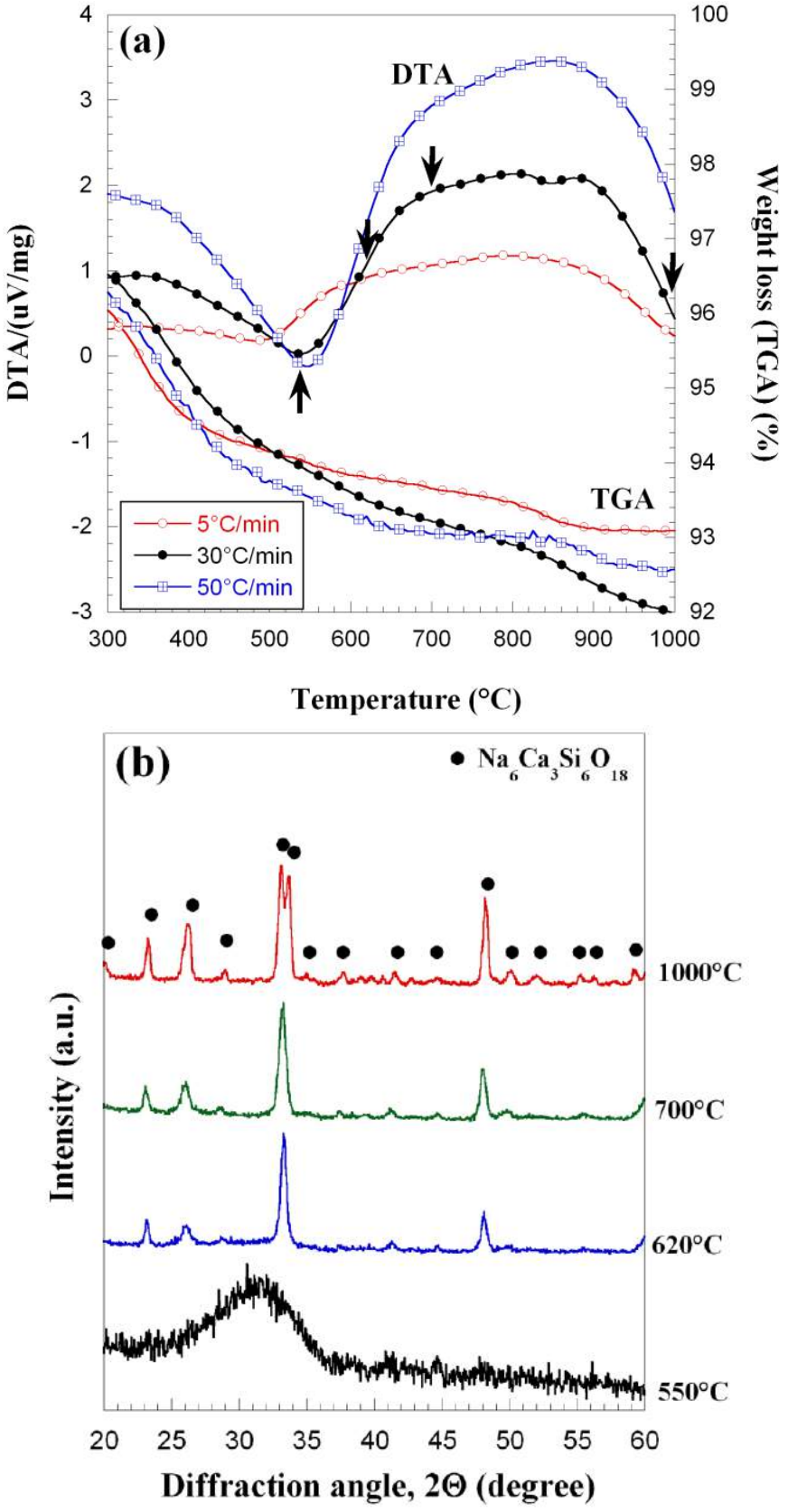

Figure 32. Results of the differential thermal analysis of BG_45S5 powders in air (100 ml/min): (a) TGA/DTA curves at different heating rates and (b) compositional changes (30°C/min).

However, other sodium calcium silicates such as $Na_2Ca_2Si_3O_9$[26,41,51] or $Na_2CaSi_3O_8$[43], are also reported as possible crystalline phases deriving from the devitrification of BG_45S5. Such discrepancies can be due to several factors, in particular the characteristics of the raw powders (particle size, preparation method) and the heating conditions adopted[42]. Figure 32(b) also indicates that no additional phases are formed when the temperature during TGA is further augmented up to 1000°C.

The only change observed is related to the decrease of the diffraction peaks' width and their increased intensity. The latter feature can be readily ascribed to the crystallite growth taking place when the BG_45S5 material experiences higher temperature levels.

Figure 32(a) shows also a marked decrease of the TGA curves as a manifestation of the significant mass reduction (up to about 8%) of this bioglass during thermal analysis. This phenomenon is mainly confined to low temperature levels, i.e. before crystallization takes place (Figure 32(b)), and can be likely ascribed to the evaporation of free water and loss of OH groups[27]

As shown in Figures 33(a)-33(b), a markedly different behavior is displayed by the CaO-rich bioglass during TGA. Firstly, only minor changes in the mass of the sample (< 1%) are observed during the heating process up to 1000°C. In addition, the amorphous nature of the material is preserved for temperature higher than 800°C. On the other hand, the XRD analysis evidenced the formation of crystalline phases in powders exposed to 900°C, with the detection of $CaSiO_3$ in both the α- (pseudo-wollastonite, high-temperature phase) and β- (crystalline wollastonite, low-temperature phase) forms. In addition, it was found that a further temperature increase to 1000°C during TGA determined the transformation of the α- to the β- $CaSiO_3$.

DTA curves reported in Figure 33(a) clearly indicate that the position of the exothermic peaks is shifted towards higher temperatures, as BG_Ca/Mix powders are heated faster. This finding is well known in the literature and can be exploited to estimate the activation energy of the crystallization process. In particular, following the Kissinger theory[52], the temperature T_p corresponding to the

exothermic peak in the DTA curve depends on the heating rate ***r*** according to the following expression:

$$\ln\left(\frac{r}{T_p^2}\right) = -\frac{E_c}{RT_p} + C \qquad (1)$$

where R is the universal gas constant and E_c is the effective activation energy of the crystallization process. Hence, by plotting $\ln\left(\frac{r}{T_p^2}\right)$ as a function of $\frac{1}{T_p}$ a straight line is expected. This fact is undoubtedly confirmed by the Kissinger plot shown in Figure 34 where the data obtained at heating rates in the range 5-50 °C/min are reported. From the adopted fitting procedure, a value of about 520.8 kJ/mol is estimated for E_c. It should be noted that the latter value is significantly higher with respect to those ones calculated for other bioglass products, including BG_45S5 (230-338 kJ/mol), following the Kissinger approach[52]. This provides a further proof of the relatively reduced tendency to crystallize of BG_Ca/Mix bioglass.

2.3.2 Sintering of bioglass powders

Examples of the temperature cycles imposed during Spark Plasma Sintering of BG_45S5 and BG_Ca/Mix powders are reported in Figures 35 along with the corresponding sample shrinkage (S) and shrinkage rate (SR) time profiles. Specifically, these data refer to the T_D values of 550 °C and 720°C, for the cases of BG_45S5 and BG_Ca/Mix, respectively. The motivation for lowering the heating rate when the thermal level approaches the final T_D value was to attenuate the typical temperature overshooting with respect to the set-point value. Indeed, this fact could induce the occurrence of crystallization phenomena.

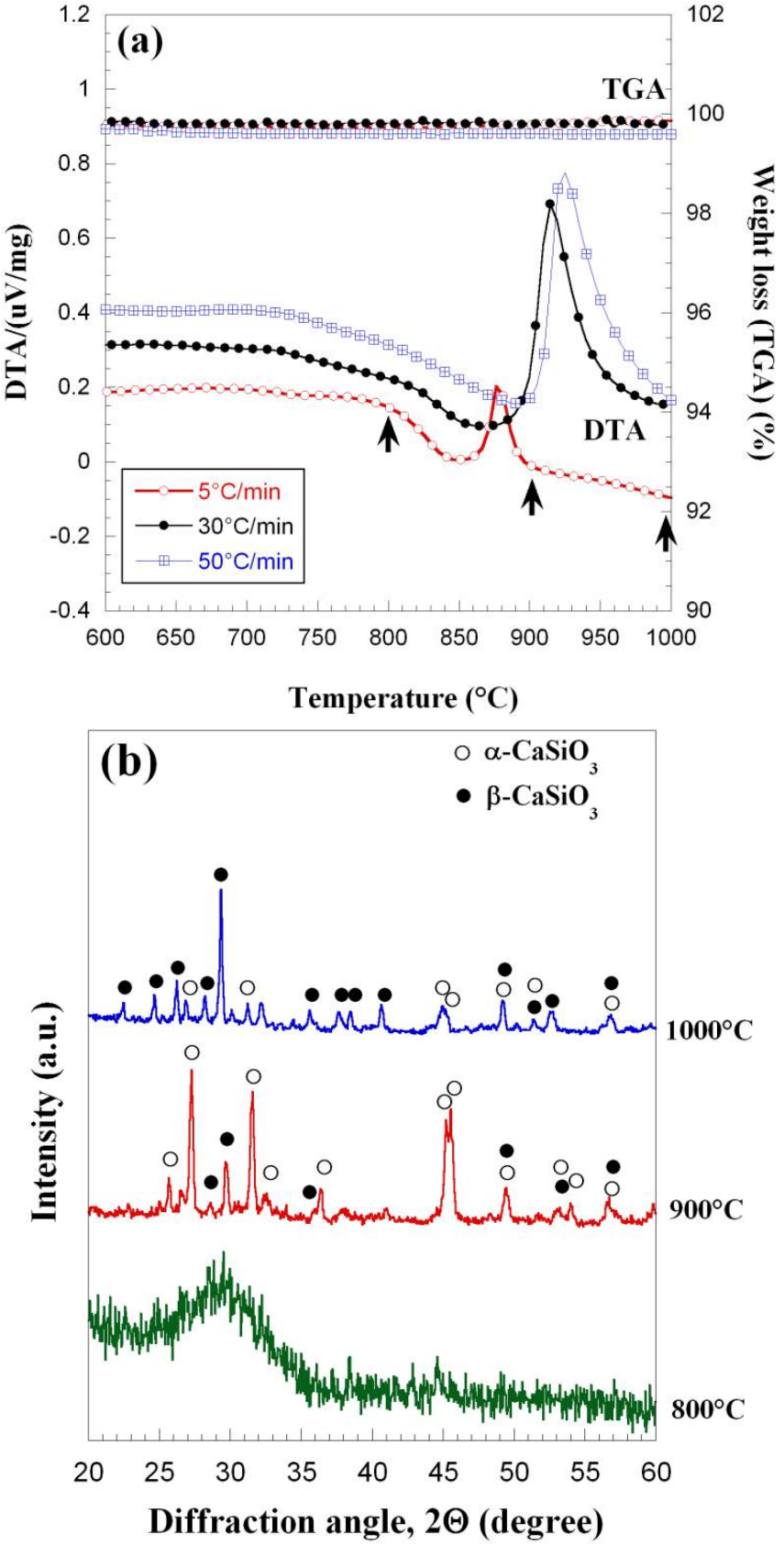

Figure 33. Results of the differential thermal analysis of BG_Ca/Mix powders in air (100 ml/min): (a) TGA/DTA curves at different heating rates and (b) compositional changes (5°C/min).

As far as the BG_45S5 system is concerned (Figure 35(a)), it is seen that powder densification starts to take place immediately after the application of the electric current, i.e. at relatively low temperature levels. However, the shrinkage rate rapidly increases at approximately 500°C to reach its maximum value at about 540 °C. A sample shrinkage level of about 1.6 mm is finally obtained when the dwell temperature is achieved.

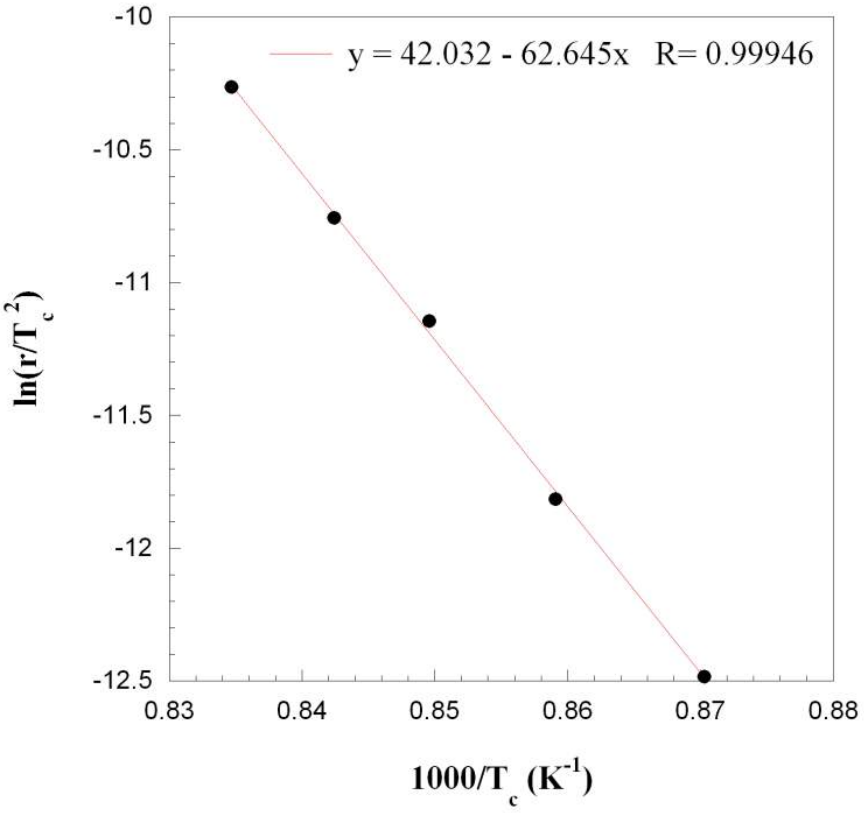

Figure 34. Kissinger plot for the BG_Ca/Mix powders based on DTA tests conducted in air at various heating rates.

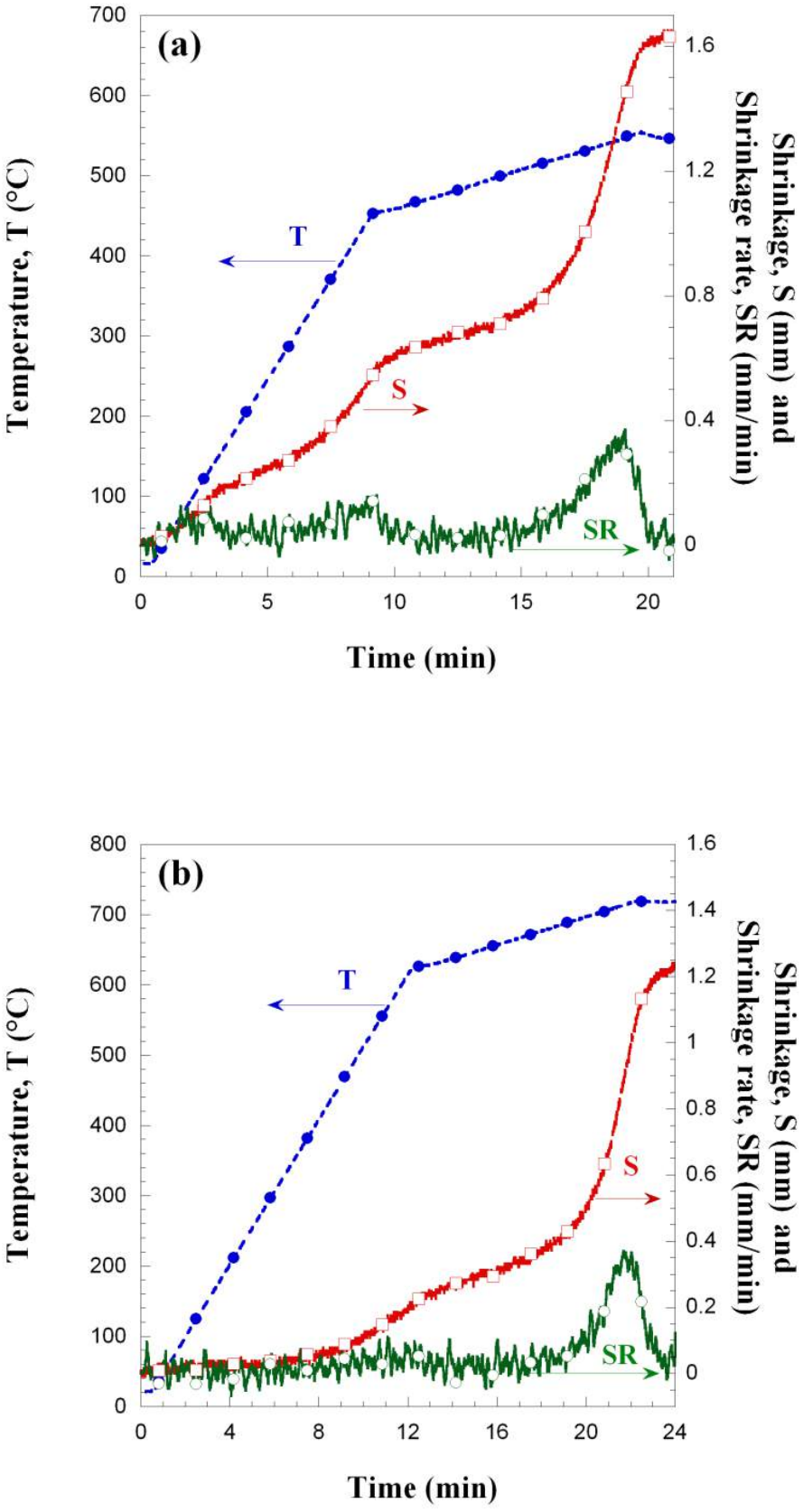

Figure 35. Temporal evolution of temperature, sample shrinkage and shrinkage rate during consolidation by SPS of (a) BG_45S5 (T_D = 550°C) and(b)BG_Ca/Mix (T_D = 720°C) powders.

In contrast, Figure 35(b) clearly indicates that the BG_Ca/Mix powders required markedly higher thermal levels to consolidate. Indeed, the related shrinkage value displays only negligible changes for temperatures below 450°C, i.e. during the first 8 min of the SPS process. Then, powders start to consolidate slowly while, for temperatures of about 680°C, the shrinkage rate increases significantly until a maximum value at about 720°C is achieved. The shrinkage value finally reached was approximately 1.2 mm.

The effect of the holding temperature on the density and XRD patterns of SPSed products is shown in Figure 36(a)-(b) for the 45S5 system. All the reported data refer to sintering experiments conducted at 70 MPa and t_D=2 min.

Figure 36(a) shows that the sample densification was progressively improved as the sintering temperature was augmented. The theoretical density value was achieved at 550°C. Only a slight density decrease resulted when the temperature level was further increase to 600°C. The corresponding structural changes were first monitored by XRD (Figure 36(b)). The incipient formation of the first crystalline phase, $Na_6Ca_3Si_6O_{18}$, was clearly evidenced in BG_45S5 samples sintered at 525°C. However, the glassy nature in the SPS material is apparently predominant up to 550°C. On the other hand, the typical broad amorphous band in the XRD pattern tends to vanish when the T_D value is increased to 600°C. The temperature levels needed to induce crystallization phenomena in the BG_45S5 powders undergoing SPS are quite consistent with the TGA results described previously (Figure 32).

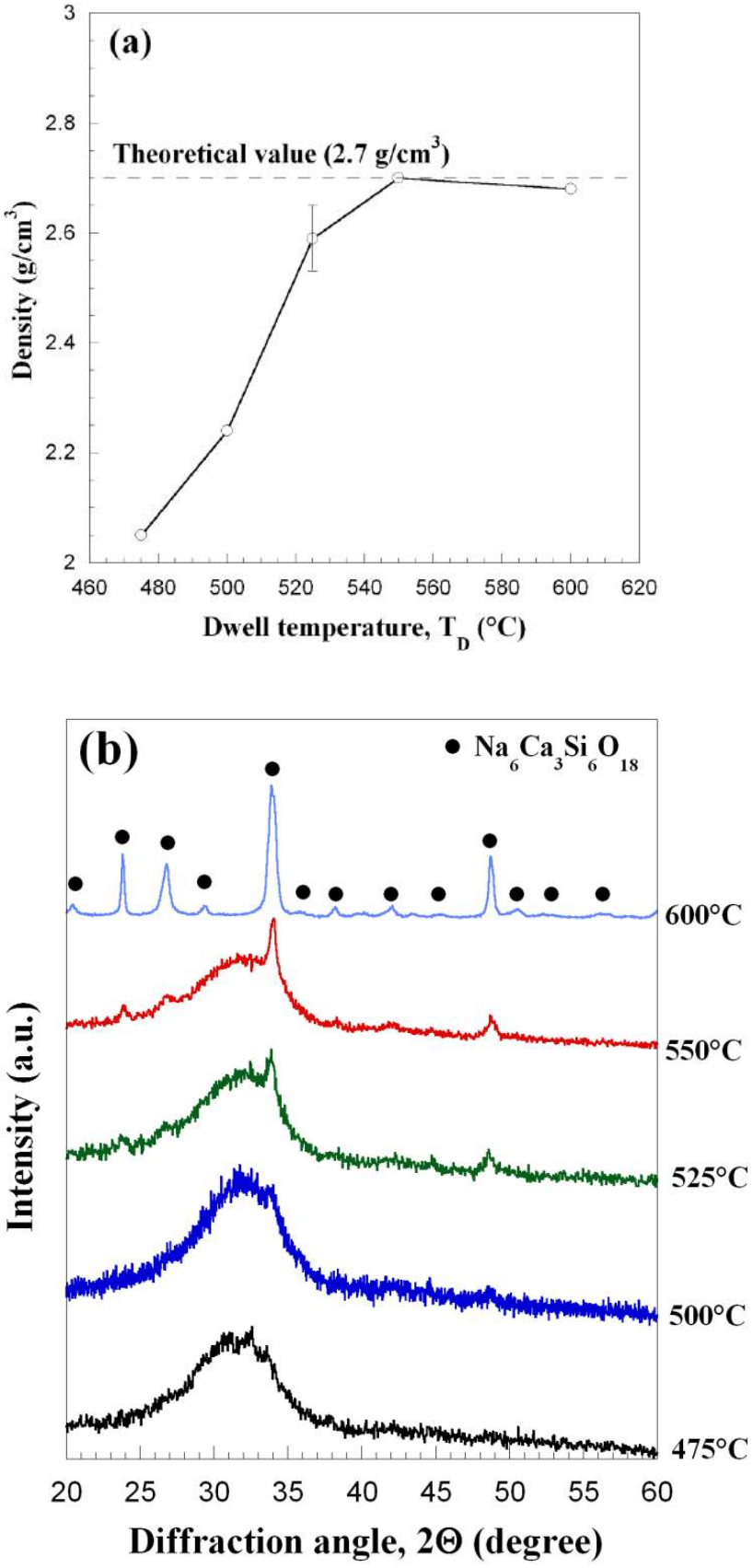

Figure 36. Influence of the (a) sintering temperature on the density of the BG_45S5 products obtained by SPS (t_D=2 min, P=70 MPa) and (b) related XRD patterns.

The fact that, in contrast with the SPS samples, no crystalline phases were detected in the XRD pattern of the TGA sample processed at 550°C might be ascribed to the unavoidable difference in the temperature measurements adopted during the heat treatments performed. Indeed, since during SPS the thermocouple is inserted in a small hole of the graphite die, as it cannot be directly embedded into the processing powders, the recorded temperature value underestimates the actual level reached inside the compact.

Furthermore, the results obtained in the present investigation, i.e. the temperature at which the BG_45S5 bioglass crystallizes during SPS as well as the composition of the resulting crystalline phase, are also well in agreement with those ones reported in a recent paper addressed to a similar subject[42].

Structural changes of the obtained BG_45S5 products can be also deduced by the SEM micrographs shown in Figure 37(a)-(b), corresponding to chemically etched products obtained by SPS at two different temperatures. Specifically, grains of $Na_6Ca_3Si_6O_{18}$ down to 100 nm sized are already formed in samples processed at 525°C. As the temperature is increased to 600°C, these grains tend to agglomerate, become coarser and replace the amorphous matrix.

The dependence of sample density and crystallization evolution on the dwell time is also investigated for the BG_45S5 bioglass. In particular, the obtained density data and the XRD patterns of the corresponding products are reported in Figure 38(a)-(b) for the case T_D= 550°C. It is observed that the decrease of t_D from 2 to 1 min or shorter times leads to less crystallized samples, but residual porosity remains significantly high.

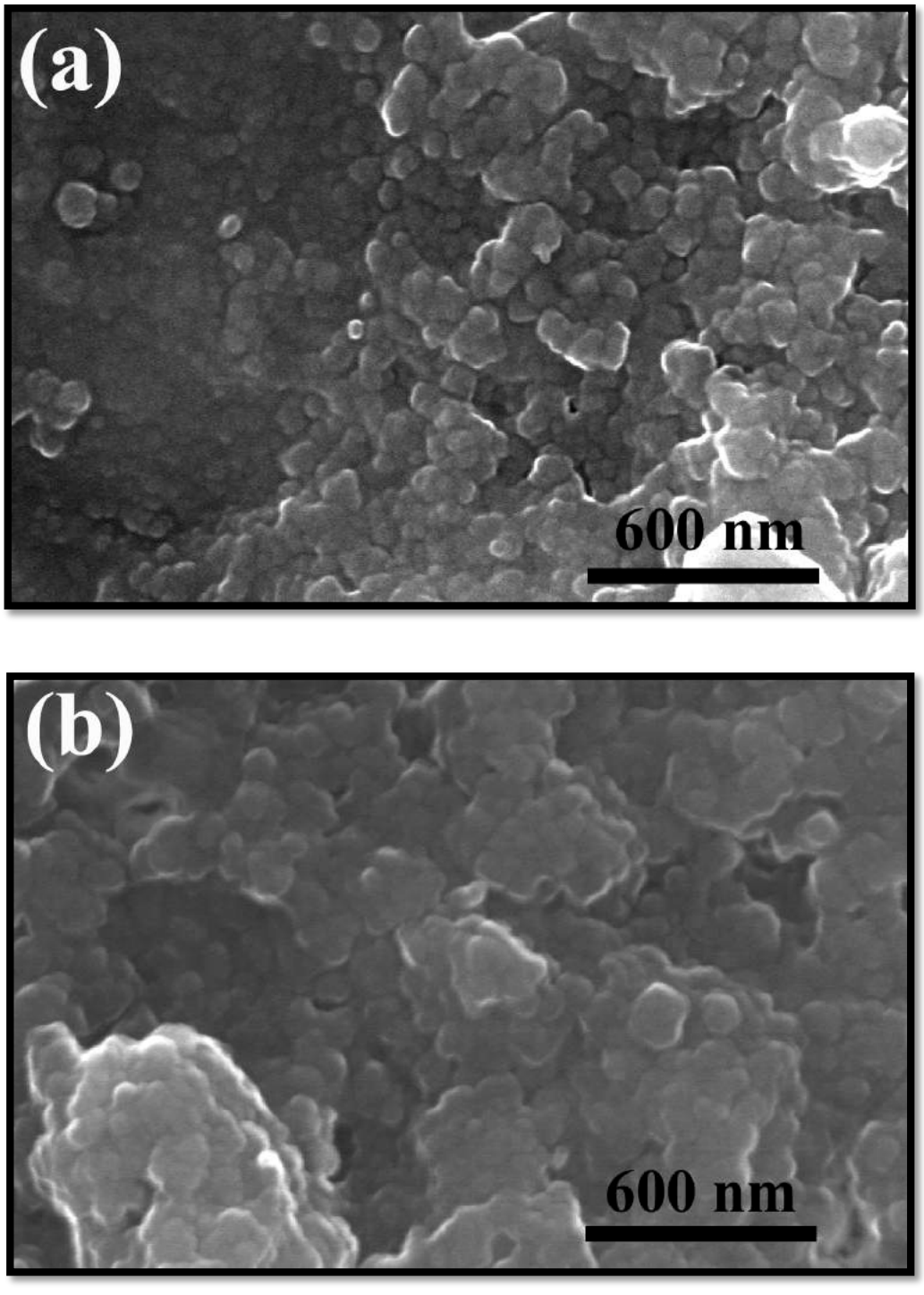

Figure 37. SEM images of chemically etched bulk BG_45S5 products obtained by SPS at different sintering temperatures: (a) 525°C and (b) 600°C.

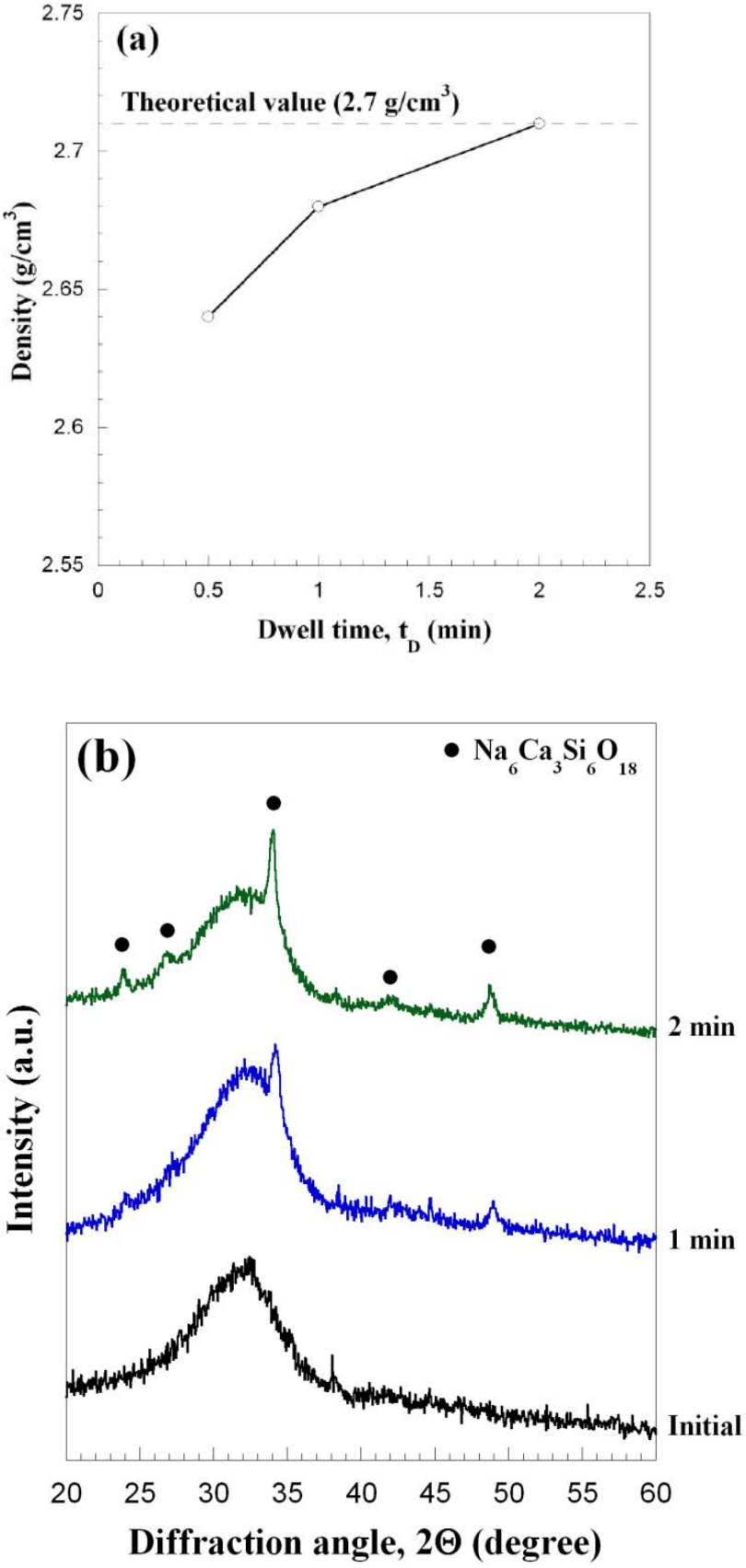

Figure 38. Influence of the (a) sintering time on the density of the BG_45S5 products obtained by SPS (T_D=550°C, P=70 MPa) and (b) related XRD patterns.

For the value of comparison, the effect of the holding temperature on product density and crystallization progress was also systematically investigated for the case of the CaO-rich bioglass powders. The obtained results are shown in Figure 39(a)-(b) for different mechanical pressure levels. In agreement with the indication provided by SPS outputs shown in Figure 35, it is confirmed that relatively higher sintering temperatures are required to densify the BG_Ca/Mix powders with respect to the BG_45S5 system. In particular, the optimal temperature to obtain a completely full dense product is in the range 720-730°C. Correspondingly, no crystalline phases are evidenced by the XRD analysis of the obtained sintered material (Figure 39(b)). Thus, the BG_Ca/Mix system confirms a relatively lower propensity to crystallize with respect to BG_45S5.

In order to identify the SPS conditions required to induce crystallization in BG_Ca/Mix, the dwell temperature was further increased. However, when the consolidation process was conducted under pressure levels equal or higher than 30 MPa, the graphite die broke during the sintering process. This is likely caused by the stresses the sample/die ensemble is subjected to, when in presence of relatively high mechanical loads, the glass transition temperature conditions are approached during sintering. To avoid the latter drawback, the mechanical pressure applied for higher temperature levels was thus lowered down to 16 MPa. As reported in Figure 39(a), the complete densification was correspondingly obtained when the dwell temperature is equal or above 730°C. Furthermore, Figure 39(b) indicates that no traces of crystalline phases can be detected by XRD up to T_D= 800°C. A diverse situation was encountered when the dwell temperature was further augmented to 830°C. Indeed, under the latter condition, the presence of α-$CaSiO_3$ was detected along with the incipient formation of the β-phase. Nevertheless, the broad halo in the XRD pattern of the resulting material indicates that the amorphous character was still preserved.

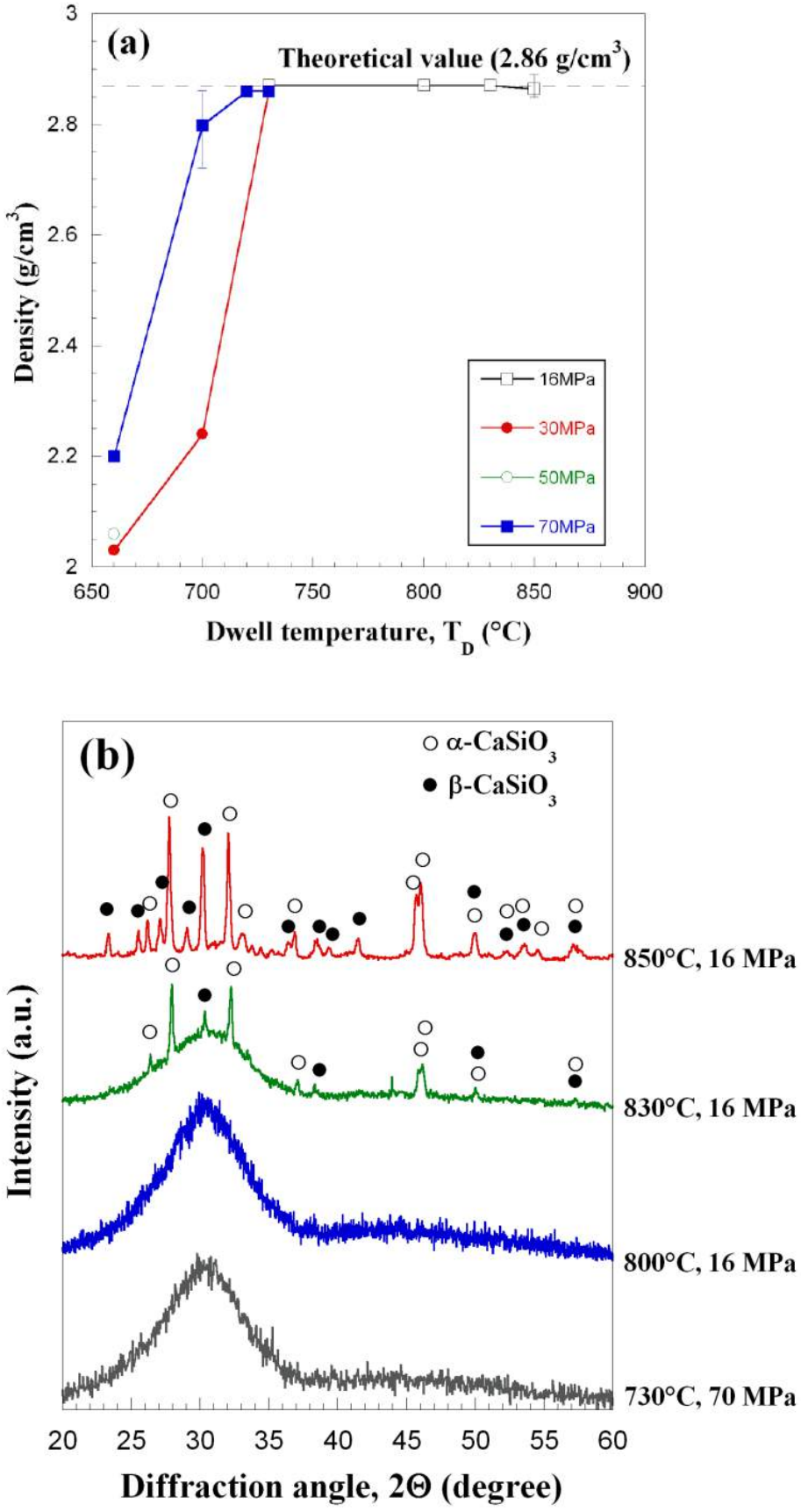

Figure 39. Influence of the (a) sintering temperature and applied pressure on the density of the BG_Ca/Mix products obtained by SPS (t_D=2 min) and (b) related XRD patterns.

Finally, as the dwell temperature was set to 850°C, crystallization phenomena proceeded, mostly with the formation of β-$CaSiO_3$, and the amorphous halo disappeared from the pattern. Thus, consistently with the TGA/TDA tests, the end product obtained by SPS at 850°C consisted of a mixture of both the α- and β-$CaSiO_3$ phases. This result is also in agreement with SEM observation. Indeed, as shown in Figure 40(a), the occurrence of the incipient crystallization in SPS products obtained at 830°C is confirmed by the presence of nanometric sized grains evidenced by this analysis. In addition, the progress of crystallization phenomena when the sintering temperature was increased to 850°C is proven by the micrograph of the corresponding chemically etched material reported in Figure 40(b).

The identification of the crystallization temperature of about 830°C for BG_Ca/Mix powders processed by SPS is well in agreement with the results of the TGA-DTA tests shown in Figure 33. More important is that fully dense and completely amorphous BG_Ca/Mix bioglass products can be obtained by SPS at 720-730°C, 10-50°C/min heating rate and 2 min dwell time. Such conditions are considerably more convenient with respect to those ones (800°C, 5°C/min heating rate, 3h) adopted to consolidate the same powders by pressureless sintering [21] .

The obtained results evidenced that the two systems displayed a marked different sintering behavior. It should be noted that a certain role might be played in this regard by their diverse particle size. Indeed, the starting BG_Ca/Mix glass powders used in this work were relatively coarser with respect to the 45S5 ones. Thus, to evidence more reliably the effect of glass composition on the sintering conditions requires to obtain fully dense products, the BG_Ca/Mix products should be further ground and sieved to reach particle size comparable to that of the other glass ceramic. Nonetheless, such treatment is not expected to produce significant changes in the optimal SPS conditions, compared to those ones identified in this work, to achieve the complete powder consolidation.

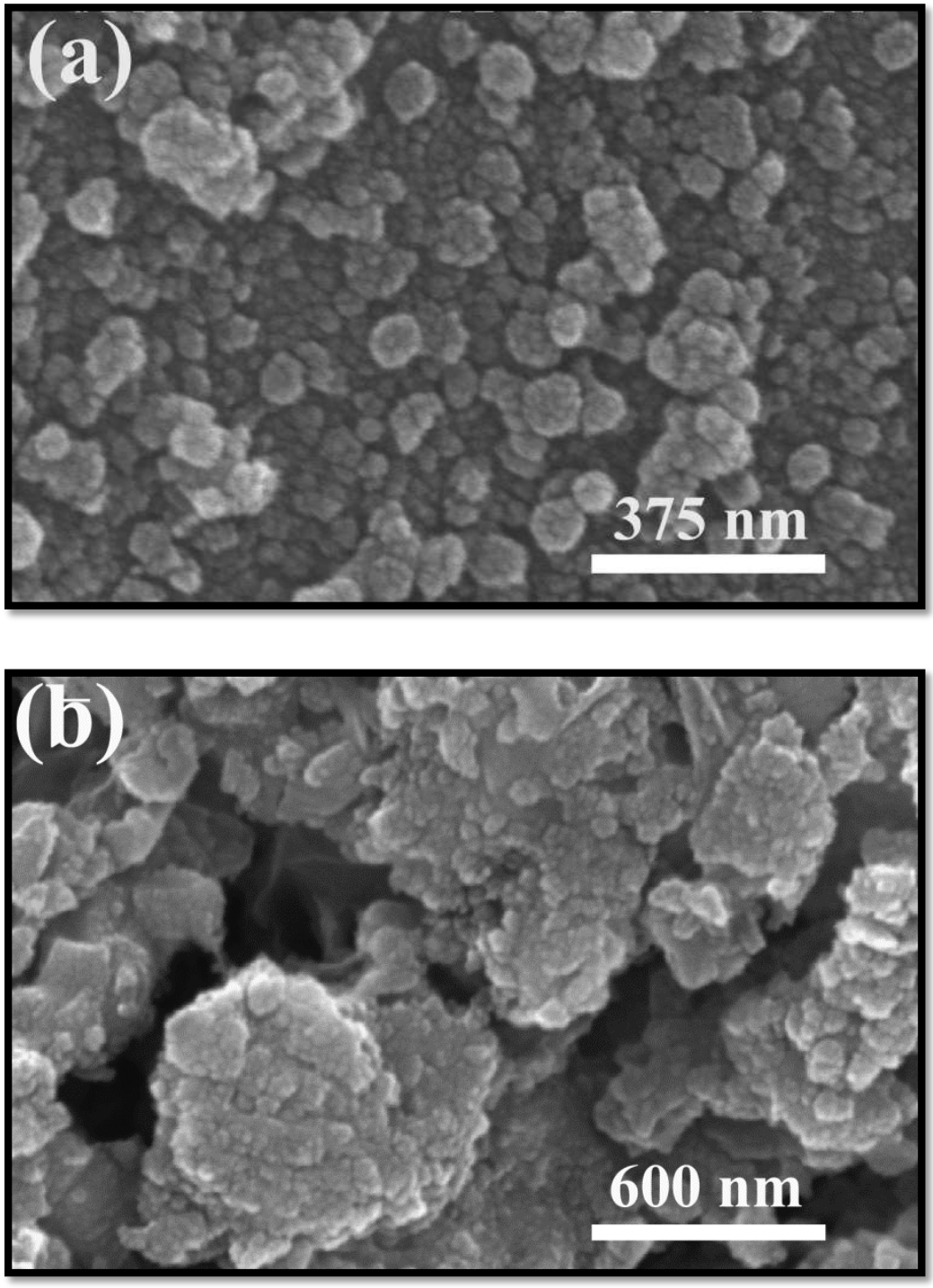

Figure 40. SEM images of chemically etched bulk BG_Ca/Mix bioglass products obtained by SPS at different sintering temperatures: (a) 830°C/16MPa, and (b) 850°C/16MPa.

2.3.3 Mechanical characterization

The mechanical characterization was addressed to highlight the effect of the crystallization process and, with this aim, two samples were considered for each type of glass, namely:

BG_45S5_a: sample sintered at 550°C, 70MPa – mainly amorphous (Figure 36(b))

BG_45S5_c: sample sintered at 600°C, 70MPa – mainly crystalline (Figure 36(b))

BG_Ca/Mix_a: sample sintered at 730°C, 70MPa – mainly amorphous (Figure 39(b))

BG_Ca/Mix_c: sample sintered at 850°C, 16MPa – mainly crystalline (Figure 39(b))

The histograms in Figure 41(a) and Figure 41(b), which refer to the local elastic modulus and to the Vickers hardness, respectively, show that an increase in T_D marginally affects the mechanical properties of BG_45S5-based materials. However, the values detected for the sample BG_45S5_a, which is mainly amorphous, are slightly higher than those observed for the sample BG_45S5_c, which is mainly crystalline.

Generally speaking, the devitrification of a glass is expected to improve the mechanical properties, because usually crystalline materials are mechanically stronger than their parent glass[53]. Nevertheless, the development of crystalline phases also determines changes in specific volumes, which may be responsible for a decrease in compactness, as observed for SPSed BG_45S5 samples in Figure 36(a).

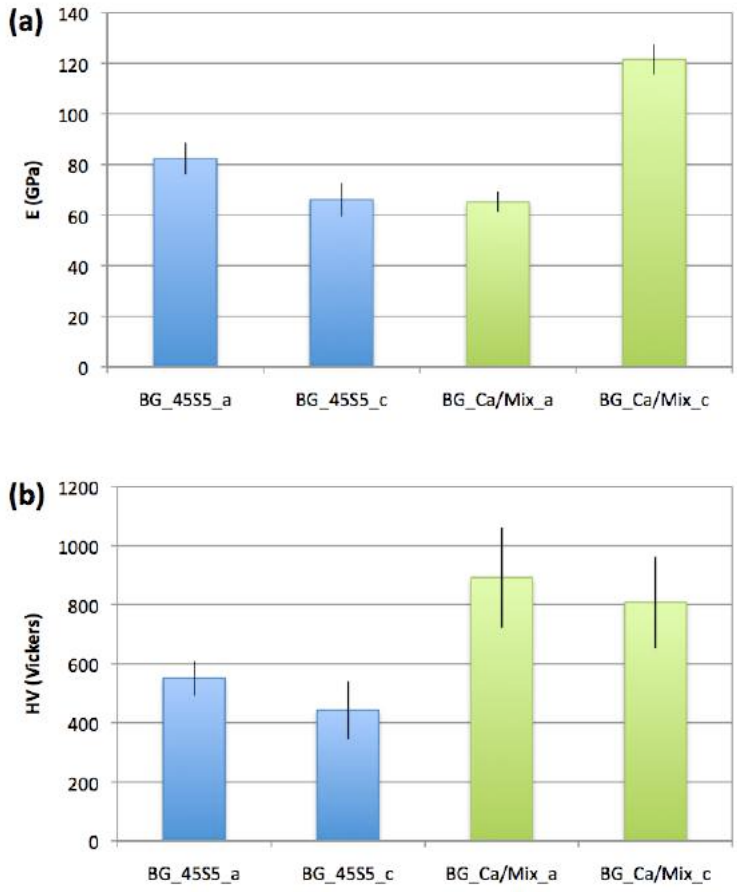

Figure 41. Local elastic modulus, E (a), and Vickers hardness, HV (b), of the samples BG_45SS and BG_Ca/Mix processed by SPS under different conditions.

A reduction in density, in its turn, is usually associated to a decrease of the mechanical performance. According to the results in Figure 41, for the samples of the BG_45S5 type, the negative effect of the structural re-arrangement counterbalances the positive effect of the crystallization. If the BG_Ca/Mix samples are considered instead, the Vickers hardness remains substantially unchanged (Figure 41(b)), whereas the local elastic modulus greatly increases after crystallization (Figure 41(a)). This is probably due to the significant difference in mechanical properties existing between the glass and the newly formed crystalline phases (wollastonite minerals have indeed an acicular structure, which allows them to compete with other fibers, including glass fibers and ceramic fibers, as a reinforcement phase[54]) and, most of all, to the very high density, almost identical to the theoretical one, which is

still observed for the samples treated at 850°C, 16MPa (type BG_Ca/Mix_c), as shown in Figure 39(a).

Beside the consideration made above, it should be also noted that the fully dense BG_Ca/Mix products sintered at 730°C are completely amorphous, so that the effect of crystallization can be better highlighted. On the other hand, this is not the case of the BG_45S5 system obtained at 550°C, where the formation of the $Na_6Ca_3Si_6O_{18}$ crystalline phase is started to take place.

Based on the results described and discussed above, it is possible to state that the SPS technology allowed us to obtain fully dese and completely amorphous products at 730°C after 2 min holding time when starting from the CaO-rich bioactive glass powders.

Moreover, dwell temperature equal or higher than 830°C are require to promote the crystallization of α- and β- $CaSiO_3$ from the parent glass. On the other hand, crystals of $Na_6Ca_3Si_6O_{18}$ are formed in fully dense 45S5-based samples produced under the optimal conditions of 550°C and 2 min. Nonetheless, the amorphous nature is still predominant in the resulting sintered products.

As far as the mechanical properties are concerned, higher hardness and local elastic modulus are displayed by the new glass composition. Crystallization phenomena provide a further improvement. Conversely, for the case of the 45S5 system, mechanical properties become slightly worsen when considering materials with higher crystallization degree, i.e. obtained ad 600°C. The last outcome could be likely ascribed to the corresponding decrease in sample compactness which, apparently, overcomes the expected beneficial effect arising from the devitrification progress.

Chapter 3

Hydroxyapatite/Bioactive glass composites

3.1 Introduction

The repair of osseous defects caused by tumors, traumatic events or inflammatory diseases is a common clinical problem. Current lines of treatment such as autogenous bone grafts, which involve the transplantation of bone from another part of the patient, or allografts, where bone tissue is taken from donors or cadavers, are affected by specific drawbacks, i.e., donor site morbidity, disease transmission risks, high costs and potential complications like infections[55,56]. In the last 40 years an extensive amount of research works has been devoted to develop specific synthetic alternatives for the replacement of damaged or lost bones. Among these alternatives, is well known to play a prominent role in oral, maxillofacial and orthopaedic surgery since the 1980s[57,58]. Thanks to its similarity to the biological apatite, which constitutes the mineral phase of hard tissues, HA exhibits excellent biocompatibility and osteoconductivity, as it is able to promote, *in vivo*, bone tissue apposition to its surface. HA has been extensively used in form of cements, powders and granules to produce bone fillers and synthetic bone grafts for biomedical applications. Unfortunately, the poor mechanical performance of HA (in particular the tensile strength and fracture toughness) makes its use difficult in bulk form for load bearing applications. However, for the latter applications, HA utilization is mainly confined to the deposition of bioactive coatings on metallic implants[59-62].

The disadvantages associated to the use of HA also include the high sintering temperatures typically required for obtaining bulk products[63,64]; moreover, the reactivity of this material at body

temperature and physiological pH is typically low. Consequently, the osseointegration rate of HA-based grafts, which should match the rate of growth of the new tissue, is also rather modest[59,65]. This fact can be particularly detrimental for the production of HA scaffolds for bone tissue engineering, which should resorb in a predictable way, at the same rate as the tissue is repaired.

In order to overcome these limitations, several investigations have been addressed to the preparation of HA-based composites with bioactive glasses as second phase. Most of these studies involved the use of 45S5 Bioglass® (45S5[66]). As described in the precious chapters, 45S5 is a degradable glass in the $Na_2O–CaO–SiO_2–P_2O_5$ system able to form a chemical bond with both soft and hard tissues. In general, bioactive glasses bond to bone more rapidly than other bioceramics. Moreover, *in vitro* studies demonstrated that the dissolution products (e.g. Si, P, Ca) of 45S5 stimulate osteoblasts proliferation and seem to induce angiogenesis and neo-vascularization[67].

The production of HA/bioactive glass composites opens intriguing scenarios, since it allows to go beyond the intrinsic limits of the ceramic and glassy phases when considered singularly[58]. On the one hand, by varying the volume fractions of the two constituents, it is possible to control the bioactivity and the dissolution rate of the resulting material, so that innovative systems with tailored biological properties can be obtained. In addition, the use of glasses may be further exploited to incorporate specific ions, such as fluorine, silicon, magnesium or strontium, within the lattice of HA, with the aim to reproduce the composition of the biological apatite, which is intrinsically nonstoichiometric and calcium-deficient with several di- and trivalent ion substitutions[68]. Furthermore, the glass may act as sintering aid, thus promoting the densification of the composite powders[63,64].

One of the main issues concerning the production of HA/bioactive glasses composites is associated to the thermal treatment necessary to sinter them. The densification of 45S5-based composites by pressureless sintering usually requires temperatures up to 1300 °C, which exceeds the crystallization temperature of the glassy phase. On the one hand, the crystallization of the glass has an adverse effect

on the sintering process, thus limiting the densification of the final system which may be prone to unwanted residual porosity. Moreover, the HA decomposition and/or reactions between glass and apatite during the thermal treatment was also observed. Finally, the crystallization of the glassy phase may also reduce its bioactivity[57,63,64,69].

Several investigations have been devoted to understand how to tailor the glass formulation with the aim to prevent crystallization[70-72]. In recent years, a novel class of silicate glasses with lower tendency to crystallize with respect to 45S5 were produced and employed to develop HA-based composites. In particular, the so-called BG_Ca/Mix system – a CaO-rich, K_2O modified glass composition – was specifically formulated as an alternative to 45S5 to be used whenever thermal treatments on bioactive glasses are required[21,47]. A crystallization temperature of 880 °C is reported for BG_Ca/Mix, while 45S5 starts to crystallize at temperatures as low as 610 °C[39]. BG_Ca/Mix powders were recently used to produce various HA-based composites, containing up to 70 wt.% of HA[73,74]. Although it was possible to sinter the novel samples at a lower temperature with respect to HA/45S5 composites with the same HA/glass proportion, the composites with higher amounts of HA suffered for some residual porosity and poor mechanical properties. For these reasons, several efforts have been made to identify more efficient powder densification techniques, as an alternative to classical sintering.

In this regard, SPS could play an important role, also to avoid or minimize crystallization phenomena, grain growth, and/or phases decomposition have to be avoided or minimized.

Based on these considerations, two studies aimed to the consolidation by SPS of three different commercial HA powders[14] as well as 45S5 and BG_Ca/Mix bioactive glasses[75] were recently carried out. In particular, the full densification of HA CAPTAL® powders was achieved after 5 min dwell time at 1200°C and the resulting product does not present any secondary phase[14]. Moreover, as discussed in Chapter 2, concerning the bioglass powders, completely dense and fully amorphous BG_Ca/Mix materials were produced by SPS at 730°C in 2 min holding time.

In this Chapter, the SPS technique is employed for the first time to produce HA-based composites with BG_Ca/Mix glass as second phase. Specifically, a systematic study is conducted to identify the optimal sintering conditions for preparing highly dense composites by considering three different HA/BG_Ca-Mix proportions. The obtained bulk products are then characterized from the compositional, microstructural and mechanical points of view. Finally, the bioactivity of the composites is investigated *in vitro* in a simulated body fluid solution.

3.2 Experimental

3.2.1 Composites powders preparation

The raw powder reagents (commercial SiO_2, Na_2CO_3, $CaCO_3$, K_2CO_3, $Ca_3(PO_4)_2$ by Carlo Erba Reagenti, Rodano-Milano, Italy) were melted at 1450 °C for 1 hour to produce BG_Ca/Mix (composition: 47.3 mol% SiO_2, 45.6 mol% CaO, 2.3 mol% K_2O, 2.3 mol% Na_2O, and 2.6 mol% P_2O_5). Subsequently the melt was quenched in room-temperature water to obtain a frit which was dried at 110 °C for 12 hours and then milled into powder (grain size < 45 μm). BG_Ca/Mix and commercial HA powders (CAPTAL® Hydroxylapatite, Plasma Biotal Ltd, UK) were accurately mixed in a plastic bottle using a rolls shaker for 6 hours in order to prepare the following set of composites:

- 80 wt.% BG Ca/Mix and 20 wt.% HA powders ("80BG_20HA");
- 50 wt.% BG Ca/Mix and 50 wt.% HA powders ("50BG_50HA");
- 30 wt.% BG Ca/Mix and 70 wt.% HA powders ("30BG_70HA").

Moreover, SPSed pure HA were prepared and subsequently used as a control in the investigation of the composites' bioactivity (see next paragraphs). The sintering conditions for the production of the HA samples have been previously reported and discussed in Ref. [14].

3.2.2 Sintering of the composite powders

Spark plasma sintering experiments for the consolidation of 80BG_20HA, 50BG_50HA and 30BG_70HA powders were performed by means of the SPS 515S equipment (shown in Figure 28). About 1.49, 1.53 or 1.56 g of 80BG_20HA, 50BG_50HA and 30BG_70HA powders, respectively, were placed in a cylindrical die (outside diameter of 35 mm, inside diameter of 15 mm, and 30 mm high) equipped with two punches, reported in Figure 29a and 29b, respectively. Further details related to the general SPS procedure can be found in Section 2.2 of the previous Chapter.

In particular, during SPS runs for the preparation of dense composites, the temperature was first increased at a rate of 50°C/min until a value of 100°C lower than the holding temperature (T_D) was achieved. Afterwards, the T_D level was reached at a lower heating rate (10°C/min) to minimize overshooting problems. The effect of the dwell temperature was investigated in the range 730-1150°C. The sample was kept at the sintering temperature for a time interval (t_D) varying from 3 sec to 10 min. The applied mechanical pressure was varied from 16 to 30 MPa. It should be noted that the sintering conditions adopted for the preparation of bulk glass-apatite systems, were selected based on the results recently obtained when the SPS apparatus was used to consolidate separately the two composite constituents. In particular, the less severe conditions needed to obtain full dense HA and BG_Ca/Mix samples were 1200°C, 5 min and 30 MPa[14] and 730°C, 2 min, and 16 MPa as described in the previous chapter, respectively.

Finally, sintered disks with diameter of 14.7 mm and thickness of about 3 mm were obtained. For the sake of reproducibility, each experiment was repeated at least twice.

Densities of polished SPSed samples were determined by the Archimedes method. The theoretical densities of the 80BG_20HA, 50BG_50HA and 30BG_70HA systems, i.e., 2.915, 3.015 and 3.074 g/cm^3, respectively, were calculated using a rule of mixture[76]. In this regard, density values of 3.16 g/cm^3 for HA and 2.86 g/cm^3 for BG_Ca/Mix were considered.

Phase composition of differently sintered composites was determined by XRD analysis using the X-rays diffractometer (Philips PW 1830, Almelo, The Netherlands) equipped with a Ni filtered Cu K_α radiation (λ=1.5405 Å) shown in Figure 25.

3.2.3. Microstructural and Mechanical characterization

Among the sintered composite specimens, a subset has been selected, based on high values of density, for further characterization carried out at the Dipartimento di Ingegneria "Enzo Ferrari", Università degli studi di Modena e Reggio Emilia (Italy). The bulk products examined are listed in Table 5 along with the corresponding SPS conditions and densities.

The mirror polished cross-sections of the samples were observed in a Environmental Scanning Electron Microscope (ESEM Quanta 2000, FEI Co., Eindhoven, The Netherland) operating in low-vacuum conditions (~0.5 Torr). Qualitative compositional analyses were performed by means of X-ray energy dispersion spectroscopy (X-EDS) (Inca, Oxford Instruments, UK).

Sample	**T_D, t_D**	**ρ [%]**	**HV [Vickers]**
80BG_20HA_#1	770°C, 10 min	96.9	539.5 ± 31.1
80BG_20HA_#2	800°C, 10 min	98.45	553.1 ± 25.4
80BG_20HA_#3	800°C, 3 sec	96.9	586.4 ± 20.8
30BG_70HA_#1	1100°C, 3 sec	96.9	456.4 ± 38.2
30BG_70HA_#2	1150°C, 3 sec	>99.9	634.66 ± 19.9
50BG_50HA	1000°C, 3 sec	98.6	536.3 ± 29.7

Table 5. Samples, processing parameters, final density and Vickers hardness of the produced composites. Vickers hardness is expressed as mean value ± standard deviation. For sake of comparison, a hardness of 368.1 ± 83.3 Vickers is reported for 80BG_20HA composites produced by means of traditional sintering[74].

Vickers micro-indentation tests (Wolpert Group, Micro-Vickers Hardness Tester digital auto turret, Mod. 402MVD) were performed on the polished cross-sections in order to determine the Vickers hardness of the samples. For each material, at least 15 clear and crack-free indentations were performed by applying a maximum load of 100 g_f for 15 s[77].

3.2.4. In vitro bioactivity

The *in vitro* bioactivity of the produced samples was evaluated by soaking them in an acellular simulated body fluid solution for different time periods, according to the procedure developed by Kokubo and coworkers[78]. For each set of produced composites one sample was tested. The disks were soaked in flasks containing 25 ml of SBF and stored at 37 °C in an incubator. The solution was refreshed every about 48 hours. The contact between composites and the solution was interrupted after 3, 7 and 14 days. The specimens were then rinsed with water and left to dry for 24 hours at room temperature. The samples surface was observed by SEM in order to investigate microstructural changes that occurred after immersion and the possible precipitation of hydroxyapatite. Moreover, micro-Raman spectroscopy was performed, using a Jobin–Yvon Raman Microscope spectrometer (Horiba Jobin–Yvon, Villeneuve D'ascq, France), equipped with a 632.8 nm-wavelength He–Ne diode laser.

3.3 Results and Discussion

3.3.1 Powders sintering

The densification behaviour of the three composites produced under the same SPS conditions (T_D=800°C, t_D=10 min, P=30 MPa) is reported in Figure 42. The corresponding temperature profile is also shown. Similar gradual and modest changes of the S parameter are observed for the three

composite powders when they are exposed to thermal levels below 700°C. On the other hand, as the temperature was further augmented, the sample shrinkage progressively increases at a higher rate, especially for the composite powders richer in BG_Ca/Mix. At the end of the experiments, the relative densities (average values) of the obtained sintered 80BG_20HA, 50BG_50HA and 30BG_70HA products were 98.075, 88.4 and 73.8, respectively. These outcomes are perfectly consistent with the composition of the starting powders, i.e. sample density increases as the fraction of the constituent glass is progressively augmented.

A systematic investigation was conducted to identify, for the three composites under consideration, the less severe SPS conditions able to guarantee the preparation of nearly full dense products. The results obtained for the 80BG_20HA system are shown in Figure 43. As expected, it is possible to notice that an increase of the holding temperature, dwell time and/or applied pressure parameters promotes powders consolidation, so that the conditions for producing samples having density higher than 96% are identified.

Specifically, such densification degree can be reached for T_D values above 770°C when t_D=10 min. As shown in Figure 44(a), the XRD pattern of the resulting product shows a broad hump, that evidences the still amorphous nature of BG_Ca/Mix, although the small peak of α-$CaSiO_3$ provides an indication of the incipient crystallization of the bioglass. The latter phenomenon is significantly enhanced as the sintering temperature was increased to 800°C. Indeed, peaks intensity related to α-$CaSiO_3$ increases markedly. In addition, a smaller amount of β-$CaSiO_3$ was also found and, more important, the amorphous hump basically disappeared from the XRD pattern.

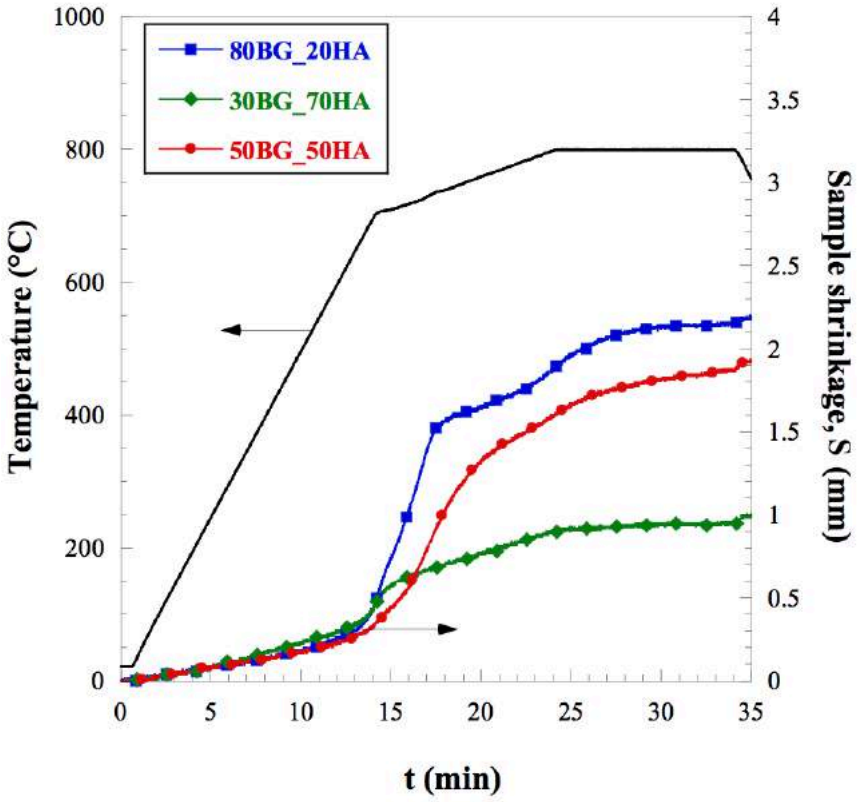

Figure 42. Temperature-time profile and the corresponding sample shrinkage curves obtained during the consolidation of the three composite systems by SPS (T_D=800°C, t_D=10 min, P=30 MPa).

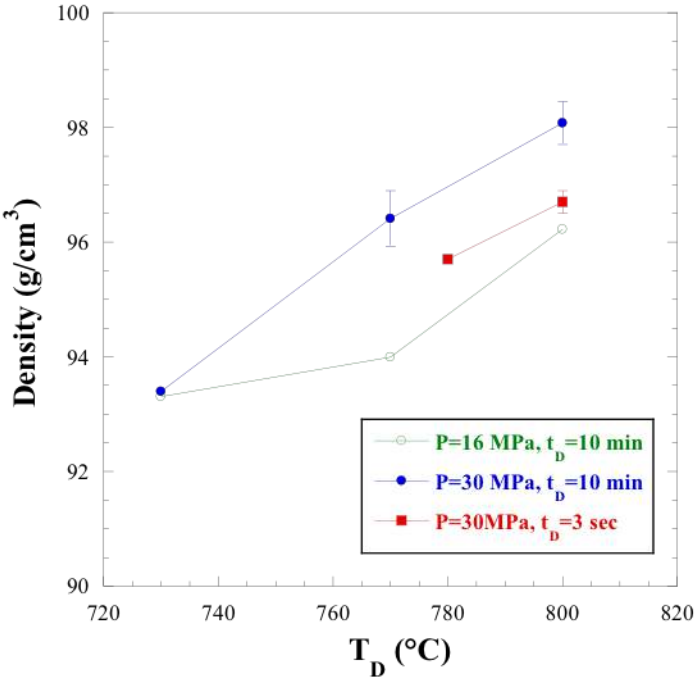

Figure 43. Effect of the sintering condition on the relative density of 80BG_20HA samples produced by SPS

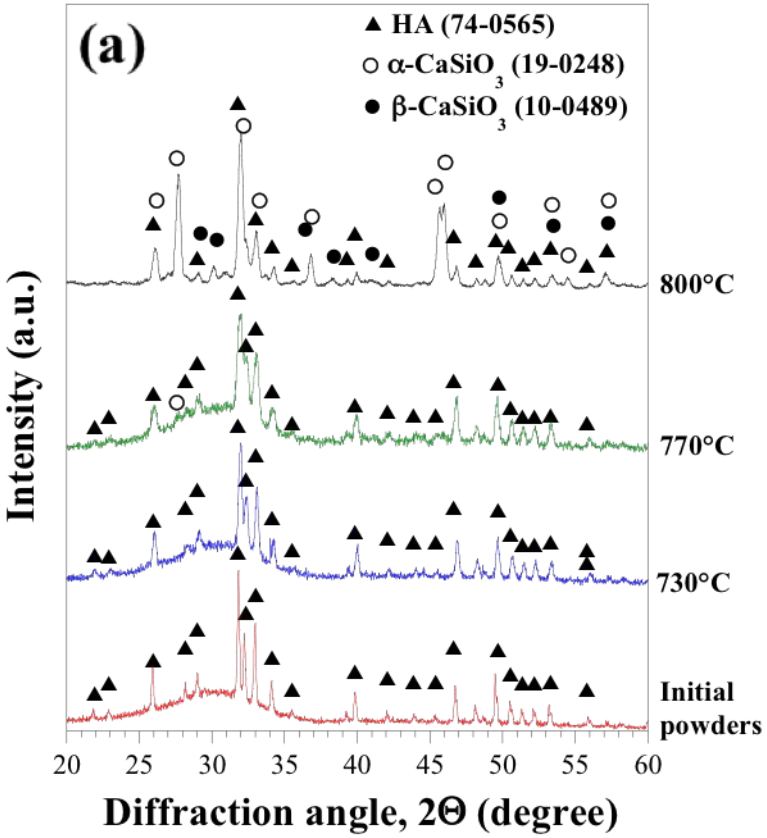

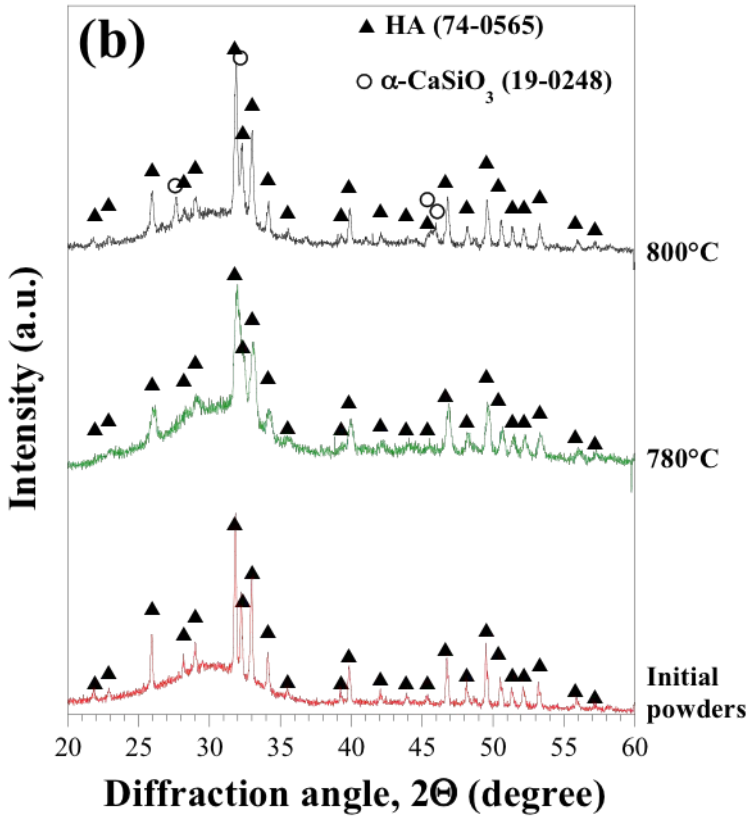

Figure 44. Effect of the sintering conditions on XRD patterns of 80BG_20HA samples produced by SPS at P=30 MPa when t_D=10 min (a) and t_D= 3 sec (b).

Crystallization phenomena can be mitigated if the holding time is sufficiently shortened while maintaining the thermal levels unchanged. In fact, as reported in Figure 44(b), no additional crystalline phases, other than HA, are detected by XRD in the 95.7% dense product obtained by SPS after 3 sec at 780°C. However, a small amount of α-$CaSiO_3$ was formed when the temperature was raised to 800°C to improve powders densification up to 96.7%, considering the same t_D and P conditions. Nonetheless, the XRD analysis revealed that in the latter case the sintered product still exhibits an amorphous character. In order to further increase the end product densities, higher temperatures or applied pressures were also considered. However, samples breakage correspondingly occurred during the SPS process.

Based on the results described above, it is possible to state that T_D=800°C, t_D= 3 sec, and P=30 MPa are the more convenient SPS conditions, among those ones investigated in the present thesis, to produce 80BG_20HA samples with average densities higher than 96.5%, where the crystallization of the bioglass is just at the early stage.

Accordingly, the optimal holding temperature for the other two composite systems examined was identified by setting the t_D and P values equal to 3 sec and 30 MPa, respectively.

Specifically, the data obtained for the 50BG_50HA sample are plotted in Figure 45. As expected, due to the presence of a larger amount of HA, the consolidation of these powders required higher thermal levels with respect to the previous system. In particular, as reported in Figure 45(a), a 90.5% dense 50BG_50HA sample (average value) was produced by SPS when the holding temperature was set at 850°C. Under such conditions, no additional phases were evidenced by the XRD analysis. On the other hand, both α- and β-$CaSiO_3$ were found in the slightly denser compacts obtained at 950°C (relative density of about 92.5%). In addition, it can be observed that a further temperature increase to 1000°C determined a partial transformation of α- to β- $CaSiO_3$. A product approximately 98% dense was correspondingly obtained.

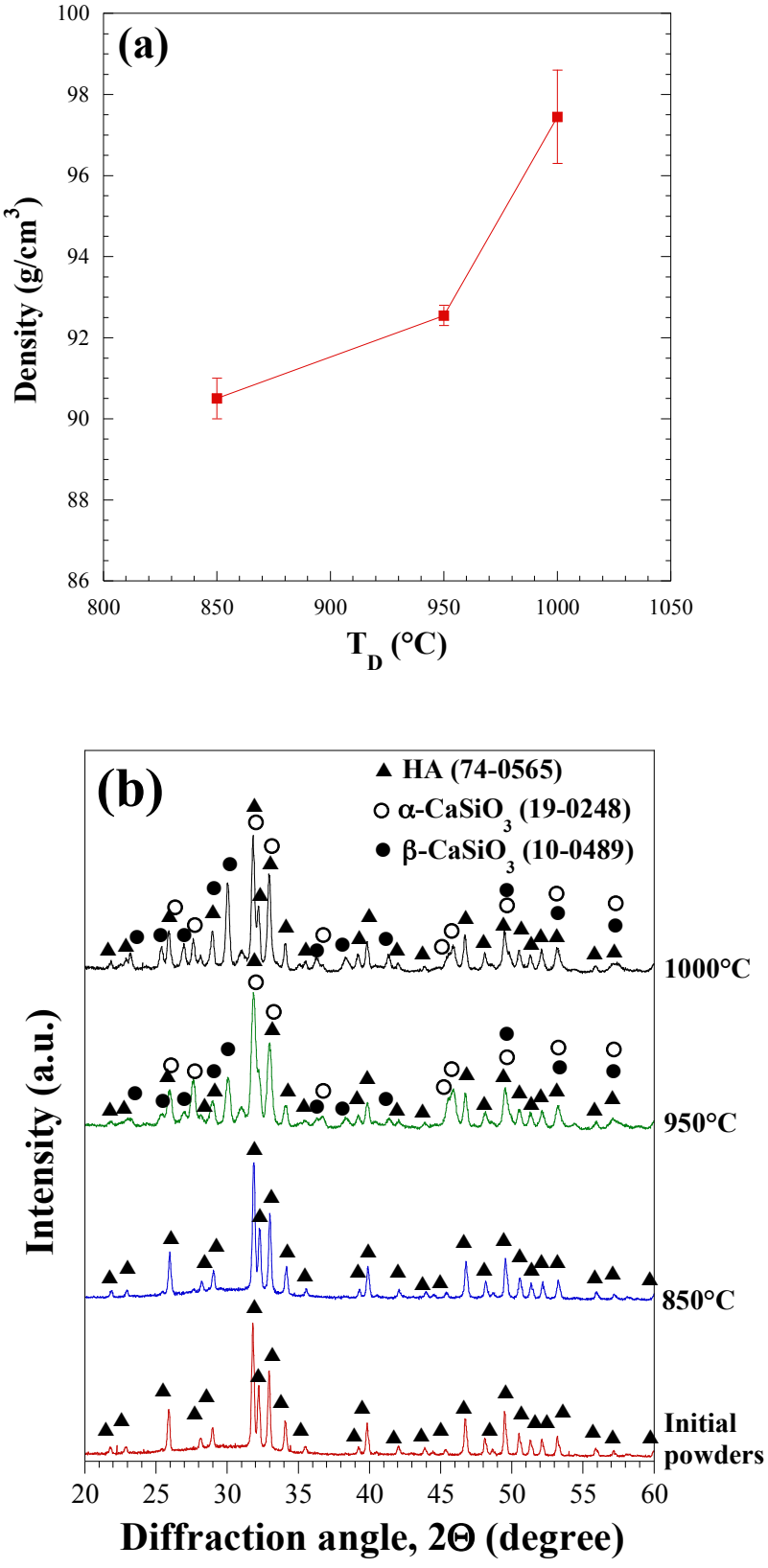

Figure 45. Effect of the sintering temperature (t_D= 3 sec, P=30 MPa) on the relative density (a) of 50BG_50HA samples produced by SPS and the corresponding XRD patterns (b).

Powder consolidation gets more difficult when the fraction of HA in the composite mixture is further increased, so that the occurrence of crystallization phenomena is favored by the higher T_D values required to reach the desired densification levels. In particular, as reported in Figure 46(a), still very porous 30BG_70HA products resulted when the holding temperature was set at 950°C. Moreover, as evidenced by the corresponding XRD pattern shown in Figure 46(b), such condition was anyway sufficient to determine a significant crystallization from the glassy phase with the formation of $CaSiO_3$, in both the α- and β- forms. The progressive increase of the temperature strongly promoted powder consolidation, so that fully dense products are obtained at 1150°C.

Based on the observed outcomes, the lowest holding temperatures, among those investigated, sufficient to produce 96.5% or denser 80BG_20HA, 50BG_50HA and 30BG_70HA specimens by SPS (t_D= 3 sec, P= 30 MPa) are 800, 1000 and 1150°C, respectively.

These findings are well in agreement with the results recently obtained when HA and BG_Ca/Mix powders were separately processed by SPS[14,75]. First of all, the beneficial role played by the glass component as sintering aid is evidenced. Indeed, it was found that the SPS conditions needed for the nearly full consolidation of BG free HA were T_D= 1200°C, t_D= 5 min and P=30 MPa[14]. On the other hand, the same goal could be reached after only 3 sec at 1150°C or lower temperatures, when at least 30% of BG_Ca/Mix are added to the mixture. Moreover, based on XRD analysis, HA did not decompose when the three composites systems under investigation were processed by SPS. This is an important outcome, since the formation of β-TCP or other secondary phases from the HA decomposition**,** which tends to occur in the powders undergoing SPS when operating at relatively higher temperatures, might reduce the bioactivity of the resulting sample. Indeed, recent studies evidenced that β-TCP exhibits a rather lower aptitude, with respect to HA, to promote the formation of new phosphate phases in the bioceramic surface during both *in vitro* (simulated body fluid) and *in vivo* experiments[79]**.**

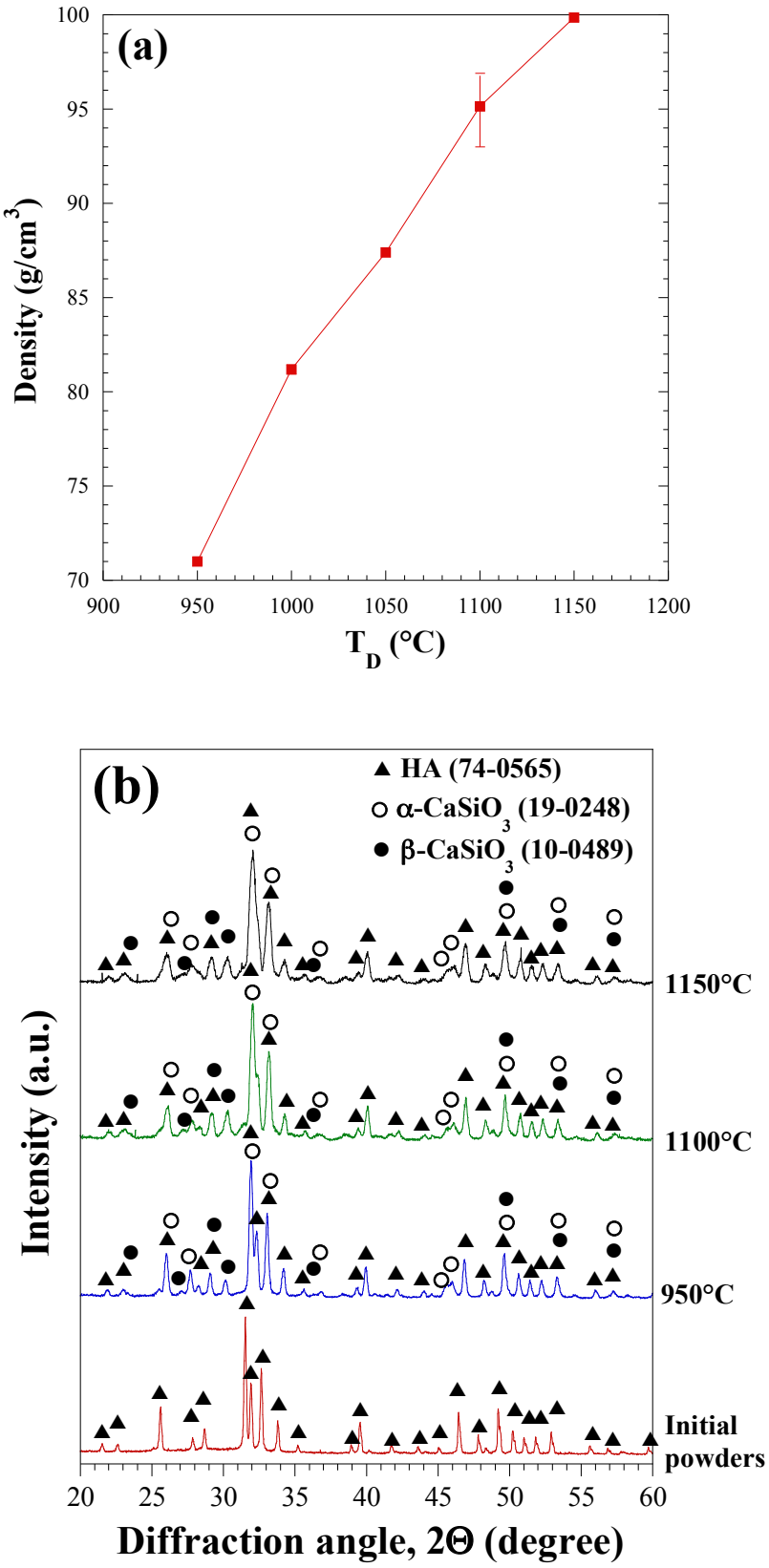

Figure 46. Effect of the sintering temperature (t_D= 3 sec, P=30 MPa) on the relative density (a) of 30BG_70HA samples produced by SPS and the corresponding XRD patterns (b).

As for the behavior of the BG_Ca/Mix constituent, it is observed that the massive composite samples with relative densities equal or higher than 96% are generally obtained in presence of a certain bioglass crystallization. The only exception is represented by the 80BG_20HA system processed for 3 sec at 780°C. On the other hand, a slight temperature increase to 800°C produced, other than an improvement of powder densification, also the formation of a small amount of α-$CaSiO_3$. This feature was relatively more accentuated when the other two composites, richer in HA, were taken into account. The latter result is readily associated to the fact that, when the relative amount of HA in the composite is progressively augmented, the dwell temperatures set to consolidate powder mixtures have to be higher. In particular, the optimal T_D values identified in this work to achieve density levels above 96% for the 80BG_20HA, 50BG_50HA and 30BG_70HA systems are 800, 1000 and 1150°C, respectively. Therefore, the crystallization of the bioglass is correspondingly favoured, as clearly confirmed by the XRD analyses of the resulting sintered samples. In particular, the temperature levels up to 1150°C needed to obtain nearly full dense 30BG_70HA materials have further promoted the formation of $CaSiO_3$, also in the β- configuration, from the glassy phase.

Nonetheless, it should be noted that devitrification phenomena as well as HA decomposition would occur at a significant higher degree if classic sintering methods, less efficient than SPS, and/or other bioglass compositions, displaying higher tendency to crystallize with respect to BG_Ca/Mix, are used.

3.3.2 Microstructural and Mechanical characterization

The bulk products examined by SEM are listed in Table 5 along with the corresponding SPS conditions and relative densities. Figure 47 and Figure 48 display some representative micrographs of the cross sections of the produced composites. Although the samples are adequately densified, some residual pores are still present. Nevertheless, several features visible in the sample images can be attributed to the preferential removal of HA-rich particles during the polishing step. This aspect is

more evident when observing the micrograph of the 80BG_20HA#1 cross section reported in Figure 49(a) and the corresponding X-EDS maps, which show the distribution of P, representative of HA in the composite, and Si, associate to the glass. In fact, the damaged areas in Figure 49(a) can be mainly identified as HA, since they are particularly poor in Si and rich in P.

Beside this feature, the cross section images show areas with different brightness (see, in particular, Figure 50): light areas should be ascribed to HA, while dark ones are representative of BG_Ca/Mix. It should be noted that the 30BG_70HA#2 sample looks particularly compact, with no traces of porosities. This finding is quite interesting, since the counterparts produced by traditional sintering suffered from widespread residual porosity and poor mechanical performance[73,74]. On the contrary, the SPS technique allowed to obtain fully dense and compact samples, regardless of the HA/glass proportions. This fact is further confirmed by the micro-hardness values of the produced samples, which are reported in Table 5. In this regard, it should be stressed that a direct comparison between the mechanical performance of the produced composites is not straightforward, since the samples differ in composition, density, microstructure, degree of crystallization of the glassy phase and mechanical properties of the formed crystalline phases. Nonetheless, on the basis of previous results obtained in the literature on the same HA and bioglass systems processed either separately by SPS or in combination using a diverse sintering technique, some considerations can be made in this context. First of all, it is important to underline that the SPSed composites obtained in this work show significantly higher hardness with respect to samples with the same HA/glass ratio prepared by traditional sintering.

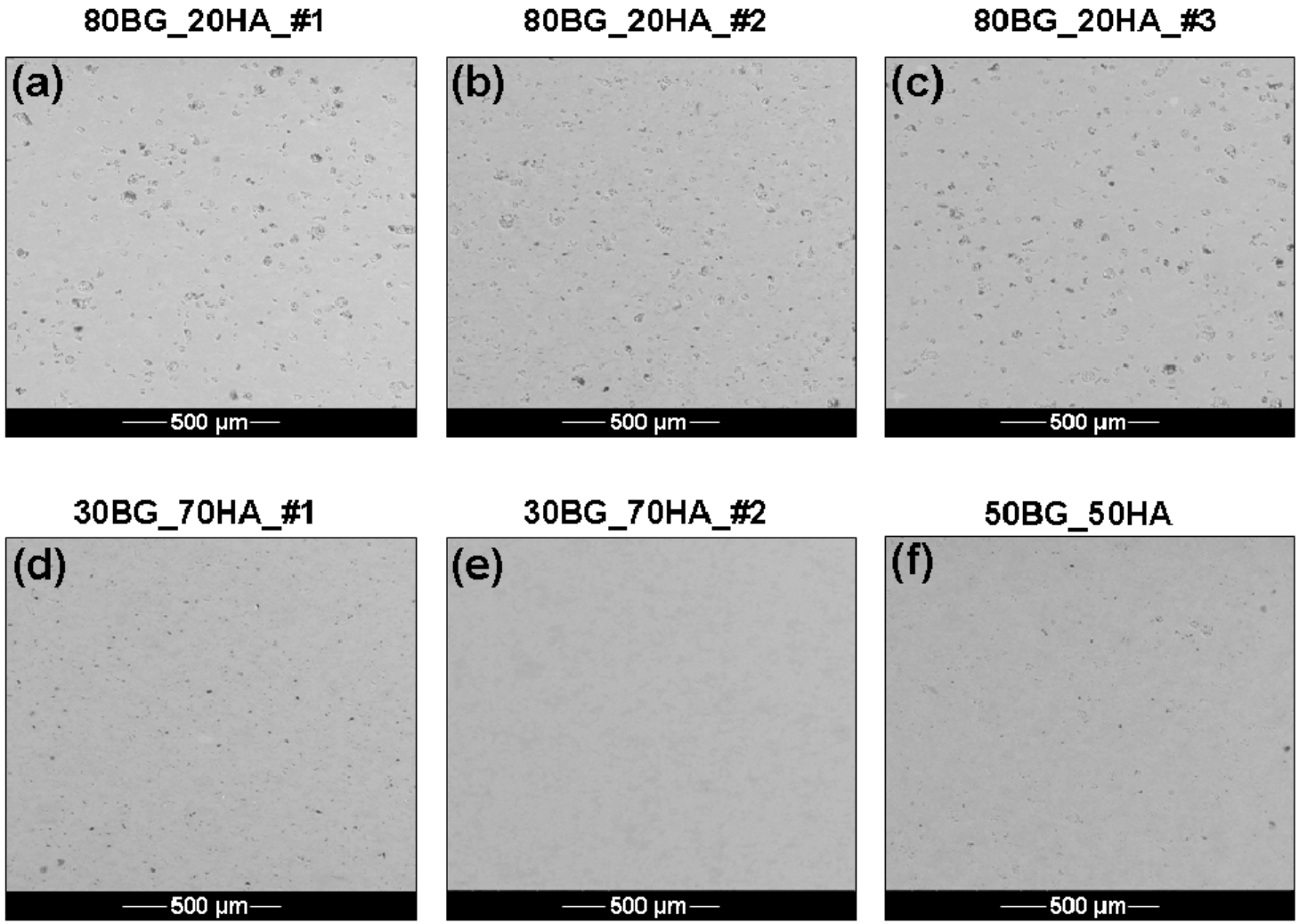

Figure 47. Cross sections of the produced composites

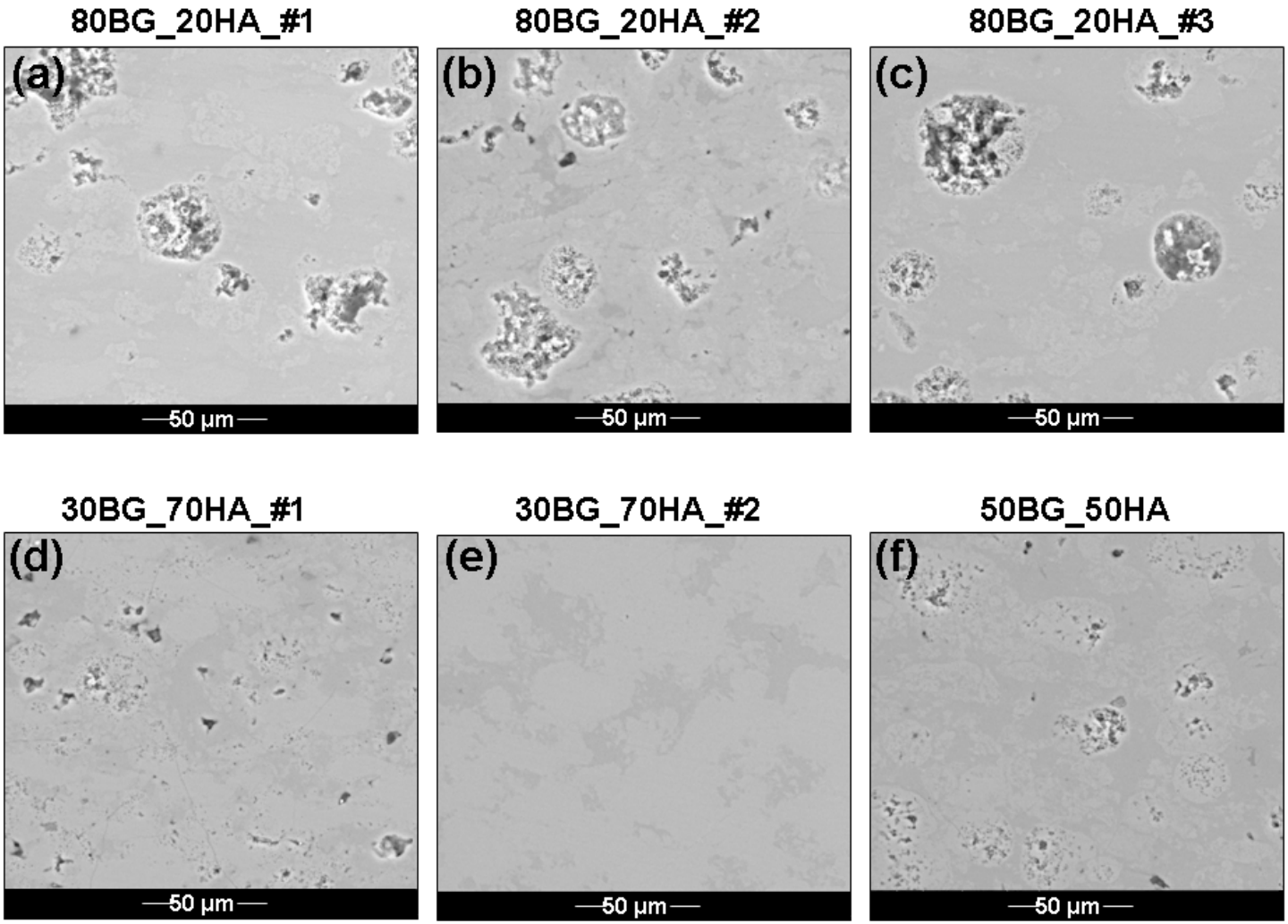

Figure 48. Cross sections of the produced composites: high magnification micrographs

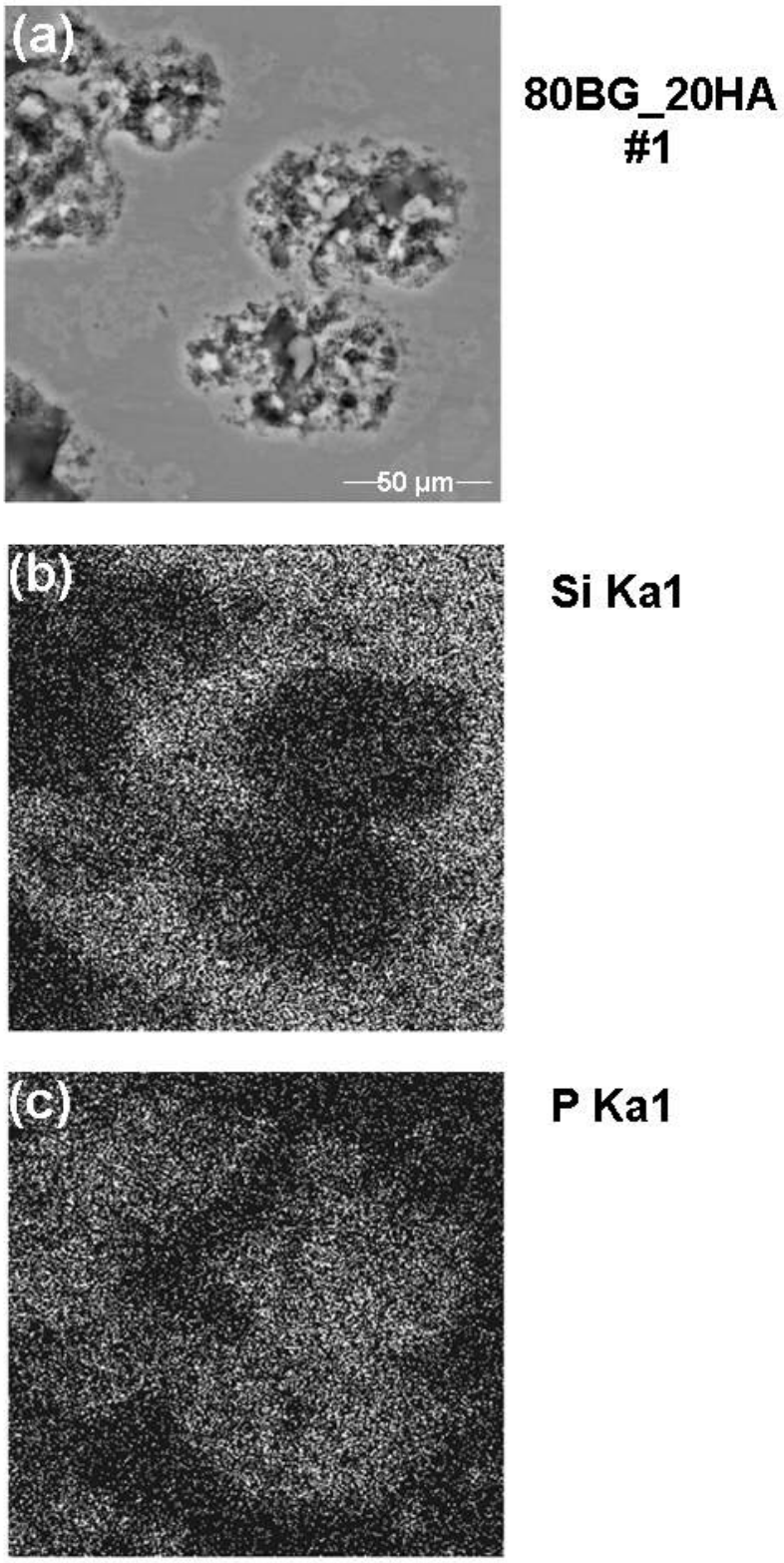

Figure 49. Micrograph of the 80BG_20HA#1 cross section (a) and corresponding X-EDS maps showing the distribution of Si (b) – representative of the glass – and P (c), representative of HA.

For sake of comparison, a Vickers hardness of 368.1 ± 83.3 was reported for 80BG_20HA composites produced by means of traditional sintering[74]. Furthermore, the residual porosity present in 30BG_70HA samples obtained using the latter approach did not permit the obtainment of reliable data for their micro-hardness[74]. In fact, indentation techniques are very sensitive to local defects, such as pores. It should be finally noted that 50BG_50HA counterparts have not been produced yet by conventional sintering.

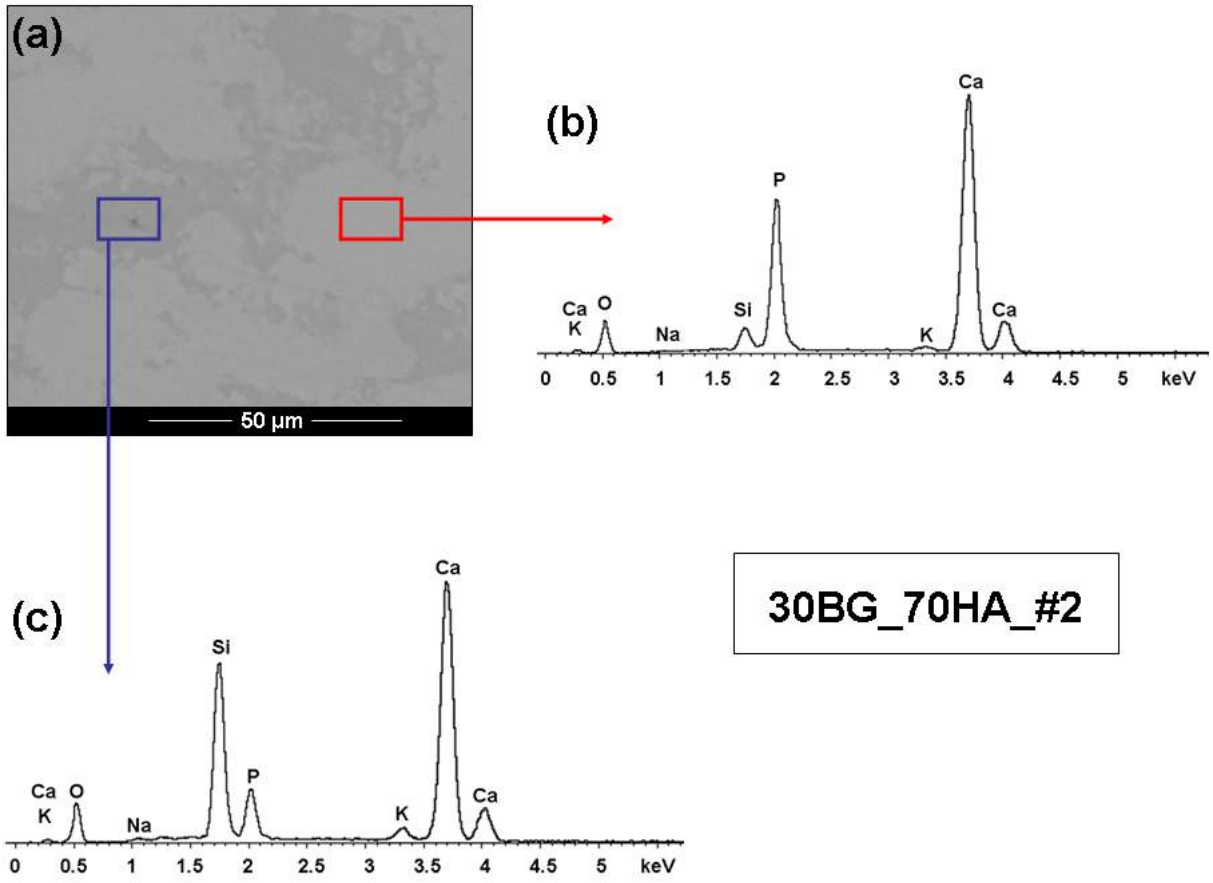

Figure 50. Micrograph of the 30BG_70HA#2 cross section (a) and results of the X-EDS analysis (b, c) performed on the areas indicated in (a).

The results reported in Table 5 indicate that the 30BG_70HA_#2 samples, which are characterized by a particularly high compactness (ρ > 99.9%) and a defects-free microstructure (see Figures 48(f)

and 49(a)), show the best performance also in terms of Vickers hardness. In contrast, the 30BG_70HA_#1 specimen has the lowest hardness among the samples examined in the present work. This result can be likely due to its lower density (ρ = 96.9%) and the relatively higher HA content. In this regard, it should be noted that two recent investigations focused on HA and BG_Ca/Mix processed separately by SPS, revealed that the micro-hardness data for BG_Ca/Mix were slightly higher than those ones found for HA[14,75]. Such finding is consistent to the lower hardness displayed by 30BG_70HA_#1 samples with respect to those ones obtained for 80BG_20HA_#1 and 80BG_20HA_#3 specimens, which have the same density but are characterized by a higher BG_Ca/Mix content. The hardness of 50BG_50HA samples is rather similar to the 80BG_20HA ones, since the negative effect due to the lower BG_Ca/Mix fraction in the 50BG_50HA composite is probably counterbalanced by its relatively higher density (ρ = 98.6%). For what concerns the 80BG_20HA samples, the 80BG_20HA_#3 has the best performance. However, in this case the analysis is made more complicated by the fact that the different degree of crystallization of BG_Ca/Mix in the composites should be taken in account. For example, the results reported in Figure 45 show that the amorphous nature of BG_Ca/Mix is better retained in 80BG_20HA#3 than in 80BG_20HA#2, although the latter one is denser. This fact could explain the slightly higher hardness of 80BG_20HA#3 with respect to that of 80BG_20HA#2.

3.3.3 In vitro bioactivity

Since the SPS method has been used for the first time to produce the composite systems under consideration, some preliminary results relative to the evaluation of their bioactivity are also reported. In this regard, the reactivity of the samples was investigated *in vitro* according to the procedure by Kokubo and coworkers[78]. This method, which aims to evaluate the apatite formation ability of bioactive glasses and bioceramics in SBF, is widely used as a preliminary screening test of the samples bioactivity.

After soaking in SBF, the characterization of the produced composites revealed the formation of apatite precipitates, which progressively spread on the samples surface. In Figures 51 and 52 it is possible to observe that the 80BG_20HA#1 surface, after 7 and 14 days of immersion, respectively, is covered by aggregates of spherical particles with the typical apatite morphology.

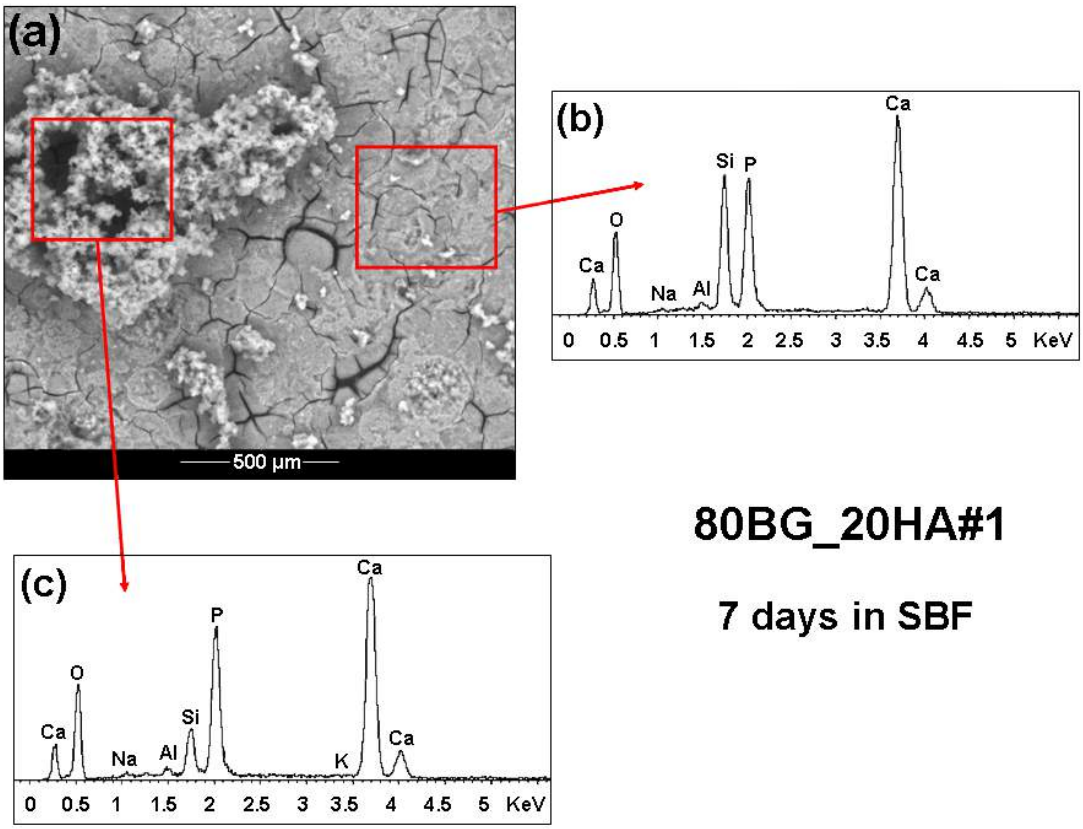

Figure 51. Micrograph of the 80BG_20HA#1 surface after 7 days in SBF (a) and results of the X-EDS analysis (b, c) performed on the areas indicated in (a).

The X-EDS analysis performed on the precipitates revealed that such aggregates are particularly rich in calcium and phosphorous (Figure 51(b, c)). Some Si is also detectable, due to the glassy phase underneath the precipitates and to the possible formation of a silica gel layer, according to the models which describe the reaction mechanisms of bioceramics and bioactive glasses in SBF reported by the

literature[27,66,80]. As shown in Figure 53, the nature of the globular precipitates was further investigated by micro-Raman spectroscopy. The Raman spectrum acquired on the 80BG_20HA#1 composite after 14 days in SBF looks rather similar to that of commercial apatite[81].

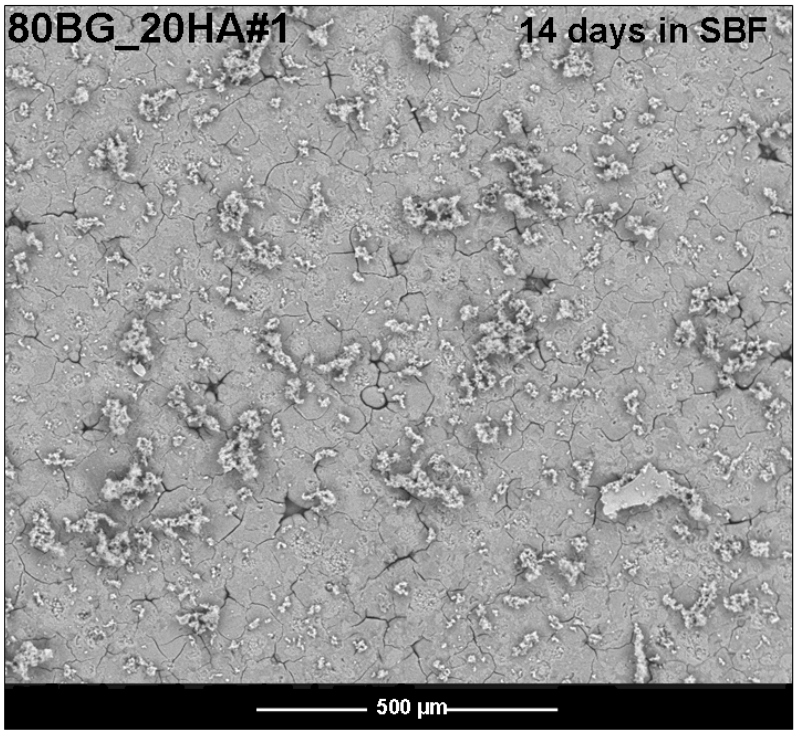

Figure 52. Micrograph of the 80BG_20HA#1 surface after 14 days in SBF.

Specifically, it is possible to identify three peaks, i.e. an intense and sharp signal at ~960 cm^{-1} and two peaks with lower intensity at ~430 cm^{-1} and ~590 cm^{-1}, which are ascribable to the PO_4 vibrations[82]. A further peak detected at ~1070 cm^{-1} can be referred to the stretching of carbonate groups[83]. In conclusion, it is possible to identify the precipitates on 80BG_20HA#1 as carbonated hydroxyapatite, thus confirming the *in vitro* bioactivity of the prepared samples.

Previous investigations have demonstrated that dense HA produced by SPS showed strong ability to induce hydroxyapatite formation *in vitro*[84,85]. Nevertheless, it should be stressed that the development of such apatite layer on the composites under consideration could be mainly ascribable

to BG_Ca/Mix, which revealed significantly higher *in vitro* reactivity. This fact is clearly evidenced in Figure 54, which shows the surfaces of SPSed bioglass-free HA, 30BG_70HA, 50BG_50HA and 80BG_20HA after immersion in SBF for three days.

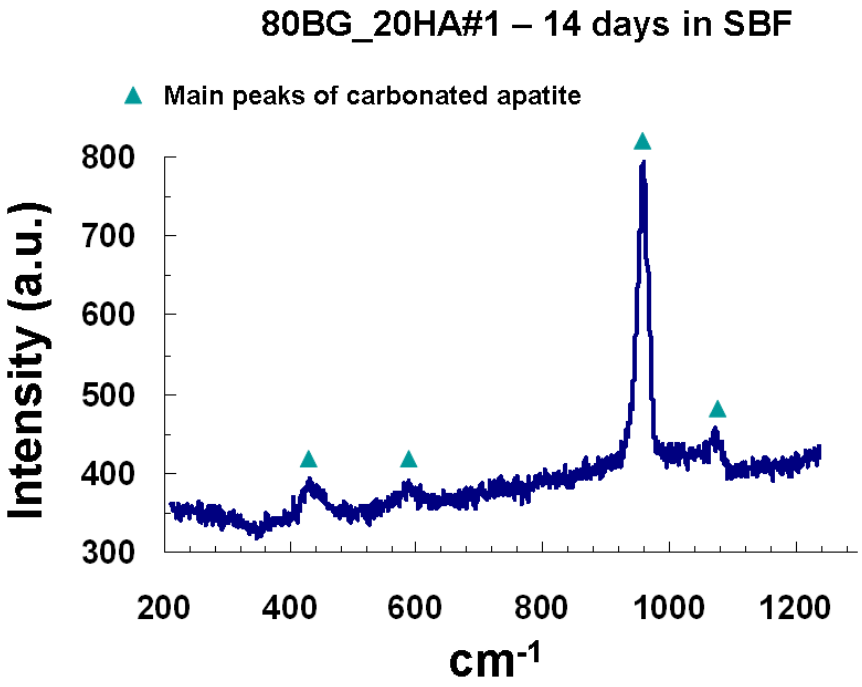

Figure 53. Raman spectra acquired on the precipitates formed on the 80BG_20HA#1 surface after 14 days in SBF.

It is possible to observe that the relative higher content of apatite precipitates on the samples surface with the increasing amount of BG_Ca/Mix in the sample. In particular, the newly formed apatite completely covered the 80BG_20HA surface, i.e., the sample with the highest content of glass. Therefore, the addition of BG_Ca/Mix may be used to modify the dissolution of the final system and to tune its biological response to the specific clinical application. It should be stressed that the latter aspect probably represents the most important advantage associated to the use of silicate-glass/HA composites. Moreover, thanks to its low tendency to crystallize, the BG_Ca/Mix in the composites maintained almost completely its amorphous nature, with positive effects in terms of the resulting bioactivity. On the other hand, the partial crystallization of BG_Ca/Mix to α- and β-$CaSiO_3$, which

belong to the family of wollastonite ceramics, is not detrimental regarding the HA-forming ability in SBF, since such crystalline phases also display a bioactive character, as reported in the literature[86-89].

For example, the bioactivity of wollastonite coatings deposited on titanium was evidenced by the formation of hydroxycarbonate apatite on the coatings surface after 1 day in SBF[86]. A good bioactivity was also shown by dense β-$CaSiO_3$ ceramics produced through SPS and subsequently tested in SBF for increasing soaking times[88]. The bioactivity in SBF of both α- and β-$CaSiO_3$ has been confirmed by Siriphannon *et al*[87] who also discussed about the differences *in vitro* between the two phases. Finally, other studies demonstrated that α- and β-$CaSiO_3$ ceramics are also able to support cell attachment, proliferation and differentiation[89].

It is important to note that the findings concerning bioactivity of the obtained composites are qualitatively analogous to those ones reported for their counterparts produced by means of traditional sintering[73,74]. However, the composites processed by SPS, in particular the 30BG_70HA and 50BG_50HA samples, exhibit far higher compactness, hardness and density. For these reasons, the SPS technology looks very promising for the production of HA/bioactive glass composites.

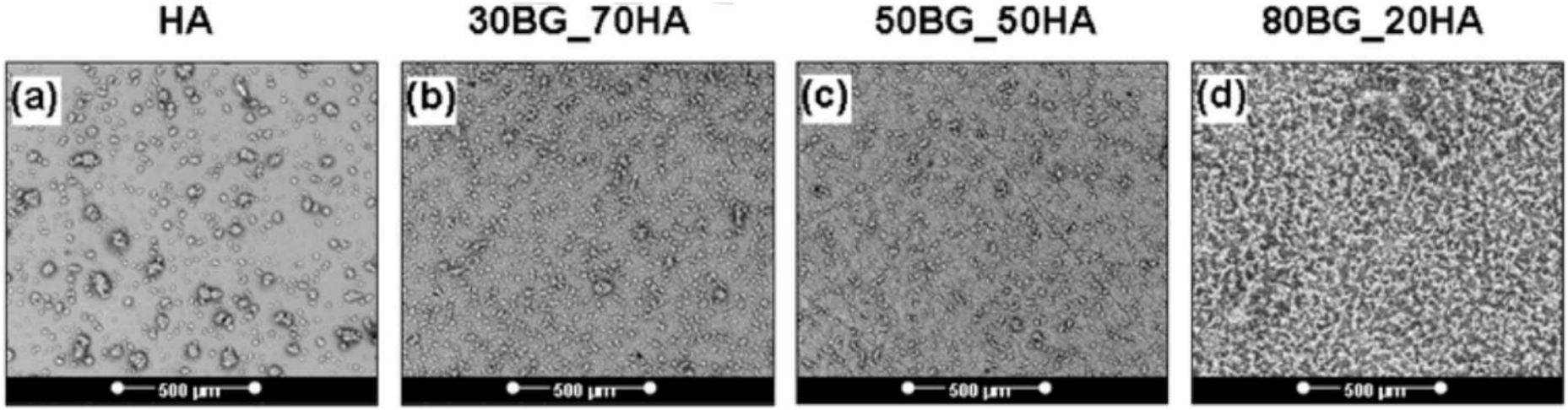

Figure 54. SEM images of the SPSed HA (a), 30BG_70A#1 (b), 50BG_50HA (c) and 80BG_20HA#1 (d) samples after 3 days in SBF.

Chapter 4

Human Cells Behavior on Calcium Phosphate Materials

4.1 Introduction

Due to their chemical composition similar to that of biological apatite, synthetic materials based on calcium phosphates (CaP) have drawn significant interest as bioceramics in the last decades[6]. In particular, no undesired host-tissue reactions are generally observed during *in-vivo* tests involving CaP systems with Ca/P atomic ratio in the range 1-1.7[6] . In this context, as already stated in previous chapters, the most representative member of this class of material is hydroxyapatite, which has already been widely used as powder, coating, porous or dense forms in several orthopedic and dentistry applications for bones/teeth substitution or restoring[90].

It is well known that heat treatment processes for the consolidation of HA powders often lead to chemical decomposition phenomena of the original phase[91]. As a consequence, the biological properties of the initial powders could be modified, often negatively, because of the high temperature adopted for their densification, particularly when considering conventional pressureless or hot-pressing methods. Changes in the composition of the material undergoing consolidation could be avoided, or relatively mitigated, when taking advantage of more efficient techniques, such as the Spark Plasma Sintering technology, because of the relatively milder processing conditions generally needed for the obtainment of fully dense products[36]. Nonetheless, the use of the latter technique is

not sufficient to overcome the drawbacks mentioned previously, since sintering temperatures, as well as composition, microstructure, and mechanical properties of the end bulk products are also strongly affected by the characteristics of the starting HA powders, as clearly demonstrated[14]. Specifically, the best mechanical properties obtained in the latter study corresponded to sintered samples where the decomposition of HA to β-Tri-Calcium Phosphate (β-TCP) was avoided during SPS and the resulting microstructure was relatively finer.

In addition to these previous aspects, it should be noted that SPS also offers a rapid tool to obtain highly dense CaP products for subsequent characterization, particularly from the biological point of view. In this regard, it is well established that the behavior of CaP systems during *in-vitro* or *in-vivo* experiments depends on several interconnected physico-chemical factors, such as the material composition, surface/volume ratio, porosity, surface roughness, grains size, etc. [6]. For instance, it is reported that fully dense and highly crystallized HA samples tend to maintain unchanged their size in an organism for years. On the other hand, a porous HA material with the same composition could be entirely bioresorbed in less than one year[6] .As far as the influence of the composition of CaP samples is concerned, a recent study evidenced that β-TCP displays relatively lower ability, with respect to other bioceramics including HA, to promote the formation of new phosphate phases in the material surface during *in-vitro* (simulated body fluid without cells) and *in-vivo* (rabbit muscle sites) experiments[79]. Also sample roughness, which is directly associated to surface area, not only influences its dissolution rate but also cells adhesion[6].

In this context, some recent studies have been addressed in the literature to evaluate the behavior of different cell cultures with HA substrates obtained by SPS[92-95]. In particular, it was reported that rat mesenchymal stem cells cultured on HA samples prepared by SPS were able to undergo adhesion, proliferate and differentiate to osteoblasts similarly to the case when polystyrene dishes were used as substrate[92]. The response of human osteoblasts on spark plasma sintered disks with relative density up to 99.7% and grains size of about 80 nm was examined by Li and coworkers[93]. Their results

indicated that the use of nanostructured materials promotes initial cells attachment and spreading. This outcome was ascribed to the highly dense samples obtained which, in turn, determine a decrease of the surface energy which favours cells/substract contact. Along the same line, it was found that the use of nanostructured HA enhanced osteoblasts adhesion, cells proliferation and matrix mineralization with respect to the microstructured counterpart[94]. The behavior of a human fetal osteoblast cell line cultured on monophasic HA, HA-β-TCP composite, HA-1 wt.% SiO_2, and HA-5 wt.% SiO_2 bulk samples, all obtained by SPS, was also investigated[95]. The main feature evidenced in the latter study was the positive effect produced, in terms of cells differentiation, by the introduction of small amounts of SiO_2 in the bioceramics. Nonetheless, a positive biological response was exhibited by all the systems taken into account and no noteworthy differences were found in the morphology of cells attached to the surface of the different materials.

In the present Chapter, the behavior of SaOS-2 human cells when interfaced with three different nearly full dense calcium phosphate-based materials obtained by SPS is investigated in detail. Specifically, this work is mainly address to highlight the effects of the compositional and microstructural differences among the scaffolds, whereas discrepancies in the other possibly affecting parameters, particularly surface area and material porosity, are mitigated as much as possible. Several *in-vitro* tests are conducted to evaluate cell adhesion, morphology, viability, proliferation and matrix mineralization, using glass coverslips and polystyrene wells dishes as control materials. Particular attention will be devoted to the compositional/microstructural changes induced in the SPSed supports by their interaction with the osteoblast cells. It should be noted that the latter aspect is, to the best of our knowledge, almost unexplored in the literature. Indeed, the previously mentioned *in-vitro* tests performed by Xin and coworkers[79] to compare, with respect to the formation of calcium phosphates, the behavior of different bioceramics, were conducted using SBF medium without cells. In addition, such investigation was carried out on porous scaffolds instead of dense supports as in the present work.

4.2 Experimental

4.2.1 Preparation of dense samples

Dense CaP cylindrical disks (about 15 mm diameter, 3 mm thickness) were produced taking advantage of the SPS 515S model equipment shown in Figure 28. Three different calcium phosphate-based powders supplied by Plasma Biotal Ltd (Cod. CAPTAL 60-1), Alfa-Aesar (Cod. 36731), and Sigma-Aldrich (Cod. 21223) companies, respectively, were used as precursors. The corresponding sintered specimens produced for *in-vitro* experiments will be indicated as CaP_1, CaP_2 and CaP_3, respectively. The XRD analysis of the initial powders evidenced they all consisted of HA except for the Sigma-Aldrich material, where minor amounts of $CaHPO_4$ were also present. Further details of the powders characteristics and SPS experiments are reported elsewhere[14]. Briefly, the optimal holding temperatures (T_H) required for obtaining nearly full dense products for the three systems were identified when the holding time (t_H), the mechanical pressure (P), and the heating rate were maintained constant to 5 min, 30 MPa and 75 °C/min, respectively. Relative densities of the end-samples were evaluated by the Archimedes' method by considering the theoretical value for HA equal to 3.16 g/cm^3.

The composition of the sintered bioceramics was determined by XRD using the X-rays diffractometer (Philips PW 1830, Almelo, The Netherlands) equipped with a Ni filtered Cu K_α radiation (λ=1.5405 Å) reported in Figure 25.

The microstructure and local phase composition of the SPS samples, before and after the *in-vitro* experiments, were examined using the high resolution scanning electron microscopy equipment and UltraDry EDS Detector (Thermo Fisher Scientific, Waltham, MA, USA), respectively, shown in Figure 26. In particular, the microstructure of the SPS products was observed after chemically etching their surface for 10 s using a 3 vol.% HNO_3 solution.

On the other hand, before using them for *in-vitro* experiments, all SPSed products were first accurately polished following a standard protocol.

The residual surface roughness in the polished samples was determined using the Form Talysurf Intra 50 profilometer (Taylor-Hobson ltd., Leicester, UK) shown in Figure 55. The obtained topological data were then analysed with the Ultra Software (Taylor-Hobson, Leicester, UK). The evaluation of roughness parameters was performed on 4 different profiles for each sample. Measurements involve four different disks for each group of CaP specimens. In particular, the roughness parameter *Ra*, defined as the arithmetic average of the deviation of peak heights and valleys of the roughness profile from the mean line, was considered.

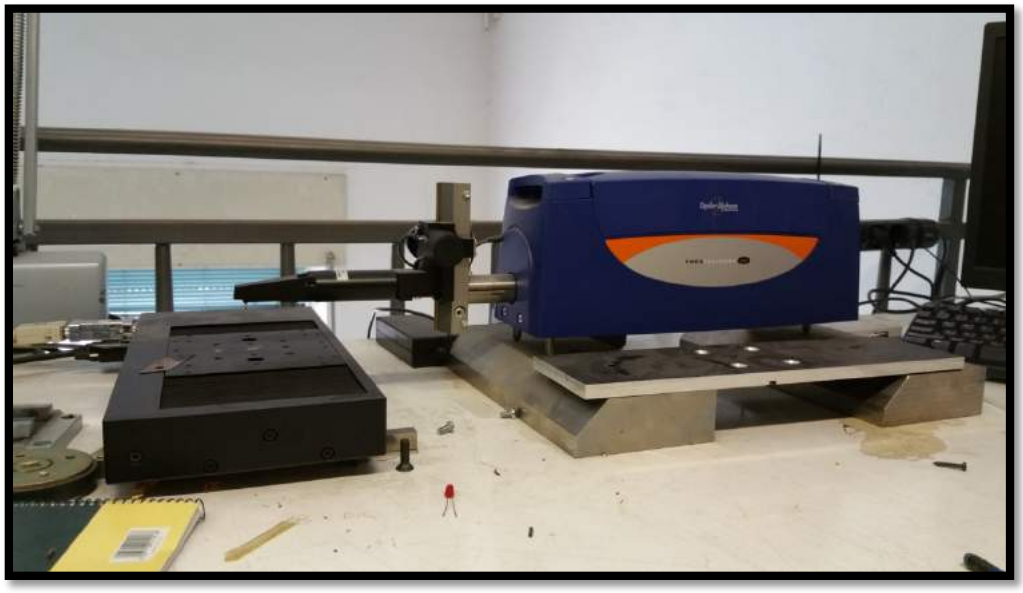

Figure 55. Talysurf intra 50 profilometer.

Wettability of polished CaP samples was determined by means of contact angle analysis using the Dataphysics Contact Angle system (mod. OCA 20, Filderstadt, Germany) reported in Figure 56. For the sake of comparison, the latter measurement was also carried out on glass coverslips (GS) and polystyrene wells without disks (PS) dishes used as control materials for *in-vitro* tests.

Figure 56. Dataphysics Contact Angle system OCA 20.

4.2.2 In vitro tests

4.2.2.1 Cell Culture

Osteosarcoma cell lines SaOS-2, purchased from Sigma-Aldrich (Sigma, St. Louis, MO, USA), were cultivated, according to the recommendations of the supplier, in McCoy's 5a medium containing 15% fetal bovine serum (FBS), 1% penicillin-streptomycin solution, 2 mM L-glutamine at 37°C in a humidified incubator with 5% CO_2. Medium and all supplements were also obtained from Sigma-Aldrich.

Prior to cell seeding, CaP disks were autoclaved at 120°C for 21 min, dried under UV for sterilization and then individually placed into the wells of a 24-well plate. Cells were then added to the top of each CaP disk at a density of $2x10^4$ cells/cm^2 with 0.75 ml media contained in each well. The cells cultured in glass coverslips and in polystyrene wells without disks were used as control. Triplicate samples per group were considered for all experiments.

4.2.2.2 Cell adhesion and morphological studies

The possible effect of the culture medium, in presence or without cultured cells, on the surface microstructure of CaP_1, CaP_2 and CaP_3 disks as well as the analysis of cells adhesion and cellular morphology on different samples was assessed through HRSEM imaging. Immediately fixed scaffolds without neither medium nor cells were used as control.

To this aim, scaffold disks and glass slides were immersed in 500 μL of the medium for 24 h or 14 days. Samples were then fixed in a mixture of glutaraldehyde 1.25% and paraformaldehyde 1% in cacodylate buffer 0.1 M (pH=7.2) for 20 min at room temperature. After rinsing in a phosphate buffer saline (PBS) solution, scaffolds were dehydrated with acetone, subjected to Critical Point Dry, mounted on an aluminum stub and sputtered with platinum (2 nm thickness) with an Emitech 575 turbo sputtering apparatus (Emitech Ltd., Ashford Kent, UK), which was suitably modified by Isola et al. [96] and Loy et al. [97]. Finally, samples were observed with a Hitachi S4000 FEG HRSEM operated at 15–20 kV. Image acquisitions were obtained by the software Quartz PCI v. 5 (Quartz Imaging Corporation, Vancouver, BC, Canada). Spectroscopy Elemental Isotope Analysis was performed by a UltraDry EDS Detector (Thermo Fisher Scientific, Waltham, MA, USA); data were collected by NSS3 Software v. 3.0 (Thermo Fisher Scientific).

Weight loss of CaP samples during their immersion for 14 days in culture medium without cells was also determined. Specifically, weighting of the specimens before and after the test was performed using a Sartorius analytical balance (± 0.00001 g precision).

4.2.2.3 Cell viability

The mitochondrial activities of the cells were evaluated using the Alamar Blue assay (Invitrogen, Italy) performed according to manufacturer's guidelines. The assay is based on detection of the metabolic activity of the cells, which chemically reduce the Alamar Blue, thus producing a color change from blue to red. Briefly, cells were seeded as previously described onto disks, glasses and polystyrene wells and left to grow for 10 days at 37°C with 5% CO_2. At the prescribed time points, 0.75 ml of fresh medium containing 10% Alamar Blue was added to each sample. Following 3.5 h incubation with the dye, absorbance was measured at 540 nm and 630 nm using the microtiter plate reader (BioTek EL800 plate reader, BioTek Instrument Inc, Winooski, VT, USA) shown in Figure 57.

Figure 57. BioTek EL800 Microtitier plate reader.

The number of viable cells was correlated with the magnitude of dye reduction and expressed as percentage of Alamar Blue reduction (% AB reduction). The calculation of the % AB reduction is carried out according to the manufacturer's protocol as follows:

$$\%AB\ reduction = \frac{(\varepsilon_{ox}\lambda_2)(A\lambda_1)-(\varepsilon_{ox}\lambda_1)(A\lambda_2)}{(\varepsilon_{red}\lambda_1)(A'\lambda_2)-(\varepsilon_{red}\lambda_2)(A'\lambda_1)} \times 100 \quad (2)$$

where, $\varepsilon\lambda_1$ and $\varepsilon\lambda_2$ are constants representing the molar extinction coefficient of AB at 540 and 630 nm, respectively, in the oxidized (ε_{ox}) and reduced (ε_{red}) forms. $A\lambda_1$ and $A\lambda_2$ represent absorbance of test wells at 540 and 630 nm, respectively, whereas $A'\lambda_1$ and $A'\lambda_2$ are the values corresponding to negative control wells measured at the same wavelengths. The %AB reduction data were corrected for background values of negative controls containing medium without cells.

4.2.2.4 Cell proliferation

As mentioned previously, SaOS-2 cells were plated onto disks, glasses and polystyrene wells at a density of $2x10^4$ cells/cm^2. Cells from three samples for each group were harvested day-by-day with the use of 0.1% trypsin (Sigma, St. Louis, MO, USA) and 0.04% EDTA (Sigma, St. Louis, MO, USA) for 6 min at 37°C. Action of trypsin was stopped with complete medium, and cells were counted using a hemocytometer (Burker Chamber, Bodanchimica, Cagliari, Italy).

4.2.2.5 Quantification of mineralization

Matrix mineralization was quantitatively evaluated on the basis of the formation of calcium phosphate by SaOS-2 cells using Alizarin red staining (ARS) based on the protocol described in literature[94]. Briefly, cells seeded onto disks, glasses and polystyrene wells, were rinsed with Dulbecco's PBS followed by fixation with ice-cold 70% ethanol for 1 h at –20°C. Afterwards, cells were washed and stained with 40 mM ARS solution (Sigma, St. Louis, MO, USA), at pH = 4.2 and room temperature, for 10 min. The washing procedure with PBS was continued till the cells were all clear off the stain debris. To quantify ARS retained in the cells, the latter ones were incubated at room temperature with 10% (w/v) CPC (Sigma, St. Louis, MO, USA) in 10 mM sodium phosphate at pH = 7 for 15 min.

The dye solution was transferred to a 96-wells plate to measure the absorbance at 540 nm. CaP disks without cells were used as background.

4.2.2.6 Statistical analysis

All quantitative experiments were performed at least three separate times. Data were presented as mean values ± standard deviation (SD). Comparison between different samples were made by the analysis of variance (ANOVA) using GraphPad Prism® 4.0 statistical software. An unpaired student's *t* test was used when only two groups were compared. Values were considered statistically different for p value < 0.05.

*4.*3 Results

4.3.1 Characterization of Sintered products

The samples obtained by SPS to be immersed in the biological medium either with or without cells during *in-vitro* experiments are listed in Table 6 along with the corresponding SPS temperatures and some relevant characteristics. The holding temperature sufficient to achieve for the CaP_2 system the complete powder consolidation in 5 min is found to be 900°C, whereas relatively higher thermal level (1200°C) are needed when the other two compositions are taken into account.

Furthermore, the XRD patterns relative to the surface of the resulting sintered specimens (Figure 58) evidenced that CaP_1 and CaP_2 still entirely consist of HA. In this regard, it was observed that while XRD peak intensities relative to sintered CaP_1 follow the same order of that one of the starting powders, which fits to the JCPDS card (74-0565) for HA, a different behaviour was displayed by the CaP_2 system. Indeed, while the angular positions of XRD reflections are still the same, a change in the sequence of peaks height was correspondingly observed subsequent to the SPS process. Such feature can be ascribed to the presence of a preferential orientation of HA crystalline planes in the

CaP_2 product, which is likely induced by the application of an electric field during sintering of fine powders. To support the latter statement, it should be noted that, when the sintered product was reduced in powder form, peaks sequence followed perfectly that one of the JCPDS card (74-0565) to indicate that the preferential orientation of the crystalline planes was consequently lost[14]. Further detailed investigation on this specific subject are currently in progress. Nonetheless, its explanation is beyond the scope of the present thesis.

More important is to underline the marked decomposition of HA during SPS to form β-TCP, when considering the CaP_3 system. Specifically, the XRD analysis indicated that the resulting massive product is mainly composed of β-TCP with minor amounts of HA and $CaHPO_4$, that was also originally present in the powders[14].

The HRSEM micrographs of the chemically etched samples, also shown in Figure 58, clearly evidenced that the three CaP materials display significant differences in their microstructures after sintering. In particular, CaP_1 consists of about 2 μm sized HA grains and exhibits a good resistance to the chemical etching. On the other hand, a relatively finer microstructure, where the size of HA grains is well below the sub-micrometer level, is obtained for the CaP_2 material. Finally, a completely different microstructure is displayed by the CaP_3 system. Indeed, the decomposition of HA to β-TCP occurring in the latter case led to SPS products with grains slightly larger than CaP_1, and the material was markedly altered after exposure to chemical etching.

To better highlight the effects of products composition and microstructure on cells behavior, the influence of other possibly affecting parameters, such as surface roughness, which are expected to play a role in this context have been minimized in the present work. Thus, the three groups of samples produced by SPS for *in-vitro* tests were all first finely polished. As expected, the resulting residual roughness was generally very low, although the control materials display relatively higher smoothness (cf. Table 6). In addition, when the comparison is only confined to the SPS products, the lower *Ra* value was obtained for the CaP_2 system.

System	Starting powders	T_H (°C)	ρ (%)	Composition	Grain size (µm)	Roughness, Ra (nm)	Contact Angle (°)
CaP_1	Plasma Biotal Ltd (Cod. CAPTAL 60-1)	1200	>99.9	HA	1-1.5	67±3	75.7±0.1
CaP_2	Alfa-Aesar (Cod. 36731)	900	>99.9	HA	0.5-0.6	38±6	61.0±0.5
CaP_3	Sigma-Aldrich (Cod. 21223)	1200	97.45±0.2*	Main phase: β-TCP Minor phases: HA, $CaHPO_4$	2-2.5	75±2	83.5±0.2
GS	Thermo Fisher Scientific (Cod. CB00140RA1)	-	-	-	-	30±2	74.2±0.6
PS	Techno Plastic Products (Cod. 92424)	-	-	-	-	26±3	32.8±0.2

*This value was determined by considering the theoretical density for HA (3.16 g/cm^3)

Table 6. Characteristics of calcium phosphate based materials investigated in this work.

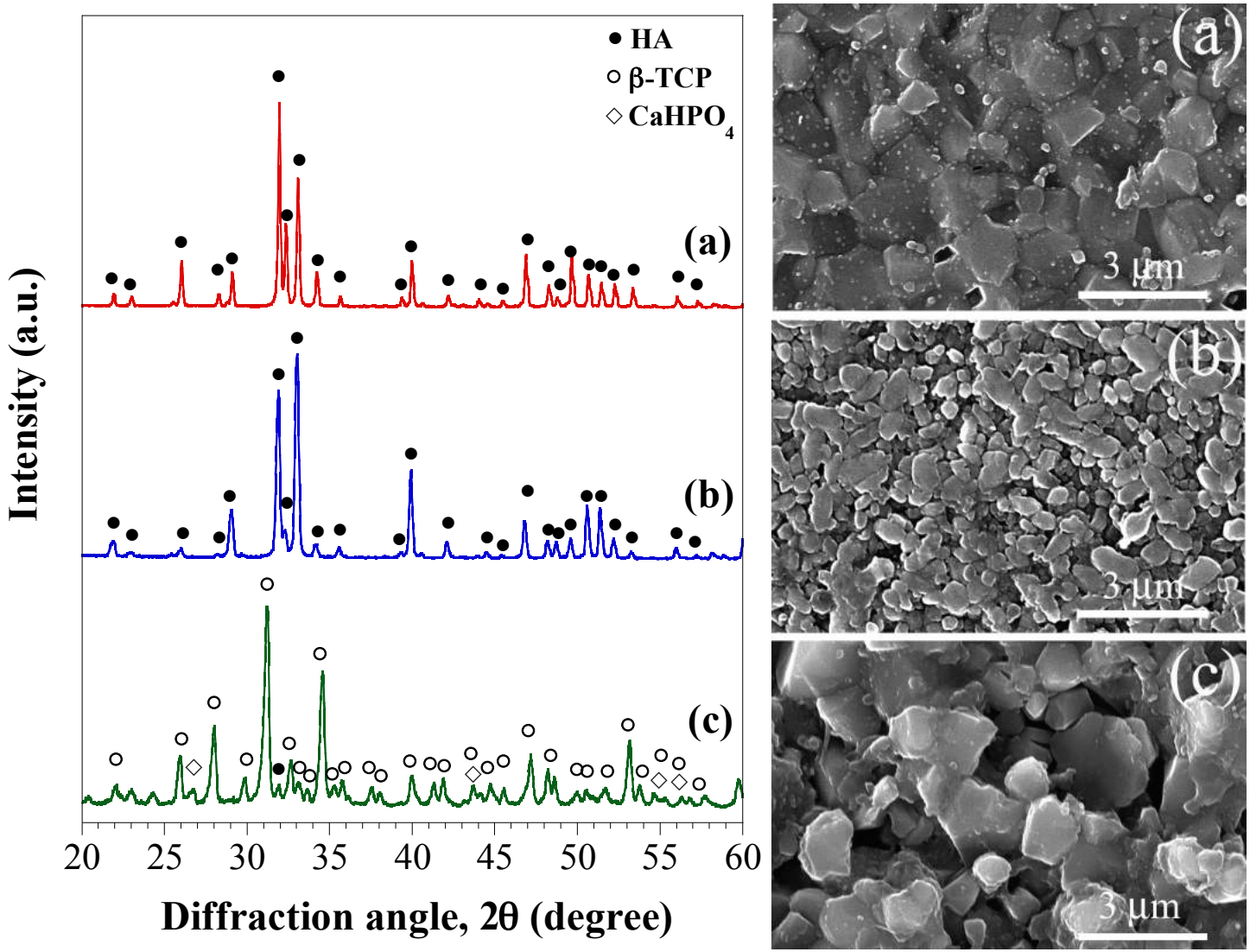

Figure 58. XRD patterns and SEM micrographs (after chemical etching) of the fully dense calcium phosphates based products to be considered for *in-vitro* tests:

(a) CaP_1, (b) CaP_2 and (c) CaP_3.

The wettability behavior of the three CaP products can be deduced by the corresponding contact angles reported in Table 6 along with those ones obtained for the tissue culture PS and GS dishes used as control. It is seen that the considered systems display their wettability in the following decreasing order: PS > CaP_2 > GS > CaP_1 > CaP_3.

4.3.2 Cells adhesion and morphology

Osteoblasts adhesion to the different substrates was examined by HRSEM at 24 h and 14 days after seeding. As shown in Figure 59, no significant differences in cell-adhesion capability on the three CaP surfaces, as well as on glass coverslips used as control, were observed after 1 day culture. In particular, cells were found well anchored to all CaP samples, exhibiting a flattened appearance with a polygonal morphology, even if few osteoblasts showed a spherical shape with blebs and short filopodia.

On the other hand, SaOS-2 cells cultured for 14 days display different morphologies, as evidenced in Figure 60. Specifically, a certain number of cells labeled 1 in Figures 60(a)-60(c) shows a rounded shape. Their external surface is, in few cases, smooth while, more frequently, displays an irregular morphology, characterized by the presence of several blebs. Moreover, numerous thin filopodia originated from the cell spread roughly along the radial direction towards the scaffold surface. Two additional classes of cells, both showing a star-shaped morphology with linear or polygonal soma, indicated with 2 and 3, respectively, can be also identified in Figures 60(a)-60(c). In particular, type 2 cells display a “Ω shape” with distal part flattened and the central side bulged.

On the other hand, cells labeled 3 are mostly flattened. Numerous elongated filopodia extend from the edge of these cells to the substrate surface. Some bleps are observed in the cellular membrane especially in type 2 cells. The features described above are better evidenced in Figure 61, where some detailed views of the three classes of osteoblasts after 14 days culture are reported.

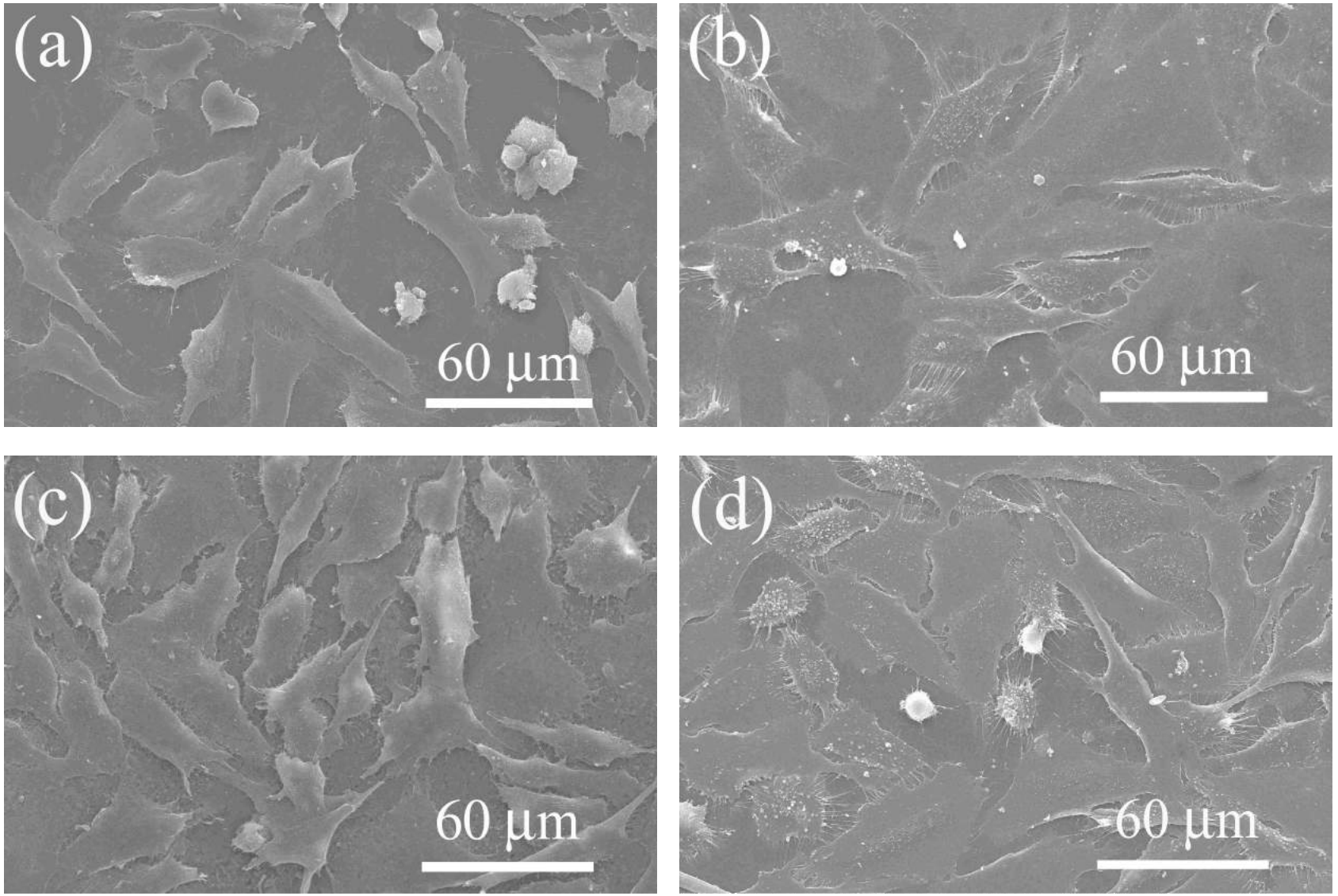

Figure 59. HRSEM micrographs of Saos-2 cells after 24 h seeding on different substrates: (a) CaP_1, (b) CaP_2, (c) CaP_3, and (d) GS control.

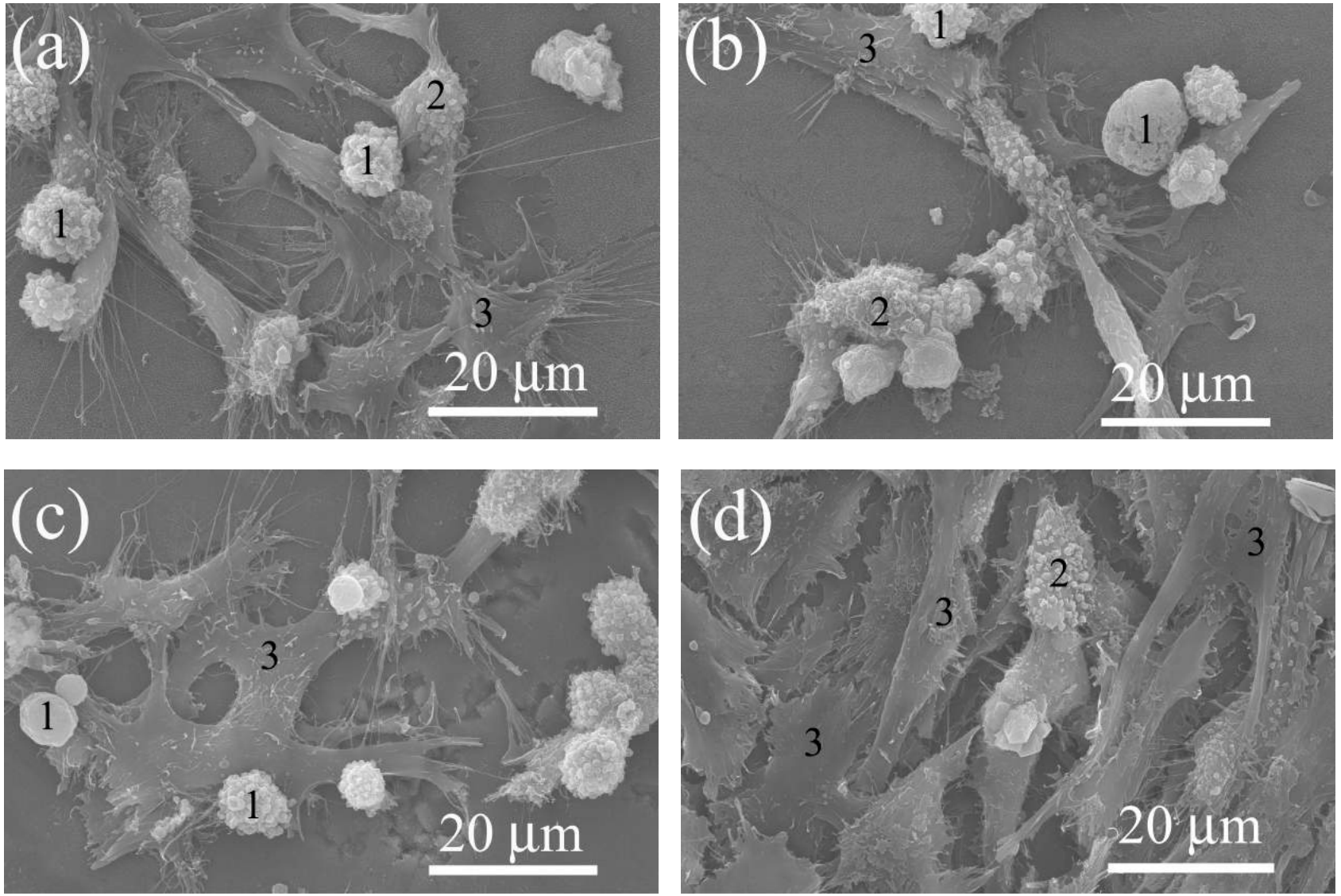

Figure 60. HRSEM micrographs of SaOS-2 cells after 14 days seeding on different substrates: (a) CaP_1, (b) CaP_2, (c) CaP_3, and (d) GS control.

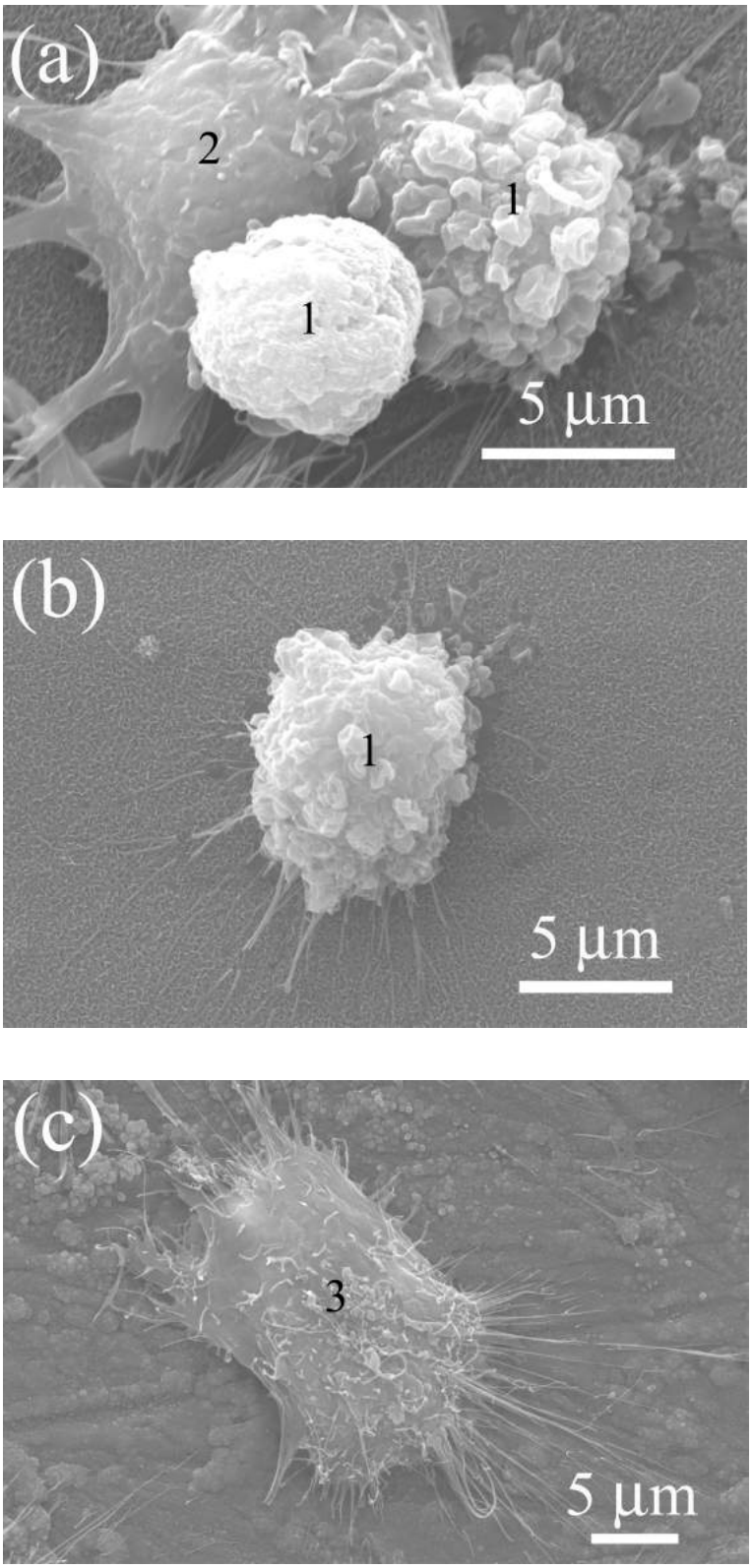

Figure 61. Detailed HRSEM micrographs of the osteoblasts cells contacted for 14 days on the surfaces of the three different CaP samples: (a) CaP_1, (b) CaP_2, and (c) CaP_3.

It should be noted that the three kind of morphologies previously described, e.g. rounded, Ω-shaped and flat, are generally observed at the same time within each sample. Moreover, different types of cells appear often connected each other through filopodia. Finally, when GS slides were used, large, flat and polygonal osteoblasts, belonging to the type 3 cells category, are mainly detected on the substrate surface (Figure 60d).

4.3.3 Cell viability

The viability of SaOS-2 cells on CaP disks, glasses and polystyrene wells was assessed using the Alamar Blue assay. The obtained results, expressed in terms of dye reduction according to Eq. (2), are reported in Figure 62. It is observed that cells activity progressively increases up to 8 days, while remains about constant as the culture time was further prolonged to 10 days. The latter feature was somehow expected, since the dye, whose initial amount is the same regardless the time point considered, tends to reduce completely as the cells number increases. Furthermore, Figure 62 also evidences that the different CaP samples and control substrates behave similarly, to manifest their comparable ability to keep cell viability after seeding.

4.3.4 Cell proliferation

Osteoblasts growth after their seeding on CaP disks, glass coverslips and polystyrene well, was monitored by direct cells counting at various time points using a hemocytometer. As shown in Figure 63, the SaOS-2 cells continuously proliferated on the different supports as the culture time was increased up to 21 days. However, as indicated by Figure 63, the number of cells interfaced with CaP_2 disks from the seventh to the fourteenth day of incubation was apparently lower with respect to the other samples. Nonetheless, when the culture time was further extended to 21 days, the number

of osteoblasts became similar for the three CaP systems as well as for GS slides, while relatively fewer cells were detected on the PS support.

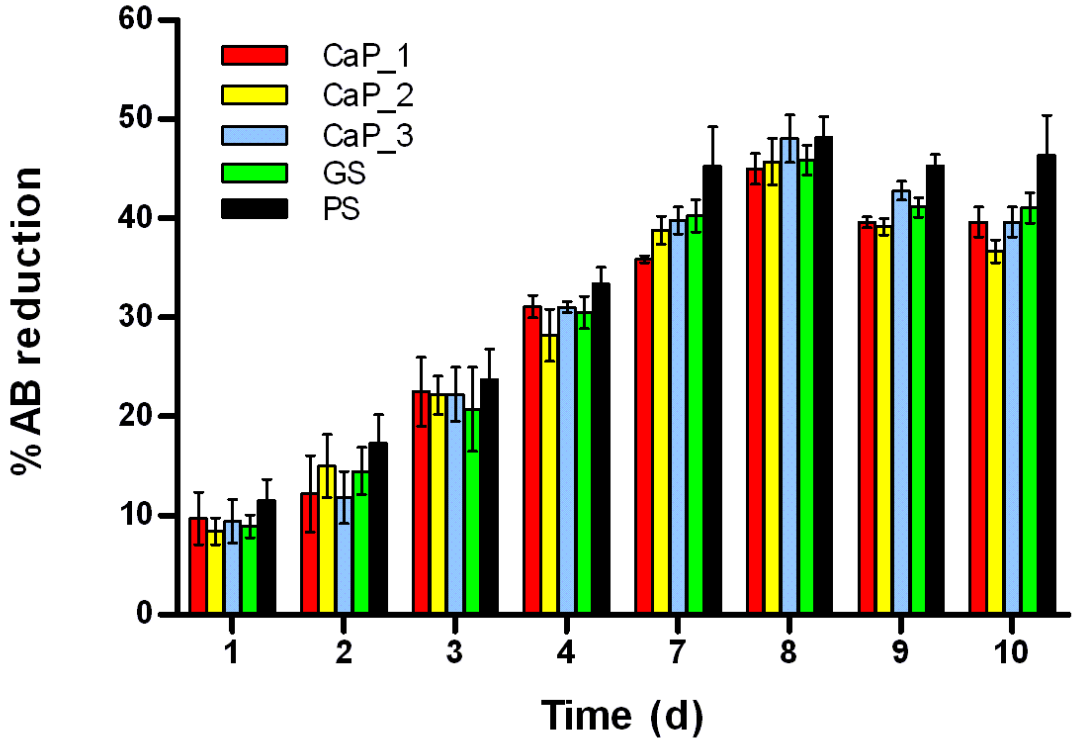

Figure 62. Temporal changes in the percentage reduction of Alamar blue dye (cf. Eq.(2)). The data are shown as the mean value ± standard deviation (SD) of three independent experiments.

4.3.5 Quantification of mineralization

In the present study, mineralization of matrix by SaOS-2 osteoblasts was assessed by quantifying calcium deposition on disks using a modified Alizarin red method. Figure 64 shows the absorbance values measured at 540 nm for the different substrates seeded with SaOS-2 cells at prescribed time intervals. It is possible to state that during the first 10 days incubation, a similar amount of calcium was detected in all CaP samples, albeit that one revealed in GS and PS controls was relatively higher.

However, the situation changed completely for prolonged culture times. Indeed, a significant increase in calcium deposits was manifested after 14 days culture in CaP_1 and, particularly, CaP_2 samples, whereas only negligible changes were observed in CaP_3 disks as well as GS coverslips and PS wells. This outcome was even more enhanced when examining Alizarin red staining data after 21 days in culture. Therefore, the capability of SaOS-2 cells to generate mineralized matrix in presence of the three calcium phosphate systems, as provided by the corresponding absorbance measurements at 540 nm, was in the following decreasing order: CaP_2 >> CaP_1 > CaP_3.

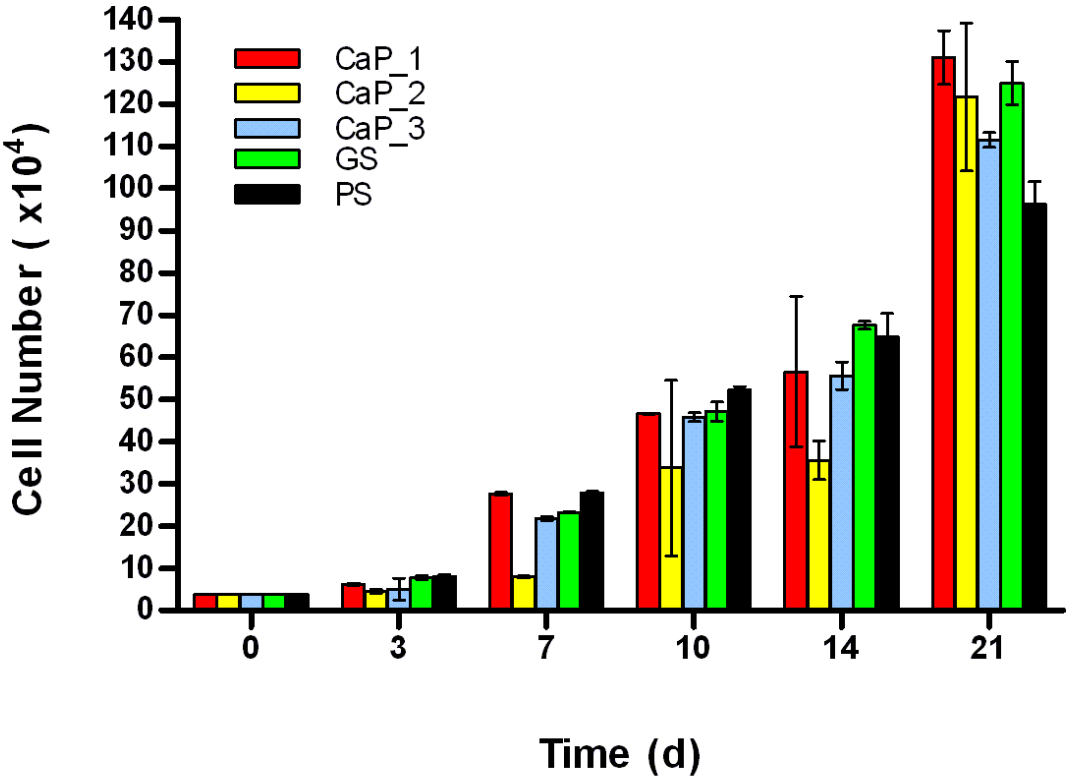

Figure 63. Osteoblasts growth on the surface of the various CaP and control substrates. Cells number was calculated at days 0, 3, 7, 10, 14, and 21 by counting cells with a hemocytometer. The data are shown as the mean value ± standard deviation (SD) of three independent experiments.

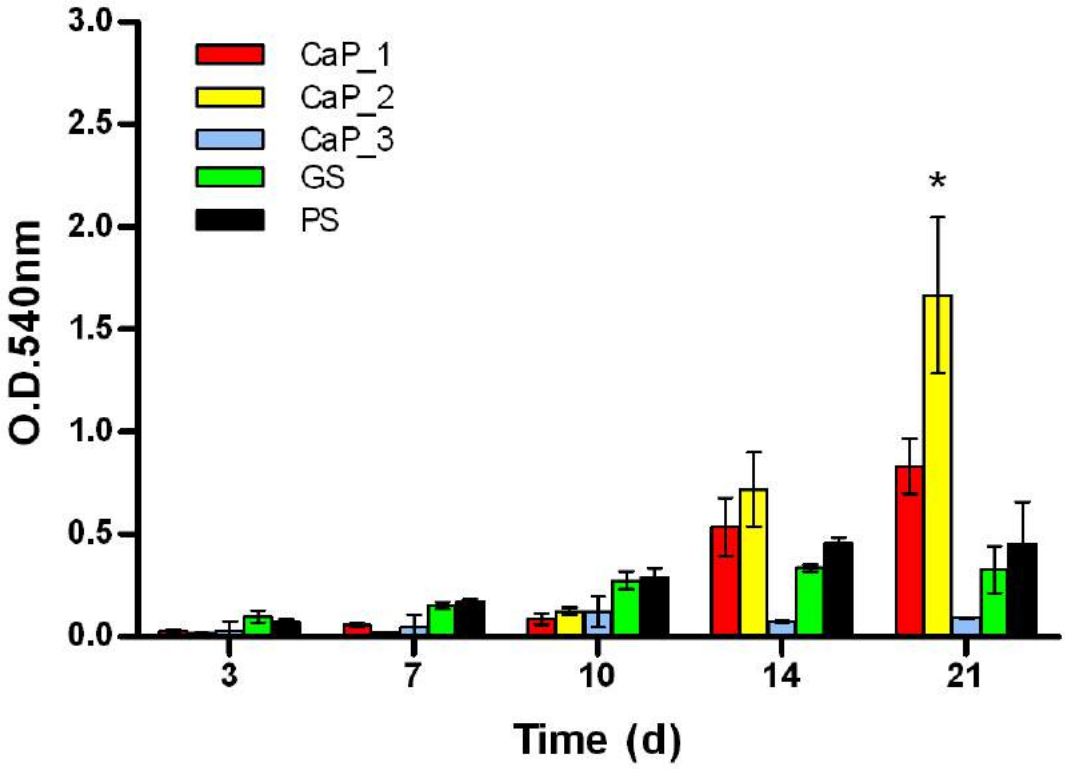

Figure 64. Quantification of mineral deposition by Alizarin Red-S staining. The data represent the mean value ± standard deviation (SD) of three independent experiments. Statistical analysis was compared between CaP_1, CaP_2, CaP_3, GS and PS. * $p<0.05$ after student's *t* test.

4.3.6 Microstructural changes in substrates surface

The possible formation of new phases on the surface of CaP disks as a result of their interaction with cells and/or culture medium was first ascertained by XRD analysis. The related patterns, corresponding to samples immersed for 14 days, are compared in Figure 65. No additional phases, other than those ones originally present in the substrates surface (cf. Figure 58(a)), could be detected by this analysis. Nonetheless, it should be noted that HA peaks appearing in XRD patterns of CaP_1 and CaP_2 samples are relatively broaden, as compared to those ones recorded prior the *in-vitro* tests. In contrast, no noteworthy changes in this regard are found when considering the CaP_3 specimens.

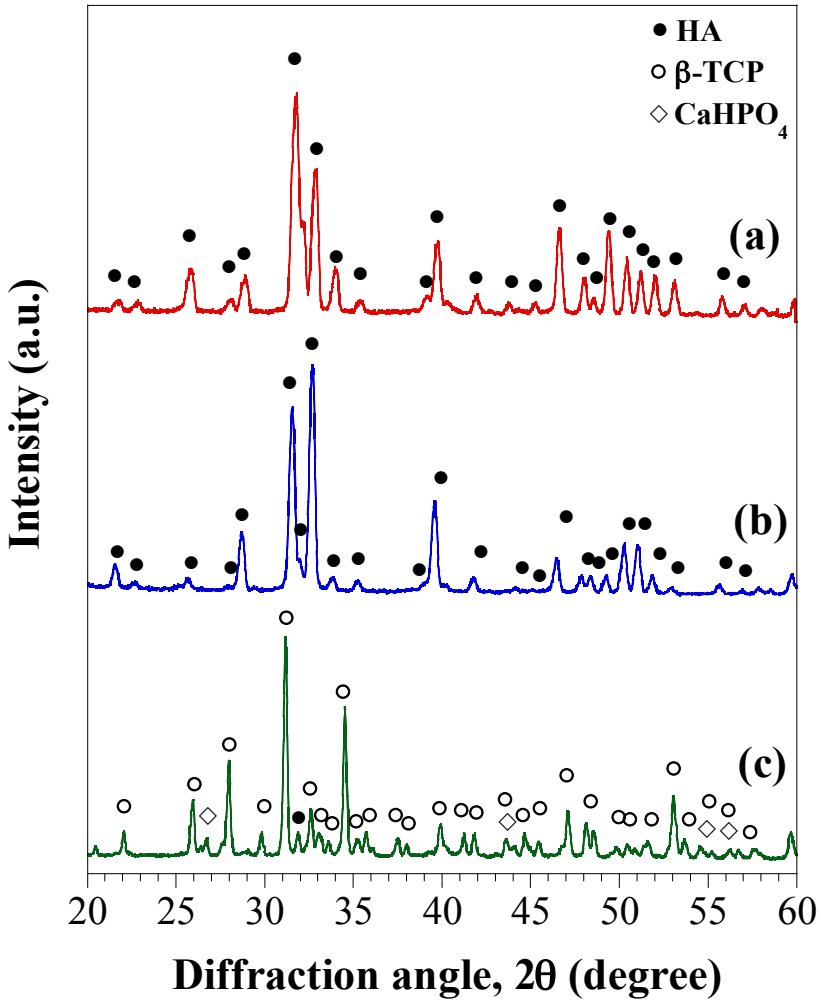

Figure 65. XRD patterns of calcium phosphates based products after 14d cells culture: (a) CaP_1, (b) CaP_2 and (c) CaP_3.

To better assess the previous issue, the three classes of CaP supports were examined in detail by HRSEM. In particular, this study involved not only samples interfaced with osteoblasts for a certain time period, but also specimens exposed to the culture medium without SaOS-2 cells. This experiment was specifically aimed to evidence the specific role played by the cells during the *in-vitro* test.

Some representative HRSEM images relative to CaP disks after 14 days incubation with osteoblasts are shown in Figures 66-68. No differences can be deduced from these micrographs when CaP surfaces are immersed for 2 weeks in the culture medium without cells. On the contrary, the CaP_1 surface undoubtedly show a marked modification in its morphology after 14 days of cell culture

(Figure 66). Specifically, the presence of a new layer which covers the surface of the scaffold can be clearly seen. Moreover, such layer consists of submicrometer sized grains with a lamellar distribution, well-organized and oriented as a net, similarly to trabecular bone structures (Figure 66c).

A similar situation is encountered in Figure 67, when considering the CaP_2 samples, although some differences can be evidenced. Indeed, in the latter case, the lamellar-shaped grains of the novel phase deposited on the scaffold surface are relatively finer and appear less oriented and organized with respect to the CaP_1 system. Nonetheless, based on the XRD results previously described, it is possible to state that the layer observed on both CaP_1 and CaP_2 supports is made of hydroxyapatite. Such statement was confirmed by EDS analysis as well as by XRD analysis reported in Figure 65.

In the latter regard, it should be noted that the finer grains composing the apatite layer are responsible for the XRD peaks broadening observed after the *in-vitro* experiments involving CaP_1 and CaP_2. On the other hand, no advisable morphological modifications can be seen when examining the HRSEM micrograph reported in Figure 68 relative to the β-TCP rich CaP_3 system. Also this outcome is consistent with the negligible variation of the scaffold composition after the *in-vitro* test, as evidenced by the corresponding XRD pattern shown in Figure 65.

Immersion tests of CaP samples in culture medium without cells were also useful to make a comparison between their possible weight changes. All the disks were found to decrease their weight during the test. Specifically, the values obtained after 14 days immersion for the CaP_1, CaP_2 and CaP_3 specimens, were 0.015±0.001, 0.025±0.001, and 0.24±0.13%, respectively.

Important features regarding the formation of the new apatite phase on the surface of CaP_1 and CaP_2 specimens can be ascertained when examining in detail their interaction with cells. As an example, a HRSEM micrograph related to the case of the CaP_1 system after 14 days culture is shown in Figure 69.

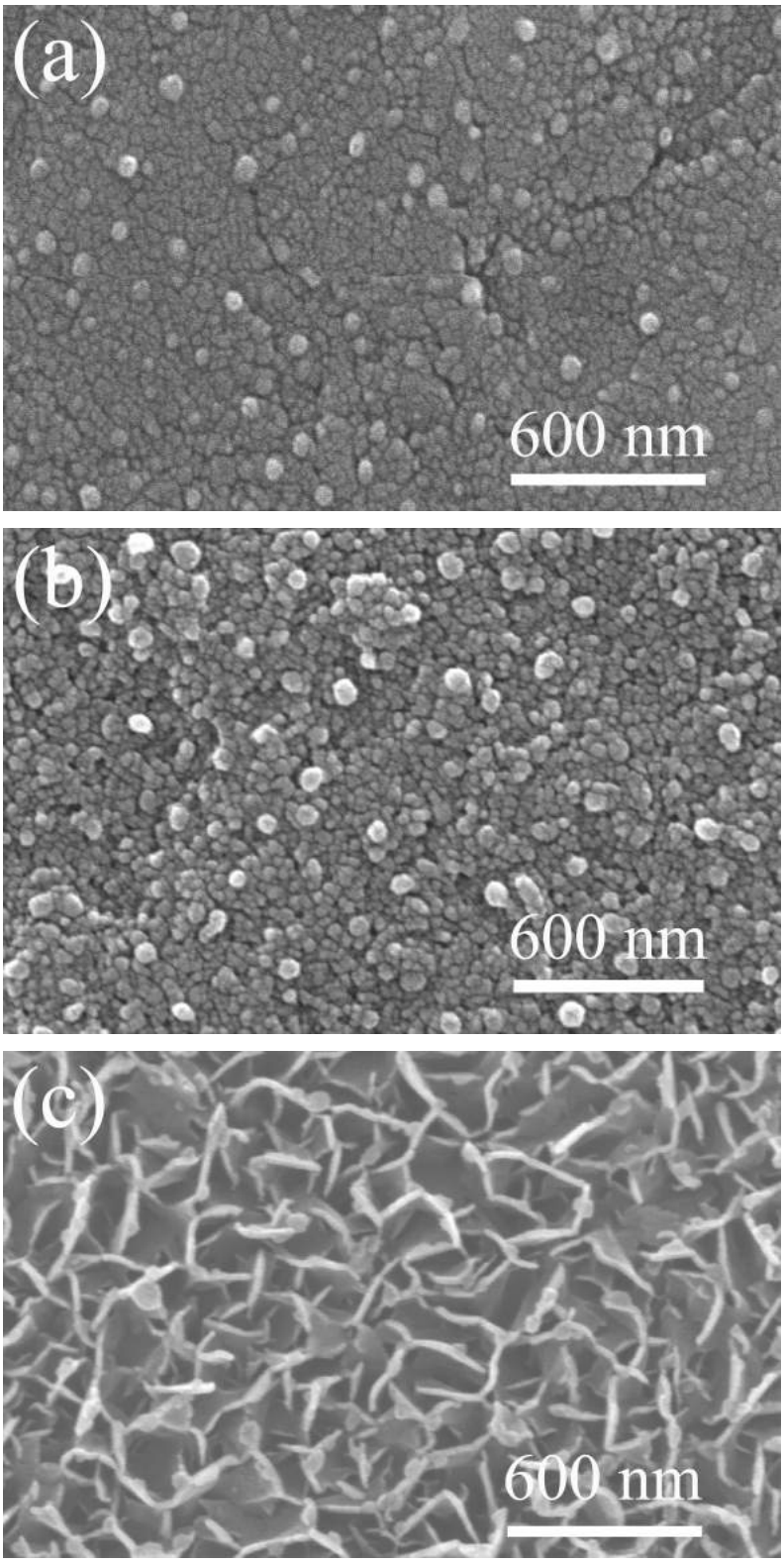

Figure 66. HRSEM micrographs relative to CaP_1 samples considered for *in-vitro* tests: (a) initial conditions, after being contacted for 14 days with the culture medium (b) without cells or (c) in presence of SaOS-2 osteoblasts.

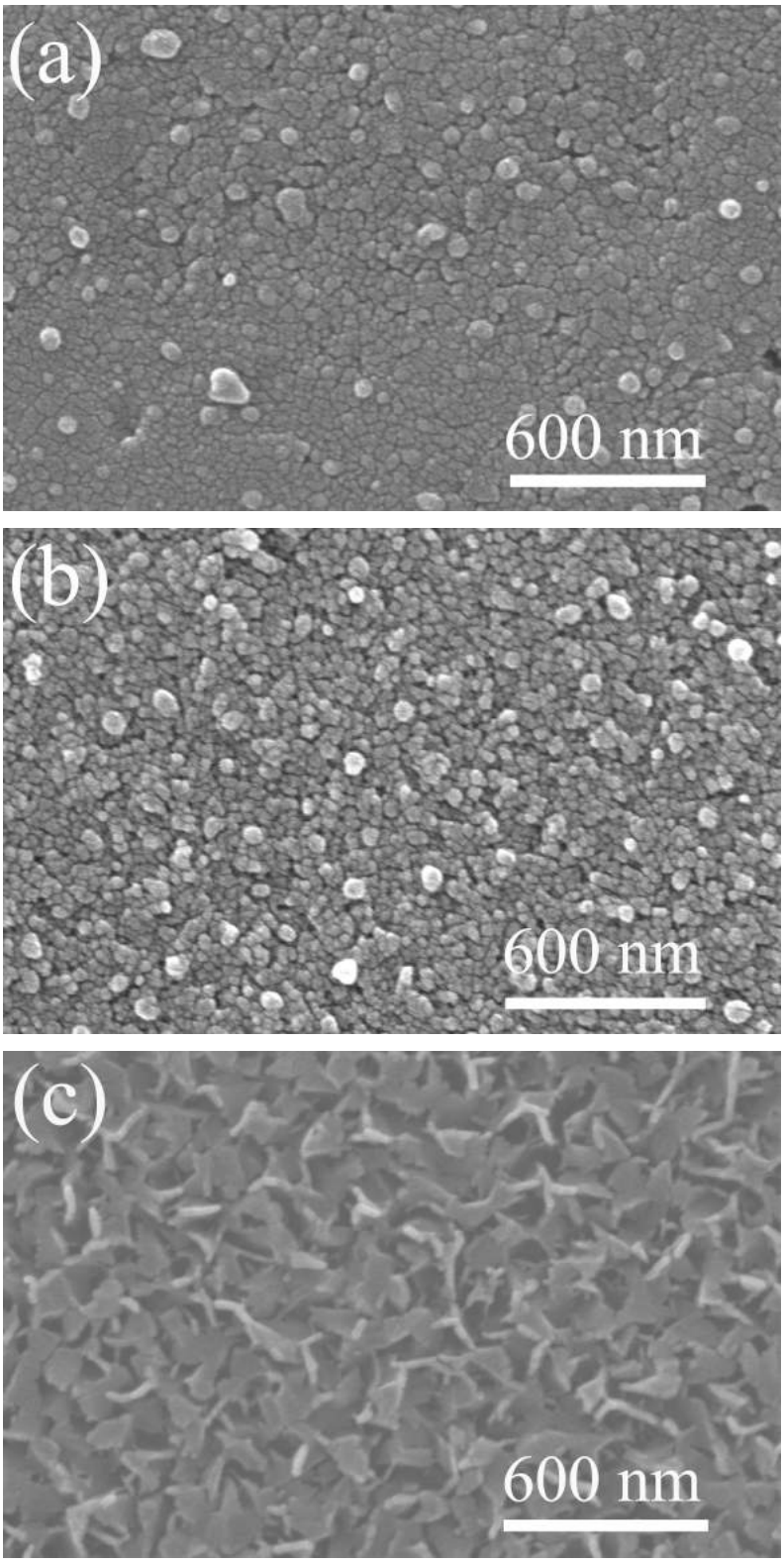

Figure 67. HRSEM micrographs relative to CaP_2 samples considered for *in-vitro* tests: (a) initial conditions, after being contacted for 14 days with the culture medium (b) without cells or (c) in presence of SaOS-2 osteoblasts.

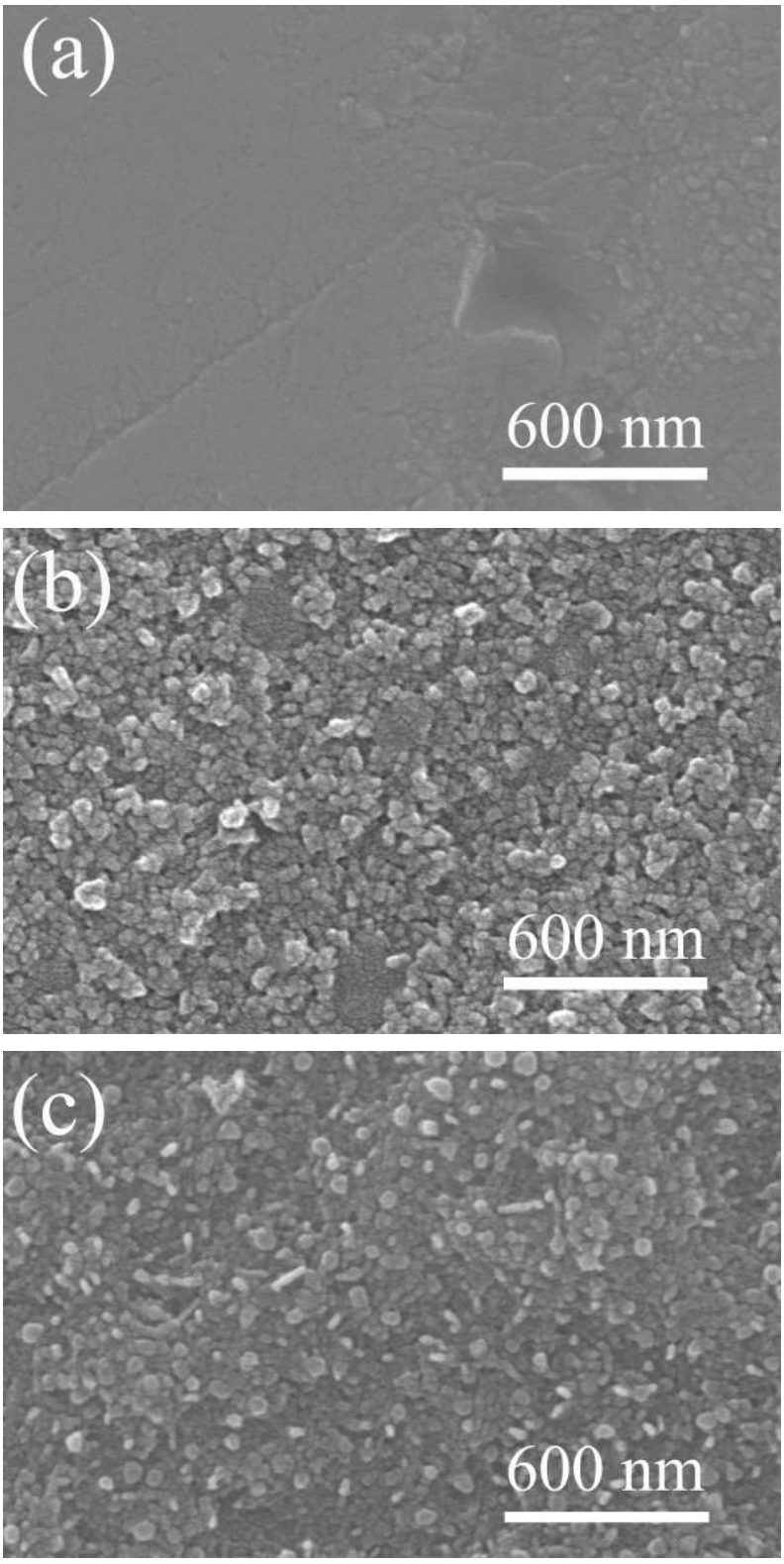

Figure 68. HRSEM micrographs relative to CaP_3 samples considered for *in-vitro* tests: (a) initial conditions, after being contacted for 14 days with the culture medium (b) without cells or (c) in presence of SaOS-2 osteoblasts.

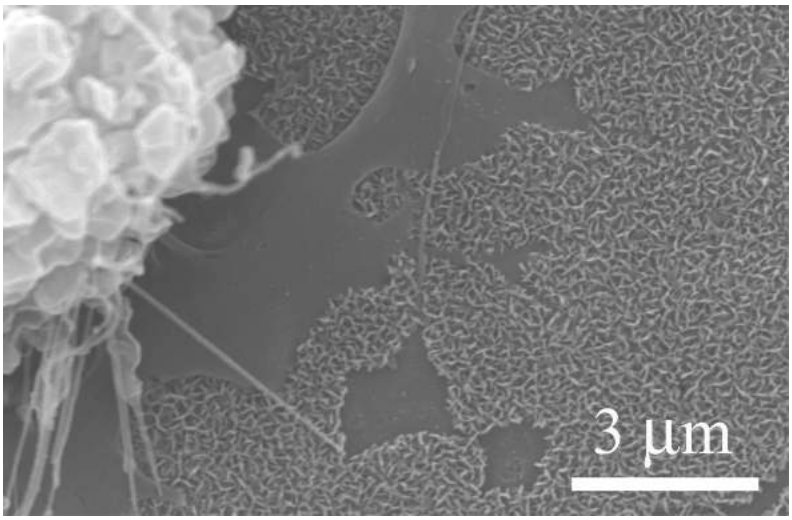

Figure 69. Detailed HRSEM micrograph showing the interaction cell-substrate for the case of the CaP_1 system after 14 days culture.

This image provides a clear evidence of the fact that the synthesis of the apatite layer, exhibiting the organized net structure shown in Figure 66c, is the result of the interaction of the SaOS-2 cells with the scaffold surface. In particular, the micrograph reported in Figure 69 shows how thin and long filopodia, starting from blebs, as well as flat branched expansions of the cells, extend, take contact and interact directly with the substrate. Analogous results are obtained for the case of CaP_2 samples.

4.4 Discussion

It is well established that the interaction between cells and biomaterials depends not only on their composition but also on surface area, porosity degree, microstructure, morphology and other aspects[6]. Consequently, the discussion of the results obtained during *in-vitro* experiments has to be preceded by the detailed examination of the samples prior the tests.

As described in Section 4.3.1, the use of highly pure and fine powders, allowed us to obtain completely dense, monophasic and relatively fine grains sized CaP_2 materials at only 900°C by SPS.

This holds also true for the CaP_1 system, except for the higher sintering temperature (1200°C) required by the relatively coarser powders to achieve their complete consolidation. On the other hand, the preparation of CaP_3 specimens was negatively affected by the presence of impurities ($CaHPO_4$) in the initial powders, which made them thermally unstable, so that the transformation of HA → β-TCP went almost to completion during the SPS process. In this regard, it should be noted that, consistently with its effective composition, the density of the obtained CaP_3 material approaches the calculated theoretical value for β-TCP, i.e. 3.066 g/cm^3[98], while the data reported in Table 6 are all referred to that of HA (3.16 g/cm^3).

Table 6 also indicates that CaP_1 and CaP_3 consisted of few micrometer sized grains, whereas CaP_2 displayed a relatively finer microstructure with average grains size down to about 500 nm.

Roughness surface might play an important role in the initial cells adhesion to the samples. In this regard, the preliminary polishing step made all the specimens to be exposed to the biological environment very smooth, although some differences were found. In particular, comparable *Ra* values were obtained for CaP_1 and CaP_3, whereas this parameter was relatively lower for the CaP_2 counterpart (cf. Table 6). Such discrepancies can be readily associated to the differences in samples microstructure, as discussed above.

Although the three categories of CaP specimens did not exhibit noteworthy differences in the measured contact angles, which provide an indication of the relative hydrophilicity (or hydrophobicity) of the various surfaces, the phosphate system with the relatively higher wettability is the CaP_2 bioceramic. On the other hand, PS dishes exhibit a significantly lower contact angle, whereas the values measured for GS slides were comparable to those one relative to CaP disks.

Based on the considerations above, two different groups of fully dense calcium phosphate samples, i.e.:

a) CaP_1 and CaP_3, with different composition but similar grains size, roughness and wettability

b) CaP_1 and CaP_2, entirely composed of HA while displaying different microstructures, roughness and wettability properties,

are made available for *in-vitro* experiments, whose results will be discussed in what follows.

The CaP_3 material, rich in β-TCP, was found to display a significantly higher dissolution extent in the culture medium with respect to the other two monophasic HA systems, which show a similar behavior. Such outcome is consistent with the hierarchy in the dissolution kinetics reported in the literature for CaP systems, i.e. β-TCP>>HA[6].

The different morphologies of SaOS-2 cells observed in Figure 60 and 61 could be related to the life-time and adhesion of the cells to the substrate. In particular, after 1 day in the media, cultured cells show a polygonal flattened morphology, to evidence their vitality, differentiation and good adhesion to the scaffolds. Based on previous studies[99,100], the spherical shape observed in few cells after 1 and 14 days suggests their good proliferative capability. For instance, a similar morphology was observed in rat osteoblast cells after 2h adhesion on supports[99]. The change in cells morphology during *in-vitro* tests is a well known phenomenon in the literature**.** For instance, normal human diploid WI-38 cells were found to modify their shape depending on time adhesion onto glass surface[101]. Specifically, at the beginning of the test, cells displayed a spherical or ovoid shape with blebs, while the development of filopodia and flattening of the entire cell was observed to occur only subsequently to their adhesion to the substrate. Some of the blebs persisted in the cellular membrane above the nucleus.

In the present thesis, filopodia are found to start from blebs mainly located on the cellular surface interfaced with scaffolds, while blebs on the free side of the cell persist, especially in correspondence of the nucleus. This feature can be probably ascribed to the characteristics of the scaffolds considered in this work, i.e. flat and fully dense, so that blebs on the opposite side of the cells membrane are filopodia free or able to produce only short filopodia. Indeed, the interaction between medium and cells, with possible growth of filopodia in additional directions with respect to the case of smoothly

polished and highly dense substrates, is favoured by the presence of porosities in the scaffolds[100]. Nonetheless, the fabrication and characterization of porous scaffolds is far beyond the scope of this thesis.

Cell viability and proliferation were assessed by Alamar Blue assay and counting cell number, respectively. The results of the Alamar Blue test show a good and comparable ability of all the examined surfaces to sustain cells metabolic activity. On the other hand, some differences in the behaviour of the considered scaffolds are found when considering proliferation data. First of all, the modest variation in cells number observed up to the third day (cf. Figure 63) could be associated to an adaptation phase for the osteoblasts, where the activity of the latter ones is mostly aimed to the production of extracellular matrix proteins rather than to cellular proliferation[102] [Dos Santos et al., 2007]. Nonetheless, a significant increase of cells number was revealed for all surfaces, except for CaP_2 disks, after 7 day of culture. Such different behaviour among the three CaP supports holds also true after 10 and 14 days. In this regard, it was reported in the literature[103.104] that the thermal levels to which HA powders are exposed during sintering, which are different for the case of the CaP_2 substrate (900°C) with respect to the other two CaP_1 and CaP_3 bioceramics (1200°C), could affect cells proliferation. In particular, when SaOS-2 osteoblasts were cultivated up to 12 days onto HA ceramics, cells growth rate was observed to increase as the sintering temperature was progressively augmented from 800 to 1200°C[104]. The latter outcome was justified by the authors on the basis of the results obtained in a previous study[103], where the interaction up to 2 days of a human monocytic cell line with HA samples sintered at 1180°C was higher with respect to that displayed by specimens processed at 600°C, which were found to generate relatively higher toxic effects during *in-vitro* tests.

Such outcomes are consistent with the results obtained up to 14 days in the present investigation, albeit the initial powders, sintering conditions, samples characteristics and *in-vitro* tests are rather different in this study. Nonetheless, Figure 63 shows that when the interaction between cells and

scaffolds was prolonged to 21 days, i.e. far beyond the time intervals considered by Laquerriere et al.[103] and Wang et al[104], cells number was about the same for all the CaP systems investigated in this work. This feature indicates that the use of the CaP_2 scaffold does not suppress osteoblasts growth, while only determines a certain extension of the adaptation time period. In conclusion, it is possible to state that the response of the SaOS-2 cells when interfaced with the three bioceramics for relatively long culture times is good and quantitatively similar in terms of proliferation rate.

Furthermore, it is worth noting that the data plotted in Figure 63 also show that cells growth on CaP samples is generally comparable, for contact times equal or shorter than 14 days, or even superior, after 21 days, with respect to PS well dishes. In contrast, it was reported that the proliferation of a phenotype of mouse MC3T3-E1 osteoblasts was markedly lower on the surface of 99.9% dense HA in comparison with plastic surfaces[105]. In this regard, it should be noted that, with respect to the present study, much more severe sintering conditions were adopted by Shu et al. [105] to obtain the HA scaffolds, i.e. (1360°C, 4h), which might negatively affect cells growth. Furthermore, Shu et al. [105] made the comparison for contact times up to 6 days, whereas the superior proliferation rate on the CaP surfaces with respect to PS well dishes was mostly manifested after 21 days in culture (cf. Figure 63). This feature likely justifies the discrepancies discussed above among the two studies.

Nonetheless, based on alkaline phosphatase activity measurements, Shu et al. [105] evidenced superior ability of MC3T3-E1 osteoblasts to produce mineralized matrix when seeded for 15 days on HA samples, instead on plastic supports. This outcome is consistent with the results shown in Figure 64 relative to the Alizarin Red-S staining test carried out in the present thesis. Indeed, the amount of mineralized matrix produced when using the samples consisting of HA only, i.e. CaP_1 and CaP_2 materials, was significantly higher with respect to that generated on PS supports. More important, it is seen that the three CaP scaffolds displayed a markedly different behavior, particularly for time periods equal or longer than 14 days. More specifically, it is possible to state that mineralization phenomena are highly promoted on scaffolds composed of HA only, whereas the opposite effect is

produced by the presence of β-TCP phase, the main constituent of CaP_3 disks. Furthermore, the data plotted in Figure 64 also evidenced that the SaOS-2 cells displayed a higher ability to produce mineralized matrix when in contact with CaP_2 specimens, i.e. those ones characterized by relatively fine grained microstructure (cf. Table 6). The latter outcome is in agreement with the results obtained by Guo at al. [94], who observed that mineralization of matrix by osteoblasts was improved after 14 days incubation by the use of nanostructured HA samples instead of the microstructured counterpart. It should be noted that, in contrast with results obtained in the present investigation, Guo at al. [94] also observed an improved proliferation rate in samples with the finer microstructure. Such discrepancy could be likely ascribed to the relatively smaller grains size, about 100 nm, of the specimens used by Guo at al. [94] with respect to that one of the scaffolds tested and reported in Table 6. Thus, it is possible that the scaffold microstructure mostly affects cells growth only when grains size is reduced at the nanoscale.

The result shown in Figure 64 are also supported by the morphological changes observed during *in-vitro* tests on the surface of the different samples. Indeed, the HRSEM micrographs shown Figures 66-68 clearly testify the different microstructures displayed by the three dense calcium phosphates considered in this work after their immersion in the medium in presence of the osteoblasts. In particular, it is seen that the formation of the new apatite phase with the previously described peculiar microstructure takes place exclusively on the surface of CaP_1 and CaP_2 samples, i.e. those ones consisting of HA only. On the other hand no new phases were formed, at least at the time periods examined, when considering the β-TCP rich CaP_3 system. Such finding can be readily associated with the data provided by Alizarin Red-S staining, where osteoblasts displayed a significantly higher mineralization activity on CaP_1 and CaP_2 with respect to CaP_3.

The fact that apatite was not formed when the various scaffolds were immersed into the culture medium without cells, evidenced the essential role played by the latter ones in this context. This statement is clearly supported by the image reported in Figure 69 showing how SaOS-2 osteoblasts

act directly on the disposition of the newly formed hydroxyapatite crystals to generate a net laminar arrangement.

Chapter 5

Concluding Remarks

The fabrication of fully dense bioceramics and bioactive glasses, where the decomposition of original phases or crystallization phenomena are avoided or properly controlled, represents a crucial issue for the optimization of the mechanical and biological properties of this class of materials.

The research activity, whose results are reported in the present PhD thesis, is intended to provide a contribution along this direction. In particular, the powder systems of biomedical interest considered in this work (calcium phosphates, bioactive glasses and HA-bioglass composites) have been processed taking advantage of the Spark Plasma Sintering technology, characterized by lower sintering temperatures and significantly shorter processing times with respect to conventional sintering methods. Thus, the drawbacks mentioned above can be suppressed or limited.

In order to achieve such goal, the SPS conditions have been properly optimize for each system investigated. Furthermore, the obtained dense samples have been characterized in detail from the compositional, microstructural, mechanical and/or biological points of view.

The most relevant results will be summarized in what follows.

The consolidation and crystallization behavior displayed during SPS by a recently developed CaO-rich bioactive glass (BG_Ca/Mix) has been compared in this Chapter 2 with that one exhibited by the commonly used 45S5 Bioglass® (BG_45S5).

Preliminary TGA/DTA analyses evidenced that the new BG_Ca/Mix bioglass displays a relatively reduced tendency to devitrificate with an activation energy for the crystallization process of about 520 kJ/mol, as estimated by the Kissinger formula.

SPS experiments indicate that the optimal sintering temperatures needed to obtain fully dense products were 550°C and about 730°C for BG_45S5 and BG_Ca/Mix, respectively. Moreover, the $Na_6Ca_3Si_6O_{18}$ crystalline phase was already formed in the resulting BG_45S5 product, although the glassy nature still prevailed in the material. On the other hand, the original amorphous character was totally preserved in BG_Ca/Mix specimens after the sintering process conducted at 730 °C. Furthermore, the incipient formation of the α- and β- $CaSiO_3$ crystalline phases in the latter system was found to occur only for sintering temperatures equal or above 830°C.

As far as the mechanical properties are concerned, it was found that BG_Ca/Mix samples obtained by SPS generally displayed higher hardness and local elastic modulus values with respect to the conventional bioglass system. In addition, a general improvement is observed after crystallization for the case of BG_Ca/Mix, as the local elastic modulus significantly increases whereas Vickers hardness remains about the same. On the other hand, relatively lower values of both properties were obtained in mainly crystalline BG_45S5 specimens, probably associated to the observed decrease in sample compactness accompanying the occurrence of crystallization phenomena in this system during SPS.

In conclusion, the electric current assisted sintering seems to provide a useful tool for controlling crystallization phenomena in both BG_45S5 and BG_Ca/Mix systems. In particular, under the experimental conditions investigated, the occurrence of crystallization cannot be completely suppressed using classical Bioglass® powders to obtain fully dense products by SPS. Nevertheless, the original amorphous nature is still predominantly preserved. Furthermore, the intrinsically low devitrification tendency of the innovative BG_Ca/Mix is even further mitigated when the initial powders are processed by SPS, so that completely amorphous dense materials can be produced very shortly.

It is apparent that the control of crystallization phenomena in the bioglass samples produced by SPS will likely play also an important role with respect to their biological response. This aspect will be

considered in the near future when the obtained sintered products will be subjected to standard bioactivity tests.

It should be noted that the results obtained from the characterization of fully dense products are expected to provide important indications in view of developing porous scaffolds from classical and new bioglass compositions. In this regard, it is important to consider that, despite its primary utilization is for the fabrication of dense materials, the SPS technology has been also recently exploited, under appropriate operating conditions and adopting specifically designed die configurations, to obtain porous scaffolds[106].

In this regard, it should be noted that to make the fabrication of porous structures possible, the presence of the mechanical load during sintering should be eliminated or significantly reduced. On the other hand, the contact between electrode and graphite plungers has to be kept during SPS to maintain the electric current flowing through the die. To satisfy both requirement, the concept of ‘’Pressureless SPS’’ is developed, as schematically represented in Figure 70. It can be observed that, using such die configuration, the mechanical load is not directly applied to the powders undergoing sintering so that the pressureless conditions can be established during the SPS process.

This approach, which allows for the obtainment of various porous materials in the literature [107,108,109], can be then adopted for the fabrication of similar structures based on bioglass and calcium phosphate systems considered in the present work.

The preparation of porous structures during pressureless can be also facilitated by the use of appropriate gasifying agents initially mixed to the glass/ceramic powders, and progressively removed during the course of the sintering process.

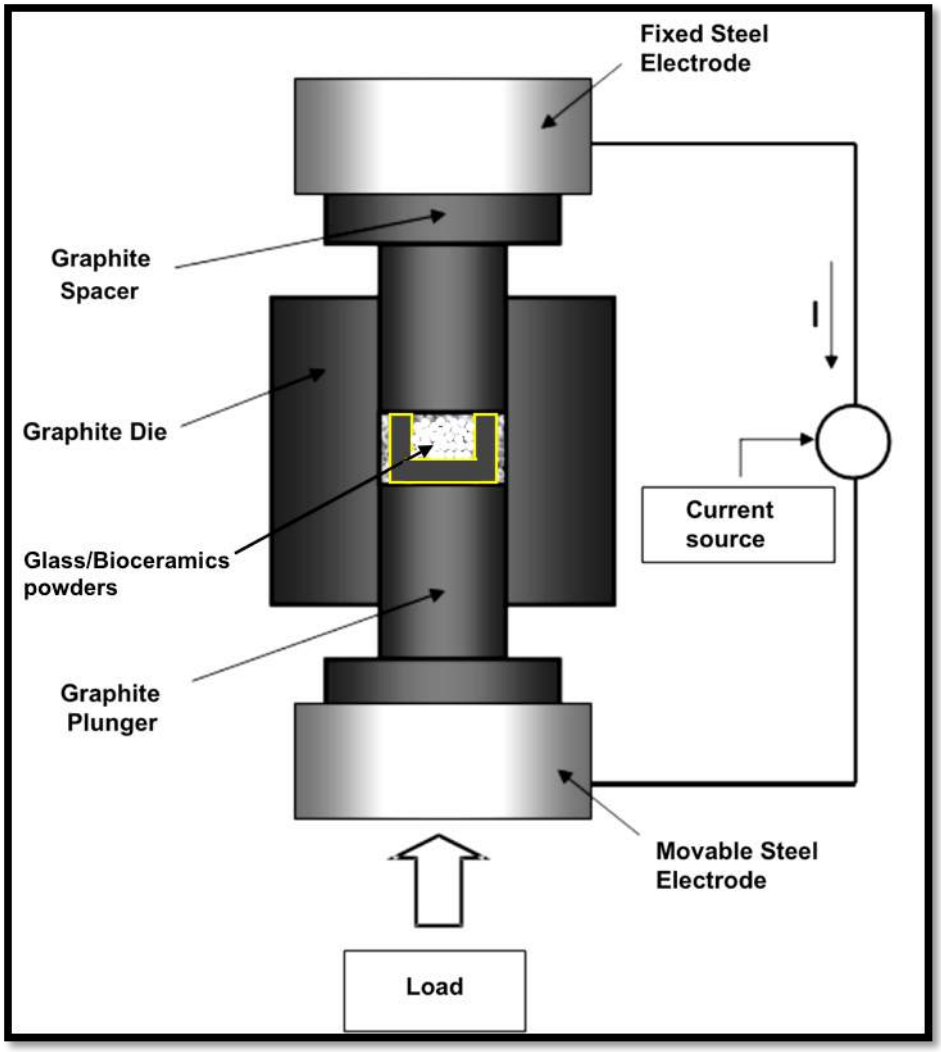

Figure 70. Principle of Pressureless Spark Plasma Sintering.

As reported in Chapter 3, SPS was also employed to produce almost completely dense and highly bioactive composites based on different mixtures of HA and of BG_Ca/Mix. The produced samples are very compact and significantly denser ($\rho \geq 96\%$) with respect to the counterparts produced by conventional sintering methods. In particular, for the first time, a set of HA/BG_Ca-Mix samples (70wt.% HA) with a density near to the theoretical value has been successfully obtained. Furthermore, thanks to the low tendency to crystallize of the innovative BG_Ca/Mix, it was possible to reduce the devitrification of the glassy phase in the samples, with beneficial effects in terms of the resulting in vitro bioactivity. Although a certain degree of glass crystallization is typically observed in fully dense composite samples, crystallization phenomena, as well as HA/glass reactions and HA decomposition, are considerably lower with respect to those observed when classic sintering methods and/or other

bioactive glass compositions are used. In conclusion, SPS was demonstrated an efficient powder consolidation technique to produce HA-based composites with bioactive glass as second phase. In addition, the BG_Ca/Mix composition is confirmed to be particularly useful whenever a thermal treatment is required to obtain dense bodies.

As far as biocompatibility is concerned, preliminary results indicated that the relative amount of apatite formation on the samples surface after few days in SBF increased as the fraction of BG_Ca/Mix in the composite was augmented.

Further studies regarding the latter issue as well as the production by SPS of HA/BG_Ca-Mix composites modified with ions of biological interest, such as strontium and/or magnesium, will be the subjects of future investigations.

Moreover, additional studies are also foreseen to examine in detail the interaction of suitable cell cultures with the newly developed HA-BG_Ca/Mix composites.

Finally, the research activity described and discussed in Chapter 4 follows a previous work [Cuccu et al., 2015] addressed to the fabrication of dense HA samples by SPS.

In particular, the in-vitro characterization of the resulting sintered material is performed in the framework of the present thesis. In this regard, it is found that the compositional and microstructural characteristics of fully dense and finely polished calcium phosphate-based disks produced by SPS from three different commercial HA powders significantly affect the biological response of SaOS-2 human cells during *in-vitro* experiments. Indeed, although a similar behavior was displayed in terms of cells adhesion, viability and proliferation rate, to indicate that the osteoblasts have a quite good affinity with the three scaffolds, important dissimilarities were evidenced when considering the amount of mineralization and the formation of an apatite layer on their surface. Specifically, it is possible to state that mineralization phenomena and the consequent formation of a new apatite phase with a trabecular-like arrangement are strongly promoted on scaffolds exclusively consisting of HA. In this regard, the specific role played by SaOS-2 cells to generate the peculiar microstructure in the

newly formed calcium-phosphate phase was evidenced. Furthermore, the amount of mineralization was markedly higher on samples exhibiting a submicrometer-grained microstructure, which was obtained when the initial fine and highly-pure powders were exposed to relatively lower thermal levels during sintering. In contrast, the chemical decomposition of HA to β-TCP during the SPS process negatively affects the biological response, as mineralization phenomena are strongly inhibited during *in-vitro* tests. Correspondingly, no apatite layer was formed on the surface of such scaffold.

Based on the obtained results, it is possible to state that CaP_2, followed by CaP_1, is the most promising system for biomedical applications, whereas the large fraction of β-TCP in CaP_3 scaffolds suppresses osteoblasts capability to generate new bone.

References

[1]. Plannel J.A., Bone Repair Biomaterials, Woodhead Publishing in Materials, (2009).

[2]. http://www.jisrf.org/unicompartmental-knee-arthroplasty-past-present-future.html

[3]. Williams D.F. , On the nature of biomaterials, Biomaterials 30 (2009) 5897-5909 pp.

[4]. Mann S. (Ed.), Biomimetic Materials Chemistry, Wiley-VCH, UK, (1996) 400 p.

[5]. Vallet Regì M., Bioceramics: where do we come from and which are the future expectations, Key Eng. Mater. 9 (2007) 1035-1050 pp.

[6]. Dorozhkin S.V., Calcium orthophosphate bioceramics. Ceram. Int. 41 (2015) 13913-13966 pp.

[7]. Kokubo T. (Ed.), Bioceramics and Their Clinical Application, Wood-head Publishing, Abington, Cambridge, UK, (2008) 784 pp.

[8]. Hench L.L. Bioceramics J. Am. Ceram. Soc. 81 (1998) 1705-1728 pp.

[9]. Jones J. R., Review of bioactive glass: From Hench to hybrids, Acta Biomaterialia 9 (2013) 4457- 4486 pp.

[10]. Deer W.A., Howie R., Zussman J., an introduction to Rock-forming Minerals. Longman: Hong Kong, (1985) 504-509 pp.

[11]. DeJong W.F., La substance minerale dans les os. Res Trav Chim 45 (1926) 445-448 pp.

[12]. http://www.azom.com/article.aspx?ArticleID=2630

[13]. http://www.chemtube3d.com/solidstate/SShydroxyapatite.htm

[14]. Cuccu A., S. Montinaro, R. Orrù, G. Cao, D. Bellucci, A. Sola, V. Cannillo, Consolidation of different Hydroxyapatite powders by SPS: optimization of the sintering conditions and characterization of the obtained bulk products. Ceram. Int. 41(1) (2015) 725-736 pp.

[15]. http://www.3dtupo.com/sc/article/3d281

[16]. Bertazzo S. Zambuzzi W.F., Campos D.D.P., Ogeda T.L., Ferreira C.V., Bertran C.A., Hydroxyapatite surface solubility and effect on cell adhesion, Colloids Surf. B 78 (2010) 177-184 pp.

[17]. Okuda T., Ioku K., Yonezawa I., Minagi H., Gonda Y., Kawachi G., Kamitakhara M., Shibata Y., Murayama H., Kurosawa H., Ikeda T., The slow resorption with replacement by bone of a hydrothermally synthesized pure calcium-deficient hydroxyapatite, Biomaterials 29 (2008) 2719-2728 pp.

[18]. Hench L. L., The story of Bioglass® , J. Mater. Sci: Mater. Med. 17 (2006) 967-978 pp.

[19]. Wilson J., Low S.B., "Bioactive Ceramics for periodontal treatment: comparative studies in the patus monkey", J. Appl. Biomater. 3 (1992) 123-169 pp.

[20]. http://www.scielo.br/img/revistas/bdj/v21n5/a01fig3.jpg

[21]. Bellucci D., Sola A., Cannillo V.,Low temperature sintering of innovative bioactive glasses, J. Am. Ceram. Soc. 95 (4) (2012) 1313–1319 pp.

[22]. Rahaman M. N., Day D. E.,. Bal B. S., Fu Q., Jung S. B., Bonewald L. F., Tomsia A. P., "Bioactive glass in tissue engineering", Acta Biomaterialia 7 (2011) 2355-2373 pp.

[23]. Gerhardt L.C., Boccaccini A., Bioactive Glass and Glass-Ceramic Scaffolds for Bone Tissue Engineering, Materials. 3 (2010) 3867-3910 pp.

[24]. Andersson O., Happonen R-P., Yli-Urpo A., "Bioceramics: 2". Volume 7, Papers from the 7th International Symposium on Ceramics in Medicine, Turku, Finland, 1994.

[25]. Kokubo T., Kim H., Kawashita M., "Novel bioactive materials with different mechanical properites", Biomaterials 24 (2003) 2161-2175 pp.

[26]. Filho O.P., LaTorre G.P., Hench L.L., Effect of crystallization on apatite-layer formation of bioactive glass 45S5, J. Biomed. Mater. Res. 30 (1996) 509–514 pp.

[27]. Boccaccini A.R., Chen Q., Lefebvre L., Gremillard L., Chevalier J., Sintering, crystallization and biodegradation behaviour of Bioglass® -derived glass-ceramics, Faraday Discuss. 136 (2007) 27–44 pp.

[28]. Lefebvre L., Gremillard L., Chevalier J., Zenati R., Bernache-Assolant D. Sintering behaviour of 45S5 bioactive glass, Acta Biomaterialia 4 (2008) 1894-1903 pp.

[29]. German R. “Sintering Theory and Practice” Wiley-Interscience Ed. (1996).

[30]. Dorozhkin S.V., Bioceramics of calcium orthophosphates, Biomaterials 31 (7) (2010) 1465–1485 pp.

[31]. http://www.ltu.se/cms_fs/1.5838!/fafc1546.pdf

[32]. http://home.anadolu.edu.tr/~esuvaci/egitim/Sintering%20of%20Ceramics-Overview.pdf

[33]. Musa C. Locci A.M., Licheri R., Orru R., Cao G., Vallauri D., Deorsola F.A., Tresso E., Suffner J., Hahn H., Klimczyc P., Jaworska L. Spark plasma sintering of self-propagating high-temperature synthesized TiC0.7/TiB2 powders and detailed characterization of dense product. Ceramic International, 35 (2009) 2587-2599 pp.

[34]. http://www.dynacer.com/processing/hot-pressing

[35]. http://www.azom.com/article.aspx?ArticleID=5769

[36]. Orru R., Licheri R., Locci A.M., Cincotti A., Cao G., Consolidation/synthesis of Materials by Electric Current Activated/assisted Sintering, Materials Science and Engineering Report 63(4-6) (2009) 127-287 pp.

[37]. Jajarmi E., Desogus L., Orrù R., Sajjadi S.A., Cao G. On the fabrication of functional graded 3Y-PSZ/316L materials by SPS: Process optimization and characterization of the obtained products, Ceramic international 42 (2016) 8351-8359 pp.

[38]. Li P. Yang Q., Zhang F., Kokubo T., The effect of residual glassy phase in a bioactive glass-ceramic on the formation of its surface apatite layer in vitro, J. Mater. Sci. Mater. Med. 3 (1992) 452–456 pp.

[39]. Lefebvre L., Chevalier J., Gremillard L., Zenati R., Thollet G., Bernache-Assolant D., Govin A.. Structural transformations of bioactive glass 45S5 with thermal treatments. Acta Mater. 55 (2007) 3305–3313 pp.

[40]. Bretcanu O., Chatzistavrou X., Paraskevopoulos K., Conradt R., Thompsond I., Boccaccini A.R. Sintering and crystallisation of 45S5 Bioglass® powder J. Eur. Ceram. Soc. 29 (2009) 3299–3306 pp.

[41]. Chen Q.Z., Xu J.L., Yu L.G., Fang X.Y., Khor K.A. Spark plasma sintering of sol-gel derived 45S5 Bioglass® ceramics: Mechanical properties and biocompatibility evaluation Mater. Sci. Eng. C 32 (2012) 494 502 pp.

[42]. Grasso S., Chinnam R.K., Porwal H., Boccaccini A.R., Reece M.J. Low temperature spark plasma sintering of 45S5 Bioglass® J. Non-Cryst. Solids 362(1) (2013) 25-29.

[43]. Porwal H., Grasso S., Cordero-Arias L., Li C., Boccaccini A.R., Reece M.J. Processing and bioactivity of 45S5 Bioglass®-graphene nanoplatelets composites J. Mater. Sci. Mater. Med. 25(6) (2014) 1403-1413 pp.

[44]. Guo H.B, Miao X., Chen Y., Cheang P., Khor K.A. Characterization of hydroxyapatite- and bioglass-316L fibre composites prepared by Spark Plasma Sintering Mater. Lett. 58 (2004) 304 307 pp.

[45]. Jia Z., Zhang J., Jia C., Nie J., Chu K., Preparation and characterization of mechanical properties of carbon nanotube/45S5 Bioglass composites for biologic applications, Mater. Sci. Eng. A 528 (3) (2011) 1553–1557 pp.

[46]. Lockyer M.W.G., Holland D., Dupree R., NMR investigation of the structure of some bioactive and related glasses, J. Non-Cryst. Solids 188 (1995) 207–219 pp.

[47]. Bellucci D., Cannillo V., Sola A. Calcium and potassium addition to facilitate the sintering of bioactive glasses Mater. Lett. 65(12) (2011) 1825-1827 pp.

[48]. Bellucci D., Cannillo V., Sola A. A new highly bioactive composite for scaffold applications: A feasibility study Materials 4(2) (2011) 339-354 pp.

[49]. Locci A.M., Orrù R., Cao G., Munir Z.A., Effect of ball milling on simultaneous spark plasma synthesis and densification of TiC-TiB2 composites, Mater. Sci. Eng. A 434 (1–2) (2006) 23–29 pp.

[50]. Oliver W.C., Pharr G.M., An improved technique for determining hardness and elastic modulus using load and displacement sensing indentation experiments, J. Mater. Res. 7 (6) (1992) 1564–1583 pp.

[51]. Clupper D.C., Hench L.L., Crystallization kinetics of tape cast bioactive glass 45S5, J. Non-Cryst. Solids 318 (2003) 43–48 pp.

[52]. Massera J., Fagerlund S., Hupa L., Hupa M., Crystallization mechanism of the bioactive glasses, 45S5 and S53P4, J. Am. Ceram. Soc. 95 (2) (2012) 607–613 pp.

[53]. Bellucci D., Cannillo V., Sola A., An overview of the effects of thermal processing on bioactive glasses, Sci. Sin. 42 (2010) 307–320 pp.

[54]. Padmanabhan S.K., Gervaso F., Carrozzo M,Scalera. F., Sannino A., Licciulli A., Wollastonite/hydroxyapatite scaffolds with improved mechanical, bioactive and biodegradable properties for bone tissue engineering, Ceram. Int. 39 (2013) 619–627 pp.

[55]. LaPrade R.F., Botker J.C.. Donor-site morbidity after osteochondral autograft transfer procedures. Arthroscopy 20 (2004) e69–e73 pp.

[56]. Palmer S.H., Gibbons C.L., Athanasou N.A.. The pathology of bone allograft. J Bone Jt. Surg. Br. 81 (1999) 333–335 pp.

[57]. Bellucci D., Sola A., Cannillo V.. Hydroxyapatite and tricalcium phosphate composites with bioactive glass as second phase: State of the art and current applications. J. Biomed. Mater. Res. Part A 104A (2016) 1030–1056 pp.

[58]. Samavedi S., Whittington A.R., Goldstein A.S.. Calcium phosphate ceramics in bone tissue engineering: A review of properties and their influence on cell behavior. Acta Biomater. 9 (2013) 8037–8045 pp.

[59]. Bohner M.. Calcium orthophosphates in medicine: From ceramics to calcium phosphate cements. Injury 31 (2000) D37–D47 pp.

[60]. Burg K.J.L., Porter S., Kellam J.F.. Biomaterial developments for bone tissue engineering. Biomaterials 21 (2000) 2347–2359 pp.

[61]. Habibovic P., Sees T.M., van den Doel M.A., van Blitterswijk C.A., de Groot K.. Osteoinduction by biomaterials—Physicochemical and structural influences. J. Biomed. Mater. Res. 77 (2006) 747–762 pp.

[62]. Bolelli G., Bellucci D., Cannillo V., Lusvarghi L., Sola A., Stiegler N., Müller P., Killinger A., Gadow R., Altomare L., De Nardo L.. Suspension thermal spraying of hydroxyapatite: Microstructure and in vitro behaviour. Mater. Sci. Eng. C 34 (2014) 287–303 pp.

[63]. Santos J.D., Reis R.L., Monteiro F.J., Knowles J.C., Hastings G.W. Liquid phase sintering of hydroxyapatite by phosphate and silicate glass additions: Structure and properties of the composites. J. Mater. Sci. Mater. Med. 6 (1995) 348–352 pp.

[64]. Santos J.D., Silva P.L, Knowles J.C., Talal S., Monteiro F.J.. Reinforcement of hydroxyapatite by adding P2O5-CaO glasses with Na2O, K2O and MgO. J. Mater. Sci. Mater. Med. 7 (1996) 187–189 pp.

[65]. Proussaefs P., Olivier H.S., Lozada J.. Histologic evaluation of a 12-year-old threaded hydroxyapatite-coated implant placed in conjunction with subantral augmentation procedure: a clinical report. J. Prosthet. Dent. 92 (2004) 17-22 pp.

[66]. Hench L.L. Bioceramics: From concept to clinic. J. Am. Ceram. Soc. 74 (1991) 1487–1510.

[67]. Gorustovich A.A., Roether J.A., Boccaccini A.R.. Effect of bioactive glasses on angiogenesis: a review of in vitro and in vivo evidences. Tissue Eng. Part B Rev. 16 (2010) 199-207 pp.

[68]. Kolmas J., Jaklewicz A., Zima A., Bućko M., Paszkiewicz Z., Lis J., Ślósarczyk A., Kolodziejski W.. Incorporation of carbonate and magnesium ions into synthetic hydroxyapatite: the effect on physicochemical properties. J. Mol. Struct. 987 (2011) 40–50 pp.

[69]. Knowles J.C., Bonfield W.. Development of a glass reinforced hydroxyapatite with enhanced mechanical properties. The effect of glass composition on mechanical properties and its relationship to phase changes. J. Biomed. Mater. Res. 27 (1993) 1591–1598 pp.

[70]. Jones J.J.. Reprint of: Review of bioactive glasses: From Hench to hybrids. Acta Biomater. 23 (2015) S53-S82 pp.

[71]. Bellucci D., Cannillo V., Ciardelli G., Gentile P., Sola A. Potassium based bioactive glass for bone tissue engineering. Ceram. Int. 36 (2010) 2449-2453 pp.

[72]. Bellucci D., Cannillo V., Sola A.. A new potassium-based bioactive glass: Sintering behaviour and possible applications for bioceramic scaffolds. Ceram. Int. 37 (2011) 145-157 pp.

[73]. Bellucci D., Sola A., Cannillo V.. Bioactive glass-based composites for the production of dense sintered bodies and porous scaffolds. Mater. Sci. Eng. C 33 (2013) 2138–2151 pp.

[74]. Bellucci D., Sola A., Anesi A., Salvatori R., Chiarini L., Cannillo V. Bioactive glass/hydroxyapatite composites: Mechanical properties and biological evaluation. Mater. Sci. Eng. C 51 (2015) 196-205 pp.

[75]. Desogus L., Cuccu A., Montinaro S., Orrù R., Cao G., Bellucci D., Sola A., Cannillo V.. Classical Bioglass® and innovative CaO-rich bioglass powders processed by Spark Plasma Sintering: a comparative study. J. Eur. Ceram. Soc. 35 (2015) 4277-4285 pp.

[76]. Matthews F.L., Rawlings R.. Composite Materials: Engineering and Science. Chapman & Hall, Great Britain; 1994.

[77]. Quinn G.D., Patel P.J., Lloyd I., Effect of loading rate upon conventional ceramic microindentation hardness. J. Res. Natl. Inst. Stand. 107 (2002) 299-306 pp.

[78]. Kokubo T., Takadama H.. How useful is SBF in predicting in vivo bone bioactivity? Biomaterials 27 (2006) 2907–2915 pp.

[79]. Xin R., Leng Y., Chen J., Zhang Q.. A comparative study of calcium phosphate formation on bioceramics in vitro and in vivo Biomaterials 26 (2005) 6477-6486 pp.

[80]. Chen Q.Z., Thompson I.D., Boccaccini A.R.. 45S5 Bioglass-derived glass-ceramic scaffolds for bone tissue engineering. Biomaterials 27 (2006) 2414–2425 pp.

[81]. Bellucci D., Bolelli G., Cannillo V., Cattini A., Sola A.. In situ Raman spectroscopy investigation of bioactive glass reactivity: Simulated body fluid solution vs TRIS-buffered solution. Mater. Charact. 62 (2011) 1021–1028 pp.

[82]. Koutsopoulos S.. Synthesis and characterization of hydroxyapatite crystals: A review study on the analytical methods. J. Biomed. Mat. Res. 62 (2002) 600–612 pp.

[83]. Awonusi, M.D. Morris, M.M.J. Tecklenburg. Carbonate assignment and calibration in the Raman spectrum of apatite. Calcif. Tissue Int. 81 (2007) 46–52 pp.

[84]. Nakahira, M. Tamai, H. Aritani, S. Nakamura, K. Yamashita. Biocompatibility of dense hydroxyapatite prepared using an SPS process. J. Biomed. Mater. Res. 62 (2002) 550–557 pp.

[85]. Gu Y.W., Khor K.A., Cheang P. Bone-like apatite layer formation on hydroxyapatite prepared by spark plasma sintering (SPS). Biomaterials 25 (2004) 4127–4134 pp.

[86]. Liu X., Ding C., Wang Z., Apatite formed on the surface of plasma-sprayed wollastonite coating immersed in simulated body fluid. Biomaterials 22 (2001) 2007–2012 pp.

[87]. Siriphannon P., Kameshima Y., Yasumori A., Okada K., Hayashi S., Formation of hydroxyapatite on CaSiO3 powders in simulated body fluid. J. Eur. Ceram. Soc. 22 (2002) 511–520 pp.

[88]. Long L.H., Chen L.D., Bai S.Q., Chang J., Lin K.L.. Preparation of dense β-CaSiO3 ceramic with high mechanical strength and HAp formation ability in simulated body fluid. J. Eur. Ceram. Soc. 26 (2006) 1701–1706 pp.

[89]. Ni S., Chang J., Chou L., Zhai W.. Comparison of osteoblast-like cell responses to calcium silicate and tricalcium phosphate ceramics in vitro. J. Biomed. Mater. Res. B Appl. Biomater. 80 (2007) 174–83 pp.

[90]. Prakasam M., J. Locs, K. Salma-Ancane, D. Loca, A. Largeteau, L. Berzina-Cimdina Fabrication, Properties and Applications of Dense Hydroxyapatite: A Review J. Funct. Biomater. (2015) 6 1099-1140 pp.

[91]. Champion E. Sintering of calcium phosphate bioceramics. Acta Biomater. (2013) 9(4): 5855-5875 pp.

[92]. Kawagoe D., Y. Koga , E. Hideki Ishida , N. Kotobuki , H. Ohgushi and K. Ioku Preparation of transparent hydroxyapatite ceramics by spark plasma sintering and cell culture test Phosphorous Research Bulletin (2006) 20 119-128 pp.

[93]. Li, H., Khor, K.A., Chow, V., Cheang, P. Nanostructural characteristics, mechanical properties, and osteoblast response of spark plasma sintered hydroxyapatite. J Biomed Mater Res A (2007) 82(2), 296-303 pp.

[94]. Guo, X., Gough, J.E., Xiao, P., Liu, J., Shen, Z. Fabrication of nanostructured hydroxyapatite and analysis of human osteoblastic cellular response. J Biomed Mater Res A (2007) 82(4) 1022-1032 pp.

[95]. Xu J. L., K. A. Khor, Y. W. Lu, W. N. Chen, R. Kumar Osteoblast Interactions With Various Hydroxyapatite Based Biomaterials Consolidated Using a Spark Plasma Sintering Technique. J Biomed Mater Res B (2007) 84B(1), 224-230 pp.

[96]. Isola, M., Isola, R., Lantini, M.S., Riva, A. The three-dimensional morphology of Candida albicans as seen by high-resolution scanning electron microscopy. J Microbiol (2009) 47(3), 260-264 pp.

[97]. Loy, F., Isola, M., Isola, R., Solinas, P., Lilliu, M.A., Puxeddu, R., Ekstrom, J. Ultrastructural evidence of a secretory role for melatonin in the human parotid gland. J Physiol Pharmacol (2015) 66(6) 847-853 pp.

[98]. Carrodeguas R.G., De Aza S. α-Tricalcium phosphate: Synthesis, properties and biomedical applications. Acta Biomater. (2011) 7(10) 3536–3546 pp.

[99]. Malik M.A., Puleo D.A., Bizios R., Doremus R.H. Osteoblasts on hydroxyapatite, alumina and bone surfaces in vitro: morphology during the first 2 h of attachment. Biomaterials (1992) 13(2) 123-128 pp.

[100]. Annaz, B., Hing, K.A., Kayser, M., Buckland, T., Di Silvio, L. Porosity variation in hydroxyapatite and osteoblast morphology: A scanning electron microscopy study J. Microsc. (2004) 215 (1) 100-110 pp.

[101]. Rajaraman R., D. E. Roundsa, S. P. S. Yenb and A. Rembaumb, A scanning electron microscope study of cell adhesion and spreading in vitro. Exp Cell Res, (1974) 88(2) 327-339 pp.

[102]. Dos Santos EA, Farina M, Soares GA. Specific proliferation rates of human osteoblasts on calcium phosphate surfaces with variable concentrations of α-TCP. Mater Sci Eng C. (2007) 27 61–66 pp.

[103]. Laquerriere, P., Kilian, L., Bouchot, A., Jallot E, Grandjean A., Guenounou M., Balossier G., Frayssinet, P., Bonhomme, P. Effect of hydroxyapatite sintering temperature on intracellular ionic concentrations of monocytes: A TEM-cryo-X-ray microanalysis study J Biomed Mater Res (2001) 58(3) 238-246 pp.

[104]. Wang, C., Duan, Y., Markovic, B., Barbara J., Rolfe Howlett C., Zhang, X., Zreiqat, H. Proliferation and bone-related gene expression of osteoblasts grown on hydroxyapatite ceramics sintered at different temperature. Biomaterials (2004) 25(15) 2949-2956 p.

[105]. Shu, R., McMullen, R., Baumann, M.J., McCabe, L.R. Hydroxyapatite accelerates differentiation and suppresses growth of MC3T3-E1 osteoblasts J Biomed Mater Res A (2003) 67(4) 1196-1204 pp.

[106]. Zhang F., Lin K., Chang J., Lu J., Ning C., Spark plasma sintering of macroporous calcium phosphate scaffolds from nanocrystalline powders, J. Eur. Ceram. Soc. 28 (3) (2008) 539–545 pp.

[107]. Sairam K., Sonber J.K., Murthy T.S.R.Ch., Sahu A.K., Bedse R.D., Chakravartty J.K., Pressureless sintering of chromium diboride using spark plasma sintering facility, International Journal of Refractory Metals and Hard Materials 58, (2016), 165–171 pp.

[108]. Yamanoglu R., Gulsoy N., Olevsky E.A., Gulsoy H.O., Production of porous Ti5Al2.5Fe alloy via pressureless spark plasma sintering, Journal of Alloys and Compounds 680, (2016), 654–658 pp.

[109]. Luca Bertolla, Ivo Dlouhýa, Peter Tatarko, , Alberto Viani, Amit Mahajan, Zdeněk Chlup, Michael J. Reece, Aldo R. Boccaccini, Pressureless spark plasma–sintered Bioglass® 45S5 with enhanced mechanical properties and stress–induced new phase formation, Journal of the European Ceramic Society, 2017

List of Publications related to the thesis:

- Desogus L., Cuccu A., Montinaro S., Orrù R., Cao G., Bellucci D., Sola S., Cannillo V. Classical Bioglass® and innovative CaO-rich bioglass powders processed by Spark Plasma Sintering: A comparative study, Journal of the European Ceramic Society 35 (2015) 4277-4285 pp.

- Jajarmi E., Desogus L., Orrù R., Sajjadi S.A., Cao G. On the Fabrication of Functional Graded 3Y-PSZ/316L Materials by SPS: Process optimization and characterization of the obtained products, Ceramic International 42 (2016) 8351-8359 pp.

- Bellucci D., Desogus L., Montinaro S., Orrù R., Cao G., Cannillo V. Innovative Hydroxyapatite/Bioactive glass composites processed by Spark Plasma Sintering for bone tissue repair, Journal of the European Ceramic Society, in press (2016) doi:10.1016/j.jeurceramsoc.2016.11.012

- Mancuso L., Desogus L., Orrù R., Loy F., Cao G. Behaviour of SaOS-2 Human Cells Cultured on Different Fully Dense Calcium Phosphate Materials Fabricated by Spark Plasma Sintering, Submitted to Material Science and Engineering C, 2016